Exceptional Event Demonstration for Ozone Exceedances in Clark County, Nevada – September 26, 2020

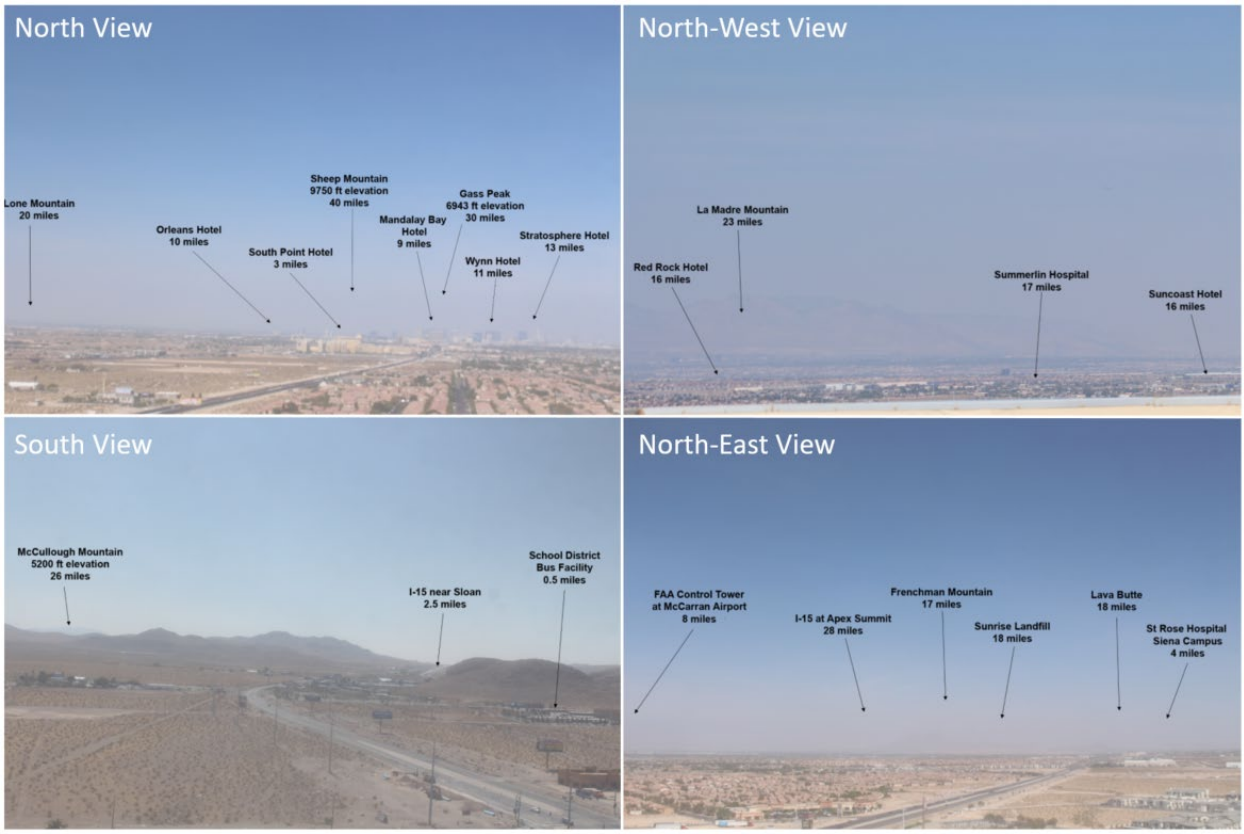

Final Report Prepared for

U.S. EPA Region 9
San Francisco, CA

September 2021

STi | Sonoma Technology

This document contains blank pages to accommodate two-sided printing.

Exceptional Event Demonstration for Ozone Exceedances in Clark County, Nevada – September 26, 2020

Prepared by

Steve Brown, PhD
Crystal McClure, PhD
Cari Gostic
David Miller, PhD
Nathan Pavlovic
Charles Scarborough
Ningxin Wang, PhD

Sonoma Technology
1450 N. McDowell Blvd., Suite 200
Petaluma, CA 94954
Ph 707.665.9900 | F 707.665.9800
sonomatech.com

Prepared for

Clark County Department of Environment and Sustainability
Division of Air Quality
4701 W. Russell Road, Suite 200
Las Vegas, NV 89118
Ph 702.455.3206
www.clarkcountynv.gov

Final Report

STI-920053-7477

September 1, 2021

The images on the cover show visibility across Clark County on September 26, 2020. These images were taken from webcams set up in Clark County, and show the impact of the exceptional event on September 26. Each image is labeled with the viewing direction and landmarks.

Contents

Figures

Tables

Executive Summary

On September 26, 2020, Clark County experienced an atypical episode of elevated ambient ozone. During this episode, the 2015 8-hr ozone National Ambient Air Quality Standards (NAAQS) thresholds were exceeded at the Walter Johnson and Joe Neal monitoring sites. The exceedance at both sites could lead to an ozone nonattainment designation for the Clark County area. Air trajectory analysis and air quality modeling results show that emissions from wildfires burning throughout southern and central California contributed to the transport to and formation of ozone in Clark County. The U.S. Environmental Protection Agency (EPA) Exceptional Event Rule (U.S. Environmental Protection Agency, 2016) allows air agencies to omit air quality data from the design value calculation if it can be demonstrated that the measurement in question was caused by an exceptional event. This report describes analyses that help to establish a clear causal relationship between wildfire smoke and the September 26, 2020, ozone exceedances at the Walter Johnson and Joe Neal monitoring sites.

The analyses conducted provide evidence supportive of wildfire smoke and impacts on ozone concentrations in Clark County. We show that (1) smoke was transported from wildfires in southern and central California to the surface in the Clark County area in the hours leading up to the exceedance date and on the exceedance date; (2) wildfire smoke impacted the typical diurnal profiles of ground-level pollution measurements, including $PM_{2.5}$, CO, and NO_2, in the Clark County area on September 25-26; (3) byproducts and tracers of wildfire combustion were present and elevated at the surface in the Clark County area on September 27, the day after the ozone exceedance; and (4) meteorological regression modeling and similar meteorological day analysis show that ozone observations on September 26 were unusual in the historical record given the meteorological conditions. Sources of evidence used in these analyses include (1) air quality monitor data to show that supporting pollutant trends at the surface were influenced by wildfire smoke; (2) air trajectory analysis to show transport of smoke-laden air to the Clark County area; (3) media coverage of wildfires and smoke impacts; and (4) meteorological regression modeling and meteorologically similar day analysis.

EPA guidance for exceptional event demonstrations (U.S. Environmental Protection Agency, 2016) provides a three-tiered approach. Depending on the complexity of the event, increasingly involved information may be required to demonstrate a causal relationship between wildfire smoke and an exceedance. Here, we provide the results of analyses conducted to address Tier 1, Tier 2, and Tier 3 exceptional event demonstration requirements.

These analyses show that smoke was transported from wildfires throughout southern and central California to the Clark County area over the hours leading up to September 26. Combined with additional evidence, such as meteorological regression modeling and meteorologically similar day analysis, our results provide key evidence to support smoke impacts on ozone concentrations in Clark County on September 26, 2020.

1. Overview

1.1 Introduction

California had an unprecedented wildfire season in 2020, with five of the six largest wildfires in the state's history occurring in either August or September (https://www.fire.ca.gov/media/11416/top20_acres.pdf). Smoke emissions from California wildfires can affect downwind areas, including Clark County, Nevada, on September 26, 2020. On this date, 2 of the 14 ozone (O_3) monitoring locations around Clark County recorded an exceedance of the 2015 National Ambient Air Quality Standard (NAAQS) for 8-hour ozone (0.070 ppm).

Emissions from wildfires can affect concentrations of ozone downwind by direct transport of both ozone and precursor gases (i.e., nitrogen oxides [NO_x] and volatile organic compounds [VOCs]). Each mechanism can enhance the overall ozone concentration and/or the amount of ozone that is produced. For example, in an area where NO_x concentrations are high, such as an urban setting like Las Vegas, Nevada, the transport of VOCs from wildfire emissions can enhance ozone production, potentially driving concentrations above the ozone standard. According to U.S. Environmental Protection Agency's (EPA) exceptional event guidance (EE) guidance (U.S. Environmental Protection Agency, 2016), EEs such as wildfires that affect ozone concentrations, can be subject to exclusion from calculations of NAAQS attainment if a clear causal relationship is established between a specific event and the monitoring exceedance.

This report describes the clear causal relationship between the large wildfires throughout southern and central California and the exceedance of the maximum daily 8-hour ozone average (MDA8) at the two Clark County monitoring sites on September 26, 2020. We correlate the following California wildfires with enhanced ozone concentrations in Clark County: SQF Lightning Complex, Blue Jay Fire, Wolf Fire, Creek Fire, Bobcat Fire, and El Dorado Fire (more details provided in Section 3.2.1). We suggest that these fires contributed ozone and ozone precursors Clark County, which enhanced ozone concentrations and caused an exceedance of the NAAQS. The evidence in this report includes all three tiers of analysis required by EPA's EE guidance: for Tier 1, ground and satellite-based measurement of smoke emissions, transport of smoke from the wildfires in California to Clark County, and media coverage of the smoke event in Clark County; for Tier 2, emission versus distance analysis, ground and satellite analysis of smoke-related pollutants, and comparison of event and non-event concentrations; and for Tier 3, vertical column analyses and statistical Generalized Additive Modeling (GAM) of the event. The wildfire that affected ozone concentrations in Clark County could not be reasonably controlled or prevented because it was caused by accidental ignition and is unlikely to recur. Table 1-1 lists the sites affected during the September 26 event, as well as their locations and MDA8 ozone concentrations.

Table 1-1. September 26, 2020, exceptional event information. All monitoring sites in Clark County that exceeded the 2015 NAAQS standard on September 26, 2020, are listed along with Air Quality System (AQS) Site Codes, location information, and MDA8 ozone concentrations.

AQS Site Code	Site Name	Latitude (degrees N)	Longitude (degrees W)	MDA8 O_3 Concentration (ppb)
320030075	Joe Neal	36.271	-115.238	75
320030071	Walter Johnson	36.170	-115.263	71

Concurrent with this document, Clark County is submitting documentation for other ozone EEs in 2018 and 2020 that were caused by wildfires and stratospheric intrusions. These events are mentioned throughout this report and are referred to as "proposed 2018 and 2020 exceptional events," recognizing that discussion with EPA is still pending. All proposed EEs for Clark County in 2018 and 2020 are listed in Tables 1-2 and 1-3. Wherever possible, we calculated statistics to provide context that both includes and excludes the proposed EEs from 2018 and 2020.

Table 1-2. Proposed Clark County 2018 exceptional events. For each site and date combination where the 2015 NAAQS standard was exceeded, the MDA8 ozone concentration is shown in parts per billion (ppb). Blank cells indicate that there was no exceedance on that site/date combination.

Date	Paul Meyer	Walter Johnson	Green Valley	Jerome Mack	Joe Neal	Palo Verde	Jean	Indian Springs	Apex	Boulder City
6/19/2018	72	72	77	75						
6/20/2018	71	74			72					
6/23/2018	72	76	75	72	72	71	77	73		
6/27/2018	75	76	78	76	72	72	81	78	74	72
7/14/2018	72		78	78						
7/15/2018		71	73	73	78					
7/16/2018	75	79	71	73	80	75				
7/17/2018	74	77				74				
7/25/2018	71	72	72							
7/26/2018	72	75	77	77					71	
7/27/2018	72	74			76					
7/30/2018			73	72						
7/31/2018		73			73					
8/6/2018	79	77	74	71	76	72			74	
8/7/2018	73	74	72	71	74				71	

Table 1-3. Proposed Clark County 2020 exceptional events. For each site and date combination where the 2015 NAAQS standard was exceeded, the MDA8 ozone concentration is shown in ppb. Blank cells indicate that there was no exceedance on that site/date combination.

Date	Walter Johnson	Paul Meyer	Joe Neal	Jerome Mack	Green Valley	Boulder City	Jean	Indian Springs	Apex
5/6/2020	78	77	76	73	72		75		76
5/9/2020	71	74							
5/28/2020	71	76							
6/22/2020	73	74	78						
6/26/2020		73							
8/3/2020	82	78	81		72	72	73	71	
8/7/2020	71		72					72	
8/18/2020	82	79	78						
8/19/2020	74	74	73		71				
8/20/2020			71						
8/21/2020		71							
9/2/2020	75	73							
9/26/2020	71		75						

1.2 Exceptional Event Rule Summary

The "EPA Guidance on the Preparation of Exceptional Events Demonstration for Wildfire Events that May Influence Ozone Concentrations" (U.S. Environmental Protection Agency, 2016) describes a three-tier analysis approach to determine a "clear causal relationship" for EEs demonstrations from an air agency. A summary of analysis requirements for each tier is listed in Table 1-4 and in the list below.

- Tier 1 analyses can be used when ozone exceedances are clearly influenced by a wildfire in areas of typically low ozone concentrations, are associated with ozone concentrations higher than non-event-related values, or occur outside of an area's usual ozone season.
- Tier 2 analyses are appropriate when the impacts of the wildfire emissions on ozone levels are less clear and require more supportive documentation than Tier 1 analyses.
- If a more complicated relationship between the wildfire and the ozone exceedance is observed, Tier 3 analyses with additional supportive documentation—such as statistical modeling of the ozone event, vertical profile analysis of smoke in the column, and meteorological analysis—should be used.

In this work, we conduct all the recommended Tier 1, Tier 2, and Tier 3 analyses.

Table 1-4. Tier 1, 2, and 3 EE analysis requirements for evaluating wildfire impacts on ozone exceedances.

Tier	Requirements
1	• Comparison of fire-influenced exceedance with historical concentrations • Key factor: Evidence that fire and monitor meet one of the following criteria: – Seasonality differs from typical season, or – Ozone concentrations are 5-10 ppb higher than non-event-related concentrations • Evidence of transport of fire emissions to monitor: – Trajectories of fire emissions (reaching ground level) – Satellite images and supporting evidence from surface measurements – Media coverage and photographic evidence of smoke
2	• All Tier 1 requirements • Key Factor #1: Fire emissions and distance of fires • Key Factor #2: Comparison of the event-related ozone concentration, with non-event-related high ozone concentrations (high percentile rank over five years/seasons) – Annual and seasonal comparison • Evidence that fire emissions affected the monitor (at least one of the following): – Visibility impacts – Changes in supporting measurements – Satellite enhancements of fire-related species (i.e., NO_x, carbon dioxide (CO), aerosol optical depth (AOD), etc.) – Fire-related enhancement ratios and/or tracer species – Differences in spatial/temporal patterns
3	• All Tier 2 requirements • Evidence of fire emissions effects on monitor: – Multiple analyses from those listed for Tier 2 • Evidence of fire emissions transport to the monitor: – Trajectory or satellite plume analysis, and – Additional discussion of meteorological conditions • Additional evidence such as: – Comparison to ozone concentrations on matching (meteorologically similar) days – Statistical regression modeling – Photochemical modeling of smoke contributions to ozone concentrations

1.3 Demonstration Outline

As discussed in Section 1.2, the "clear causal relationship" analyses involve comparing the exceedance ozone concentrations to historical values, providing evidence that the event and monitors meet the tier's key factors, providing evidence of the transport of wildfire emissions to the

monitors, and additional analyses such as ground-level measurements and various forms of modeling, depending on the complexity of the event. Table 1-5 summarizes the key factors and additional supporting evidence of the tiered approach and shows the corresponding sections in this report for each analysis.

Table 1-5. Locations of Tier 1, 2, and 3 elements in this report.

Tier	Element	Section of this Report (Analysis Type)
Tier 1	Key Factor: seasonality differs from typical season and/or ozone concentrations are 5-10 ppb higher than non-event-related concentrations	Section 3.1.1 (comparison of event with historical data)
	Evidence of transport of fire emissions to monitor	Sections 3.1.2 (maps of ozone, particulate matter with a diameter less than 2.5 micrometers ($PM_{2.5}$), fire, smoke, visible satellite imagery), 3.1.3 (HYSPLIT trajectories)
	Media coverage and photographic evidence of smoke	Section 3.1.4 (Media coverage and Images)
Tier 2	Key Factor #1: fire emissions and distance of fires	Section 3.2.1 (analysis of the relationship between fire emissions and distance [Q/d])
	Key Factor #2: comparison of event concentrations with non-event-related high ozone concentrations	Section 3.2.2 (comparison of event concentrations with non-event concentrations)
	Evidence that the fire emissions affected the monitor	Sections 3.2.3 (visibility impacts, satellite NO_x (and other pollutant) enhancements), 3.2.4 (changes in supporting measurements, differences in spatial/temporal patterns, and tracer measurements)
Tier 3	Evidence of fire emissions transport to the monitor	Section 3.3.1 (trajectory or satellite plume analysis, additional discussion of meteorological conditions, comparison to ozone concentrations on matching [meteorologically similar] days)
	Meteorologically similar matching day analysis	Section 3.3.2 (methodology and analysis for meteorologically similar days)
	Additional evidence	Section 3.3.3 (statistical regression modeling)

Tier 1 analyses are shown in Section 3.1. The key factor of Tier 1 analyses is the ozone concentration's uniqueness when compared to the typical seasonality and/or levels of ozone exceedance. The EPA guidance suggests providing a time series plot of 12 months of ozone concentrations overlaying more than five years of monitored data and describing how typical seasonality differs from ozone in the demonstration (U.S. Environmental Protection Agency, 2016). In addition, trajectory analysis produced by the Hybrid Single-Particle Lagrangian Integrated Trajectory (HYSPLIT) model, together with satellite plume imagery and ground-level measurements of plume components (e.g., $PM_{2.5}$, CO, or organic and elemental carbon) should be used to provide evidence of wildfire emissions being transported to the monitoring sites. We demonstrate the Tier 1 analysis results for the September 26, 2020, event in Section 3.1. We address the key factors in Section 3.1.1, provide evidence of wildfire smoke transport to the Clark County monitoring sites in Sections 3.1.2 and 3.1.3, and discuss the media coverage and show ground images in Section 3.1.4.

Tier 2 analyses are shown in Section 3.2. The two key factors for Tier 2 analyses are (1) fire emissions and distance of fires to the impacted monitoring sites and (2) comparison of event-related ozone concentrations with non-event-related high ozone values. We address the first factor in Section 3.2.1 by determining the emissions divided by distance (Q/d) relationship, and address the second factor in Section 3.2.2 by comparing the 5- and 6-year percentiles and yearly rank-order analysis of ozone concentrations. The Tier 2 analyses also require evidence of wildfire smoke transport to affected monitoring sites; we provide this evidence in Section 3.2.3 through satellite measurements of pollutant concentrations. In Section 3.2.4, we discuss supporting pollutant trends and diurnal patterns of $PM_{2.5}$, CO, NO_x, and total non-methane organic carbon (TNMOC) compared with ozone concentrations and wildfire tracer measurements.

Tier 3 analyses are shown in Section 3.3. We investigated total column information and event-related meteorological conditions (Section 3.3.1), analyzed meteorologically similar days to find typical ozone concentrations for the exceptional event's specific meteorological conditions (Section 3.3.2), and developed a GAM to estimate the wildfire's contribution to ozone concentrations (Section 3.3.3).

Following the EPA's EE guidance, we performed Tier 1, Tier 2, and Tier 3 analyses to show the "clear causal relationship" between the wildfires throughout California and the exceedance event in Clark County on September 26, 2020. Focusing on the characterization of the meteorology, smoke, transport, and air quality on the days leading up to the event, we conducted the following specific analyses (results of which are presented in Section 3):

- Developed time series plots that show the September 26 ozone concentrations at each affected site in historical context for 2020 and for the past five years
- Compiled maps of (1) ozone and $PM_{2.5}$ concentrations in the area, (2) smoke plumes, and (3) fire locations from satellite data
- Showed the transport patterns via HYSPLIT modeling and identified where the back trajectory air mass intersected with smoke plumes or passed over or near fires
- Discussed media coverage of the September 26 event and showed ground images

- Quantified total fire emissions and calculated emissions/distance ratio (Q/d) for the fire
- Performed statistical analysis to compare event ozone concentrations to non-event concentrations
- Provided maps showing satellite retrievals of NO_x, AOD, and CO
- Developed plots to show diurnal patterns of ozone and supporting pollutants such as $PM_{2.5}$, CO, NO_x, and TNMOC
- Examined concentrations of levoglucosan, a wildfire tracer species, during the event compared to background concentrations
- Assessed vertical transport of smoke using satellite-observed aerosol vertical profiles and ceilometer mixing height retrievals
- Performed meteorologically similar matching ozone day analysis to assess typical concentrations of ozone given meteorological parameters
- Created a GAM model of MDA8 ozone concentrations to assess the enhancement of ozone concentrations due to wildfire influence

1.4 Conceptual Model

The conceptual model for the exceptional event that led to the ozone exceedances at the Walter Johnson and Joe Neal monitoring sites on September 26, 2020, is outlined in Table 1-5. Table 1-5 provides the analysis techniques performed and evidence for each tier. This establishes a weight of evidence for the clear causal relationship between the wildfire emissions in central and southern California and the September 26 exceptional ozone event. We assert that wildfire emissions from fires in central and southern California on September 24 to 26 led to enhanced ozone concentrations in Clark County on September 26 and the MDA8 ozone exceedances at the Walter Johnson and Joe Neal sites. In support of this assertion, the key points of evidence for the conceptual model are summarized below.

1. The September 26 ozone exceedance occurred during a typical ozone season, but event concentrations at the Walter Johnson and Joe Neal exceedance sites were significantly higher than non-event concentrations. Ozone concentrations at both exceedance sites showed a high percentile rank when compared with the past six years and ozone seasons.
2. HMS smoke and fire detections, CALIPSO aerosol vertical profiles, visible satellite imagery, and aerosol optical depth observations show a consistent picture of wildfire emission plumes from central-eastern and southern California (SQF Lightning Complex, Blue Jay Fire, Wolf Fire, Creek Fire, Bobcat Fire, and El Dorado Fire) burning on September 24 through 26 that were transported eastward into Clark County on September 25 and 26.

3. Back and forward trajectories from the near-surface boundary layer at the exceedance sites at the time of maximum ozone concentration show consistent transport patterns passing over the HMS smoke plumes and regions of enhanced aerosol optical depth and CALIPSO smoke aerosol originating from the eastern and southern California fires. The combination of trajectories intersecting the fire location and/or the associated smoke plumes and a deep mixed layer over Clark County favoring vertical mixing demonstrate that wildfire emissions were transported to the surface in Clark County on September 25 and 26.
4. Meteorological conditions on September 26 did not favor enhanced local ozone production when compared with meteorologically similar ozone season days. Average MDA8 ozone across similar days was well below the ozone NAAQS and 6 and 9 ppb lower than the September 26 ozone exceedances at each exceedance site, respectively.
5. GAM model predictions of MDA8 ozone on September 26 are all below the 70-ppb ozone NAAQS at both EE-affected site.
6. Abnormal, coincident surface $PM_{2.5}$, CO, and NO_x concentration enhancements midday on the exceedance event day and the day prior, along with typical PM_{10}:$PM_{2.5}$ ratios all indicate the presence ozone precursors from wildfire emissions at the surface in Clark County coincident with the wildfire plume arrival on September 25. Additionally, levoglucosan (a wildfire tracer) concentrations were enhanced above typical ozone season levels immediately following the September 26 event.

2. Historical and Non-Event Model

2.1 Regional Description

Clark County is located in the southern portion of Nevada and borders California and Arizona. Clark County includes the City of Las Vegas, one of the fastest growing metropolitan areas in the United States with a population of approximately 2 million (U.S. Census Bureau, 2010). Las Vegas is located in a 1,600 km^2 desert valley basin at 500 to 900 m above sea level (Langford et al., 2015). It is surrounded by the Spring Mountains to the west (3,000 m elevation) and the Sheep Mountain Range to the north (2,500 m elevation). Three mountain ranges comprise the southern end of the valley. The valley floor slopes downward from west to east, which influences surface wind, temperature, precipitation, and runoff patterns. The Cajon Pass and I-15 corridor to the east is an important atmospheric transport pathway from the Los Angeles Basin into the Las Vegas Valley (Langford et al., 2015). **Figures 2-1 and 2-2** show the topography of Clark County and surrounding areas.

The Las Vegas Valley climatology features abundant sunshine and hot summertime temperatures (average summer month high temperatures of 34-40°C). Because of the mountain barriers to moisture inflow, the region experiences dry conditions year-round (~107 mm annual precipitation, 22% of which occurs during the summer monsoon season in July through September). The urban heat island effect in Las Vegas during summer causes large temperature gradients within the valley, with generally cooler temperatures on the eastern side. During the summer season, monsoon moisture brings high humidity and thunderstorms to the region, typically in July and August (National Weather Service Forecast Office, 2020). Winds in the Las Vegas basin tend to come from the southwest during spring and summer (Los Angeles is upwind), and from the northwest in the fall and winter, with air transported between the neighboring mountain ranges and along the valley.

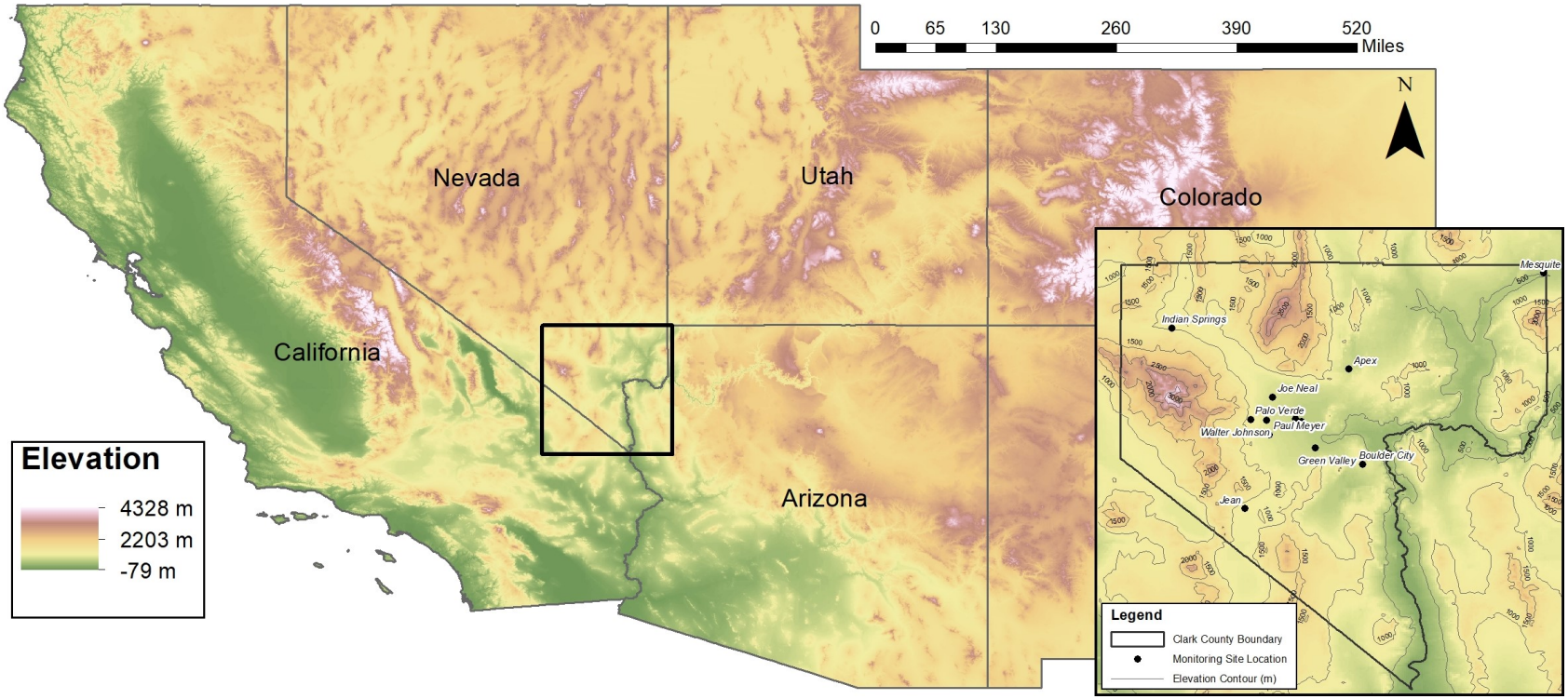

Figure 2-1. Regional topography around Clark County, with an inset showing county boundaries and the air quality monitoring sites analyzed in this report.

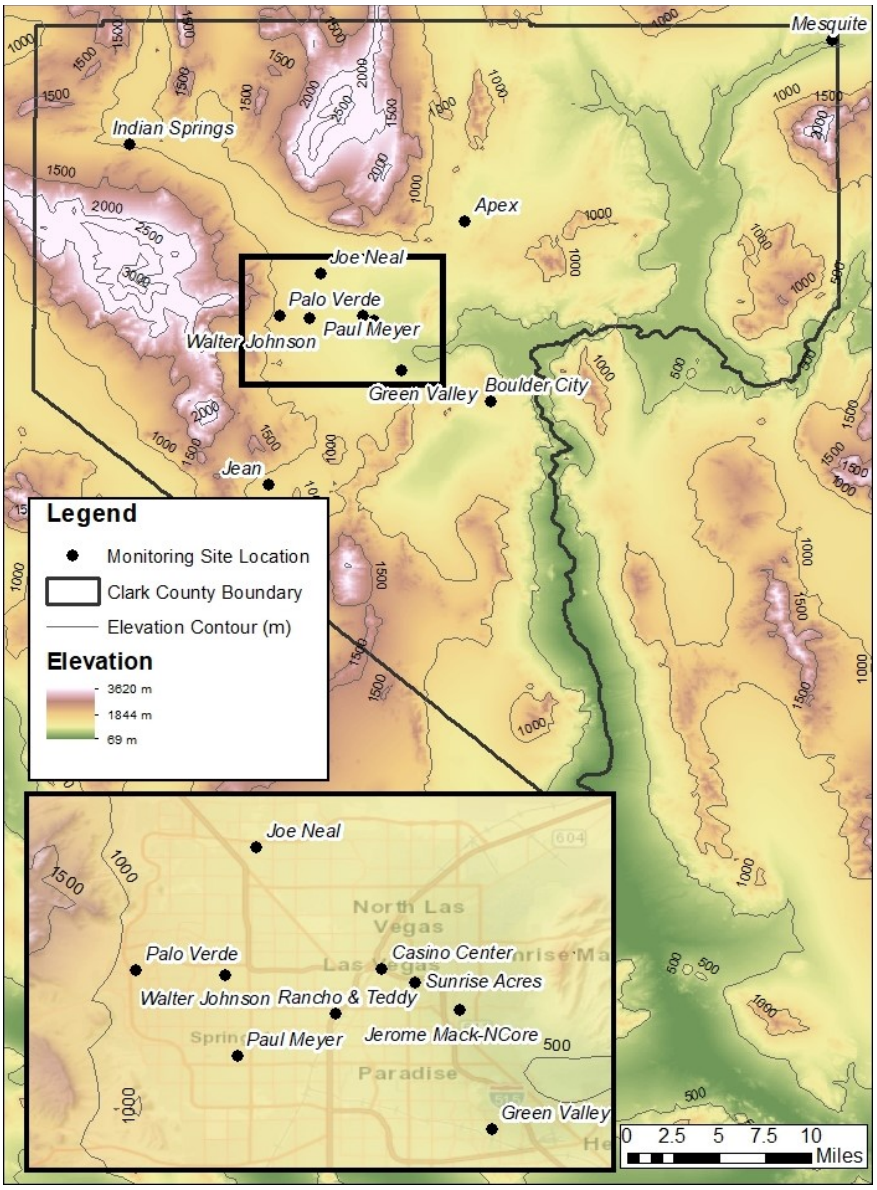

Figure 2-2. Clark County topography, with an inset showing air quality monitoring sites that measure ozone in the Clark County area.

2.2 Overview of Monitoring Network

The Clark County Department of Environment and Sustainability, Division of Air Quality (DAQ) operated 14 ambient air monitoring sites in the region during 2020 (Figure 2-2). These sites measure hourly ozone (O_3), $PM_{2.5}$, particulate matter with a diameter less than 10 micrometers (PM_{10}), nitrogen oxides (NO_x), TNMOC, and carbon monoxide (CO) concentrations along with meteorological parameters. Table 2-1 presents the monitoring data coverage across time and space for criteria pollutants and surface meteorological parameters (barometric pressure, temperature, wind speed

and direction), as well as mixing height. We examined ozone and other criteria pollutants at 11 sites around Clark County to investigate the high ozone event on September 26, 2020. DAQ's ambient air monitoring network meets the monitoring requirements for criteria pollutants pursuant to Title 40, Part 58, of the Code of Federal Regulations (CFR), Appendix D (U.S. Environmental Protection Agency, 2008). Data are quality-assured in accordance with 40 CFR 58 and submitted to the EPA's Air Quality System (AQS). The spatial distribution of monitoring sites characterizes the regional air quality in Las Vegas, as well as air quality upwind and downwind of the urban valley region (Figure 2-2). The Jean monitoring site along the I-15 corridor is generally upwind such that it captures atmospheric transport into the region and is least impacted by local sources (Figure 2-2).

Table 2-1. Clark County monitoring site data. The available date ranges of all parameters and monitoring sites used in this report for Clark County, Nevada, are shown. Casino Center and RT are near-road sites that are not used for the exceptional event analysis.

Site	AQS Sitecode	O_3	$PM_{2.5}$	CO	NO	NO_2	TNMOC	Temp.	Wind Speed	Wind Direction	Barom. Pressure	Mixing Height
Apex	320030022	2014-2020						2014-2020	2014-2020	2014-2020		
Boulder City	320030601	2014-2020									2014-2016	
Green Valley	320030298	2015-2020	2014-2020	2020				2016-2020	2014-2020	2014-2020	2014-2016	
Indian Springs	320037772	2014-2020										
Jean	320031019	2014-2020	2014-2020					2014-2020	2014-2020	2014-2020	2014-2016	
Jerome Mack	320030540	2014-2020	2014-2020	2015-2020[1,2]	2015-2020	2015-2020	2020	2014-2020	2014-2020	2014-2020	2014-2020	2020
Joe Neal	320030075	2020	2018-2020	2019-2020		2015-2020		2014-2020	2014-2020	2014-2020	2014-2016	
Mesquite	320030023	2014-2020						2014-2020	2014-2020	2014-2020		
Palo Verde	320030073	2014-2020	2020					2014-2020	2014-2020	2014-2020	2014-2016	
Paul Meyer	320030043	2014-2020	2017-2020					2014-2020	2014-2020	2014-2020	2014-2016	
Walter Johnson	320030071	2014-2020	2020					2015-2020	2015-2020	2015-2020	2014-2016	

[1] CO data invalid at Jerome Mack on Sep. 2, 2020

[2] CO data invalid at Jerome Mack Apr. 28, 2020 – May 20, 2020

2.3 Characteristics of Non-Event Historical Ozone Formation

During the ozone season (April–September) in Clark County, ozone concentrations are typically influenced by local formation, transport into the region, and, on occasion, by EEs such as wildfires and stratospheric intrusions. Transport from upwind source regions (e.g., Los Angeles Basin, Mojave Desert, Asia) occurs with southwesterly winds, and southerly transport dominates later in the season due to the summer monsoon (Langford et al., 2015; Zhang et al., 2020). Local precursor emissions in Clark County include mobile NO_x and VOC sources, natural-gas fueled power generation NO_x sources, and biogenic VOC emissions. Based on 2017 Las Vegas emission inventories, there are 98 tons of NO_x emissions per day and 238 tons of VOC emissions per day on a typical ozone season weekday (Clark County Department of Environment and Sustainability, 2020) . On-road mobile sources comprise 40% of NO_x emissions, and total mobile emissions comprise 88% of total NO_x emissions during the ozone season. In contrast, 52% of VOC emissions originate from biogenic sources within Clark County. Local emissions and/or precursors transported into the region contribute to ozone formation within Clark County (Langford et al., 2015; Clark County Department of Air Quality, 2019).

In this demonstration, we discuss the impacts of wildfire smoke on ozone concentrations in Clark County on September 26, 2020. In order to fully discern these effects, we examine the historical ozone record for all affected sites (Table 1-1). *Non-event days* refer to all days other than the September 26 event. Because percentile rankings are sensitive to including the relatively large number of potential EE days during 2018 and 2020, we also provide statistics *excluding potential EE days* (i.e., without including the 2018 and 2020 potential EE days as defined in Tables 1-2 and 1-3 in Section 1). The 8-hour ozone design value (DV) is the three-year running average of the fourth-highest daily maximum 8-hour (MDA8) ozone concentration (U.S. Environmental Protection Agency, 2015). Within Clark County, Las Vegas is classified as an EPA Region 9 marginal nonattainment region with a 73 ppb ozone DV for 2017-2019 (U.S. Environmental Protection Agency, 2020).

We identified ozone EE days as days with significant wildfire or stratospheric intrusion influence in addition to an MDA8 concentration greater than 70 ppb. By this criterion, we identified 15 possible EE days in 2018, 13 possible EE days in 2020, and no EE days in 2019.

The September 26, 2020, EE occurred late in the ozone season under hot, dry air, with upper-level high pressure and surface low-pressure meteorological conditions favoring subsidence and vertical mixing of wildfire smoke-influenced ozone and precursors to ground level (see Section 3.3.1-2). Compared with a non-event conceptual model of local precursor emissions contributing to ozone formation at ground level under similar conditions, the September 26 conditions indicate additional transport of wildfire-influenced air parcels via weak westerly and northwesterly winds aloft.

Figures 2-3 through 2-6 depict the six-year historical record and seasonality of MDA8 ozone concentrations at each monitoring site, along with the 99th percentile and NAAQS standard ozone concentrations. September 26 ranks in the top 1% for daily maximum ozone concentration at the Joe Neal site. Figure 2-7 depicts a time series diurnal cycle of 1-hour ozone concentrations beginning one week before the September 26 event and ending at the end of September. Daily maximum 1-hour ozone concentrations were the highest during this period at two of the 11 monitoring sites shown, including one of the EE-affected sites (Joe Neal).

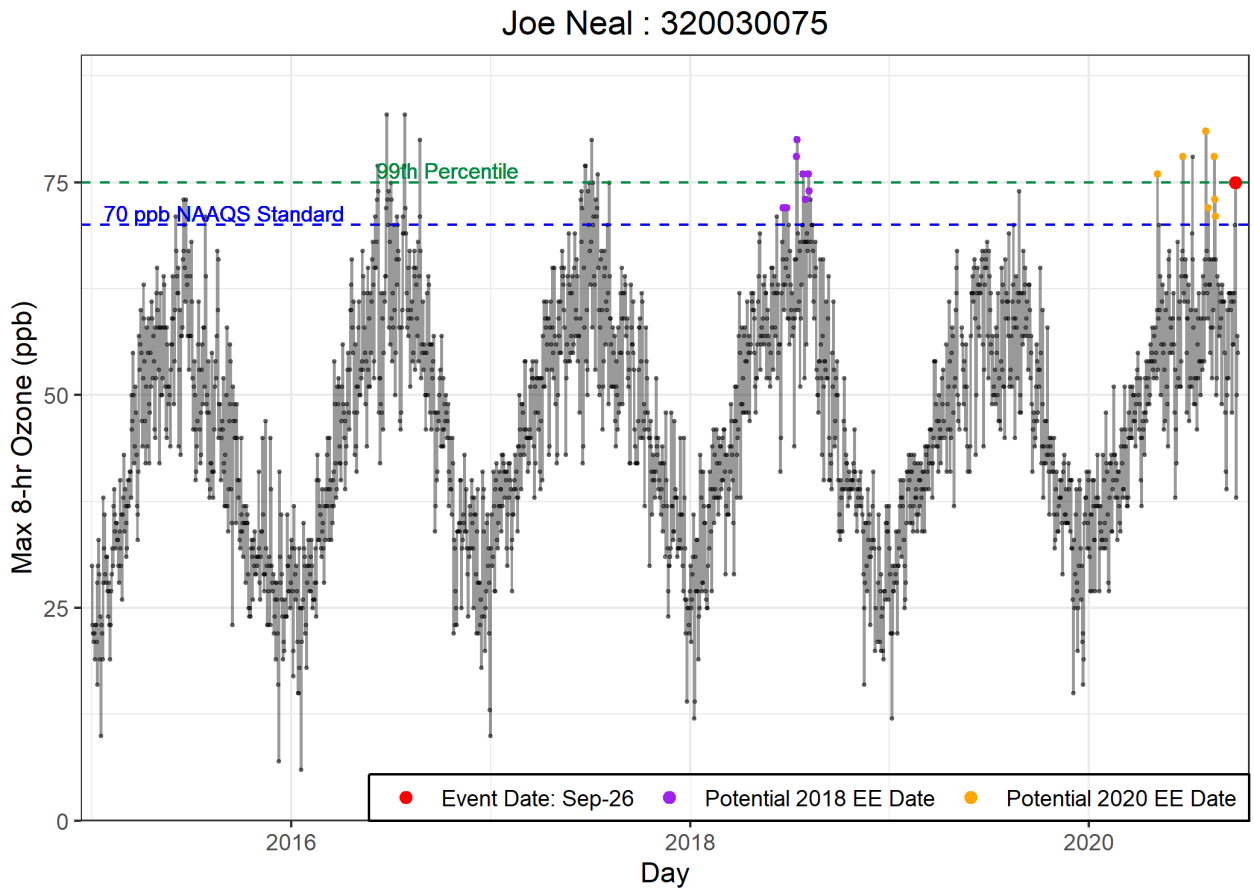

Figure 2-3. Time series of 2015-2020 ozone concentrations at Joe Neal.

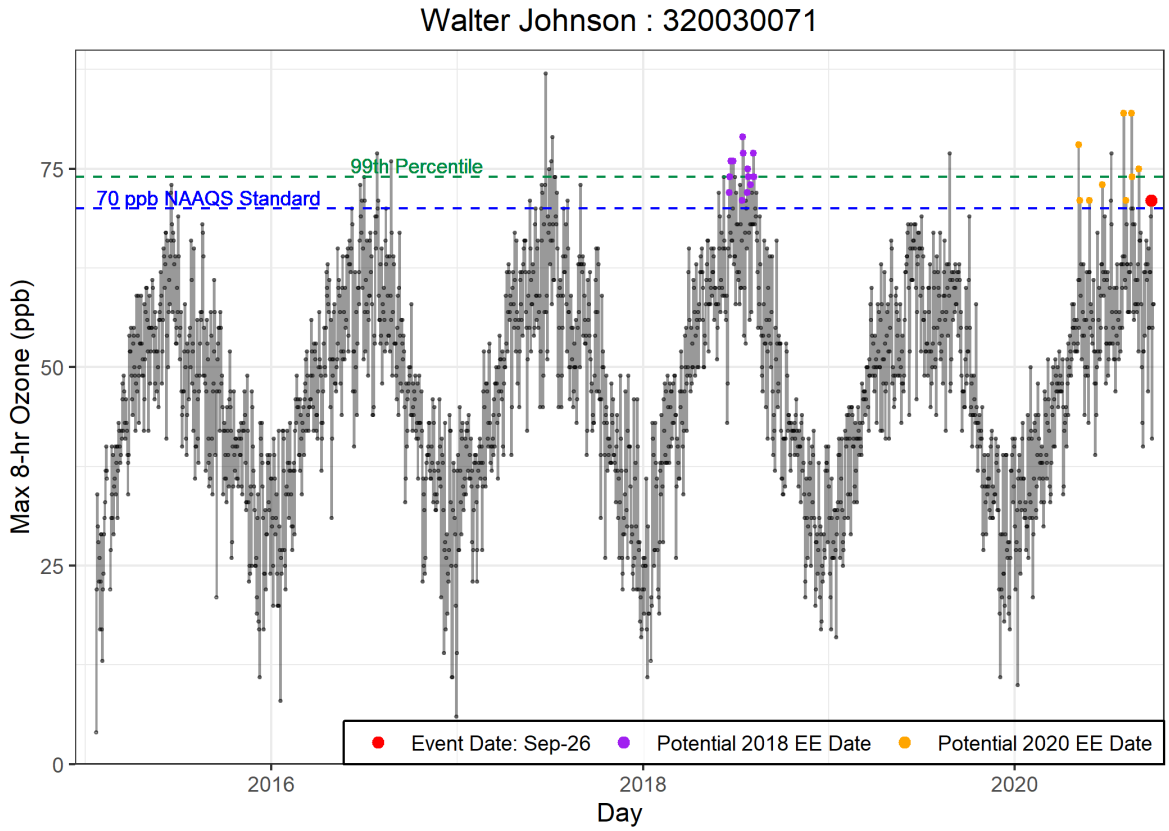

Figure 2-4. Time series of 2015-2020 ozone concentrations at Walter Johnson.

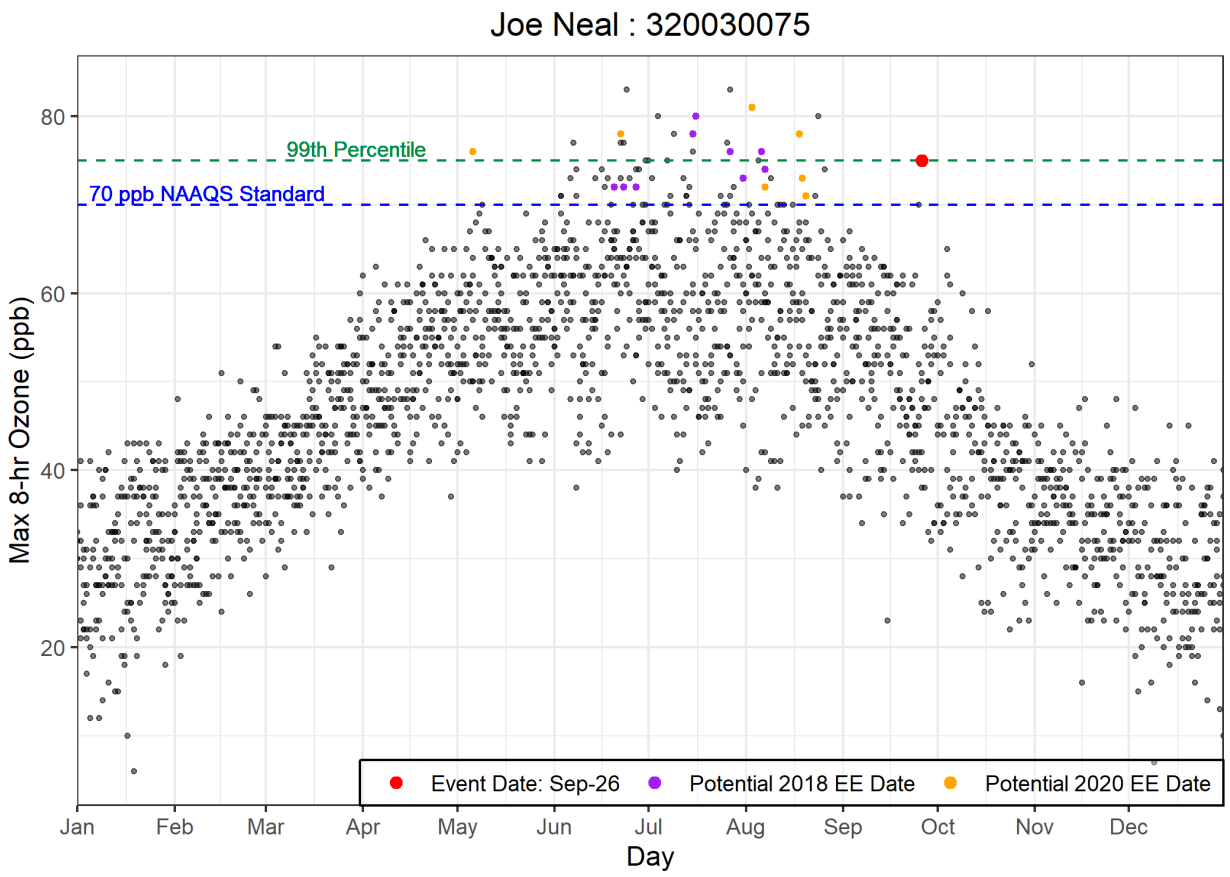

Figure 2-5. Seasonality of 2015-2020 ozone concentrations from Joe Neal.

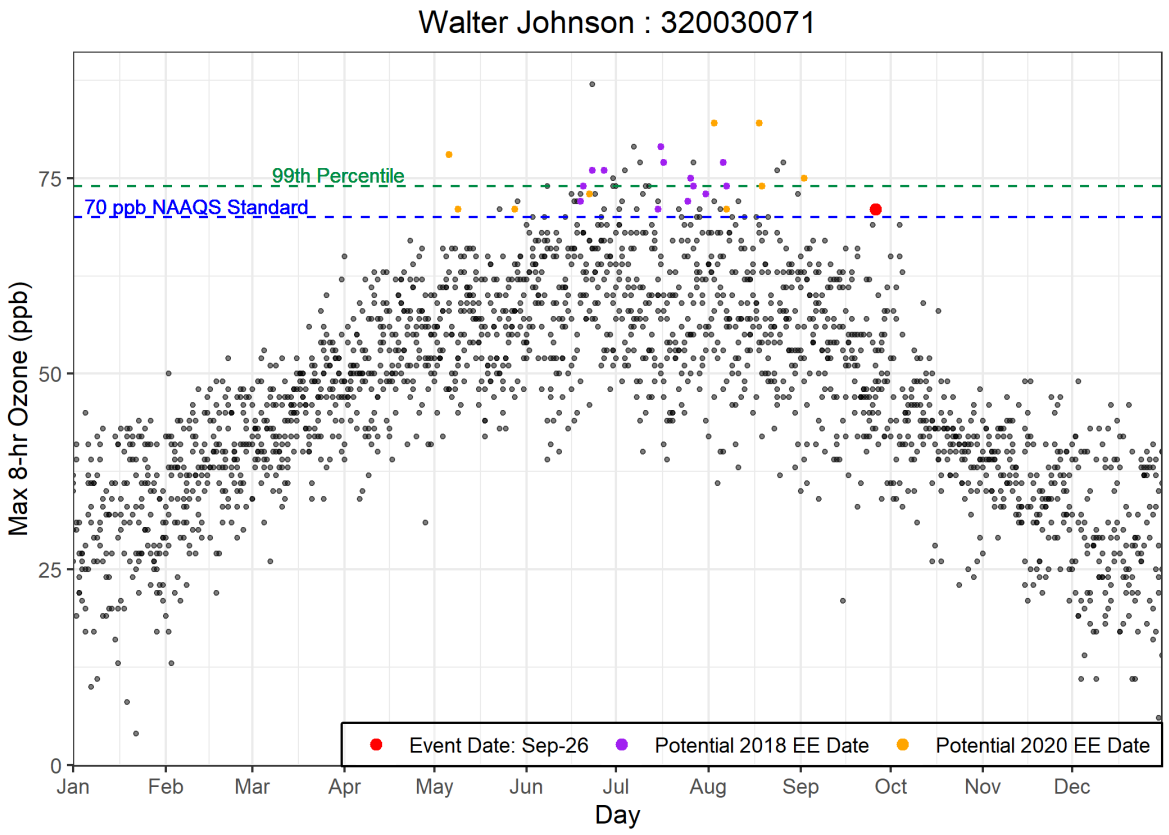

Figure 2-6. Seasonality of 2015-2020 ozone concentrations from Walter Johnson.

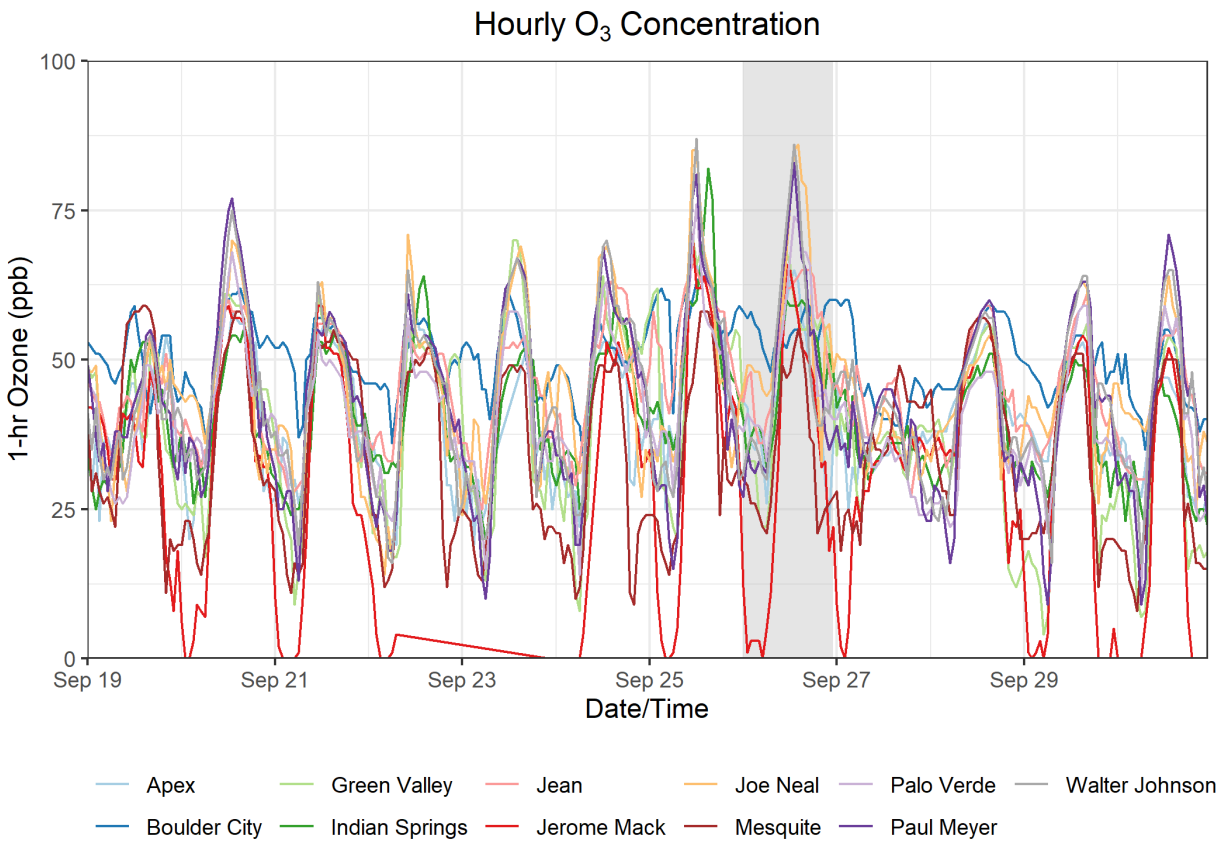

Figure 2-7. Ozone time series at all monitoring sites. Time series of hourly ozone concentrations at monitoring sites in Clark County for one week before September 26 event until September 30 are shown. September 26, 2020, is shaded for reference.

3. Clear Causal Relationship Analyses

3.1 Tier 1 Analyses

3.1.1 Comparison of Event with Historical Data

To address the Tier 1 EE criterion of comparison with historical ozone, we compared the September 26 EE ozone concentrations at each site with the 2020 ozone record, focusing mainly on the ozone season when the highest ozone concentrations occur. **Figures 3-1 and 3-2** depict the 2020 daily maximum ozone record at each monitoring site, along with the 99th percentile of previous 5-year MDA8 ozone and NAAQS criteria ozone concentrations. September 26 ranks in the top 1% for daily maximum ozone concentration during 2020 at the Joe Neal monitoring site. When compared with daily ozone rankings on September 26 over the six-year ozone record (Figures 2-5 and 2-6), the 2020 ozone concentration ranks as the highest, indicating that September 26, 2020, was an extreme event.

The September 26, 2020, ozone exceedance occurred during a typical ozone season, but MDA8 ozone concentrations on this day were the second highest compared with daily ozone concentrations excluding potential EE days (Figures 3-1 and 3-2). The MDA8 ozone concentration on September 26 was >10 ppb above the mean or median ozone concentrations for the historical ozone season non-event days at all EE-affected sites (**Table 3-1**). However, the MDA8 ozone concentrations at EE affected sites were < 5 ppb above the 95th percentile of ozone during historical ozone season non-event days (Table 3-1). Because September 26 is during the normal ozone season, and MDA8 ozone concentrations at EE affected sites could not be clearly distinguished from the 95th percentile ozone concentration during the non-event historical ozone season, the September 26, 2020, event does not satisfy the key factor for a Tier 1 EE. Tier 2 comparison of the event-related ozone concentrations with non-event-related high ozone concentrations (>99th percentile over five years or top four highest daily ozone measurements) are described in Section 3.2.2.

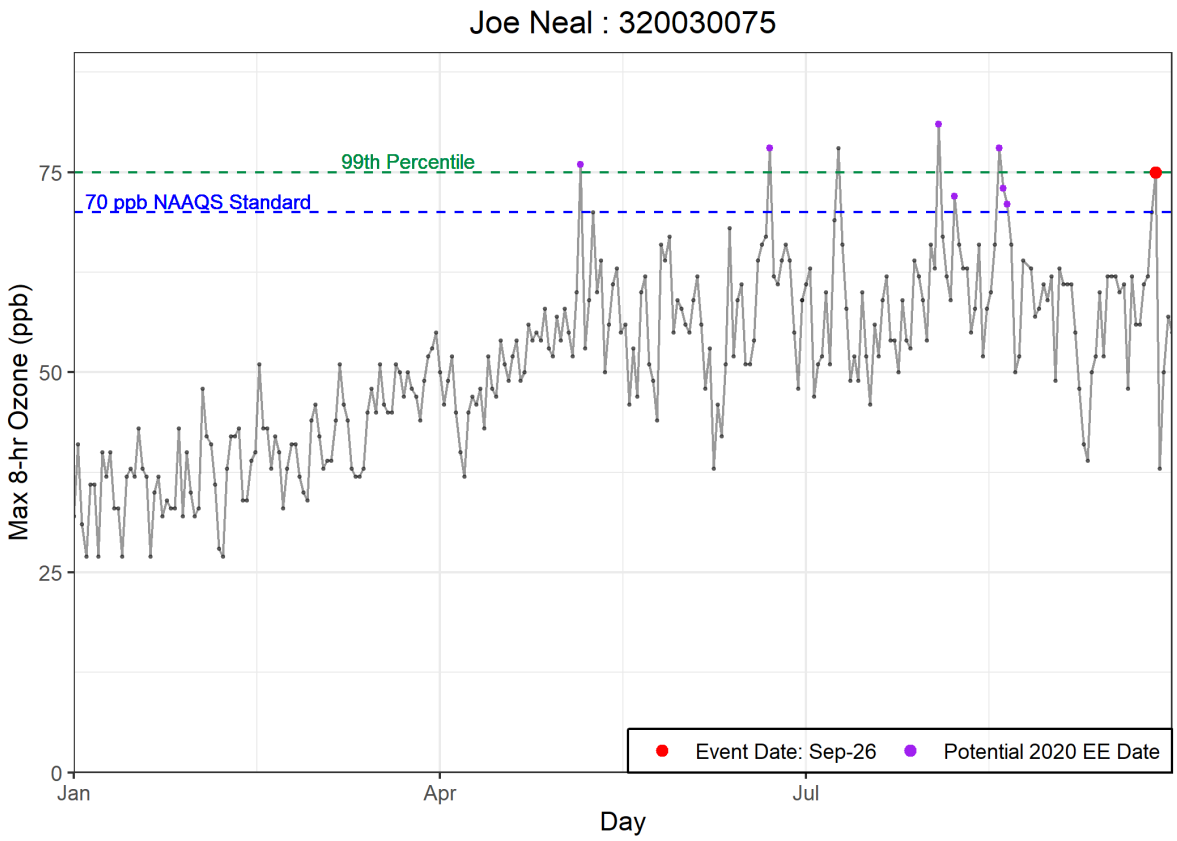

Figure 3-1. Time series of 2020 MDA8 ozone concentrations from Joe Neal.

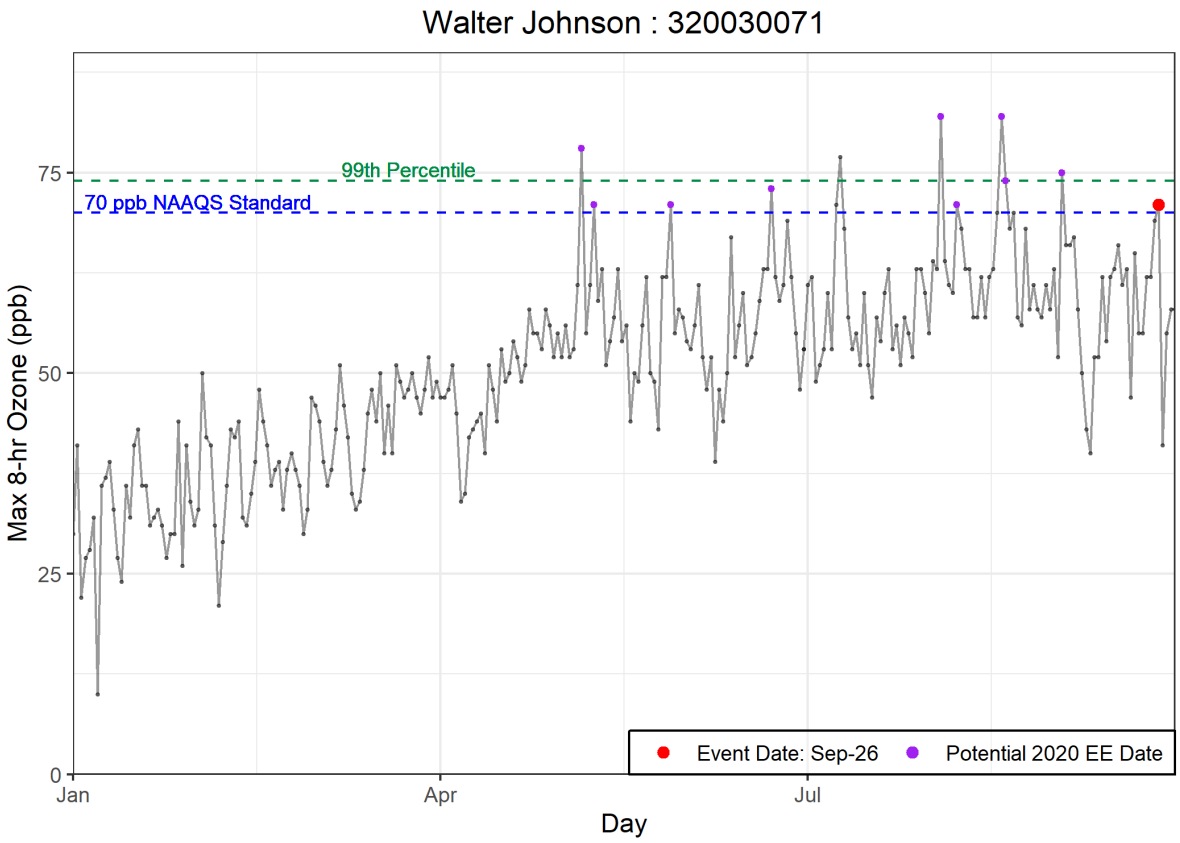

Figure 3-2. Time series of 2020 MDA8 ozone concentrations from Walter Johnson.

Table 3-1. Ozone season non-event comparison. September 26, 2020, MDA8 ozone concentrations for each affected site are shown in the top row. Five-year (2015-2019) average MDA8 ozone statistics for May through September ozone season are shown for each affected site around Clark County to compare with the event ozone concentrations.

	Joe Neal 320030075	Walter Johnson 320030071
Sep. 26	75	71
Mean	57	57
Median	57	57
Mode	62	57
St. Dev	9	9
Minimum	23	21
95 %ile	72	71
99 %ile	78	77
Maximum	83	87
Range	60	66
Count	912	917

3.1.2 Ozone, Fire, and Smoke Maps

Ozone and $PM_{2.5}$ Maps

We produced maps of ozone Air Quality Index (AQI), $PM_{2.5}$ AQI, active fire and smoke detections from satellites, and visible satellite imagery that show the transport of smoke to Las Vegas from California on September 26, 2020. These maps also show that high ozone concentrations occurred across multiple states corresponding with the presence of wildfire smoke.

From September 23 through September 26, 2020, moderate and unhealthy ground-level ozone concentrations (indicated by the yellow, orange, and red areas) were detected in the western United States (**Figure 3-3**), especially in California, Arizona, and Nevada. On September 23, high ozone concentrations (i.e., the orange and red areas) are seen in southern California, with areas of elevated ozone existing across California and southern Nevada. In the following two days, the concentrated ozone from central and southern California expanded northeastward, reaching Utah and Arizona on September 25. On September 26, elevated ozone concentrations were observed in southern California and Las Vegas, Nevada.

The spatial patterns observed in AQI plots for $PM_{2.5}$ (**Figure 3-4**) show extremely high $PM_{2.5}$ levels centered in eastern California and western Nevada, northwest of Clark County, Nevada, that persists from September 23 to 26. According to EPA guidance (U.S. Environmental Protection Agency, 2016), "if plume arrival at a given location coincides with elevation of wildfire plume components (such as $PM_{2.5}$, CO, or organic and elemental carbon), those two pieces of evidence combined can show that smoke was transported from the event location to the monitor with the enhanced ozone concentration." In Sections 3.1.2 through 3.2.4 of this report, we show that the enhanced ozone and $PM_{2.5}$ concentrations is observed in the western United States—including Clark County, Nevada—on September 26, 2020, corresponded with the arrival of a smoke plume from California fires including the SQF Lightning Complex, Blue Jay/Wolf Fires, Creek Fire, Bobcat Fire, and El Dorado Fire.

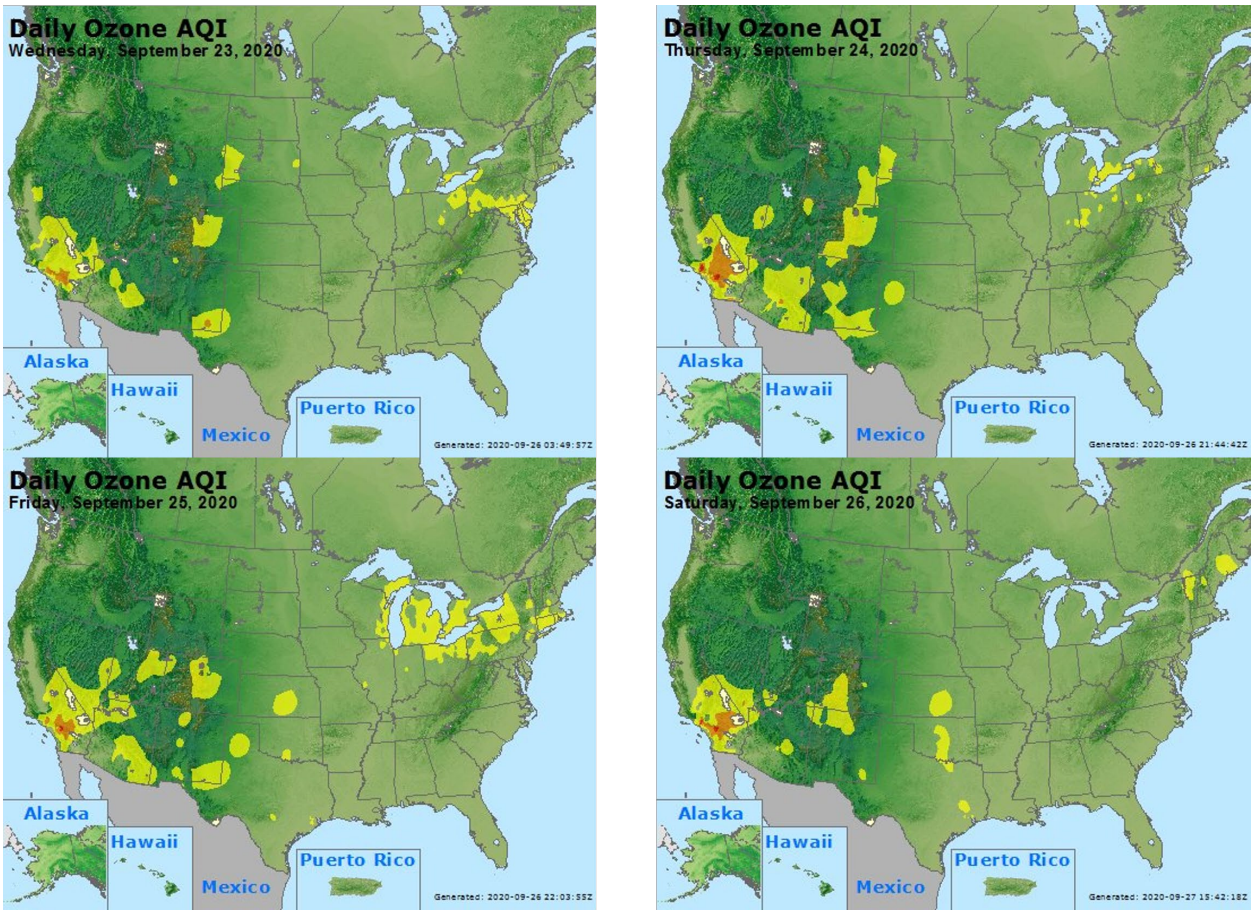

Figure 3-3. Daily ozone AQI for the three days before the September 26 event and the day of the event.

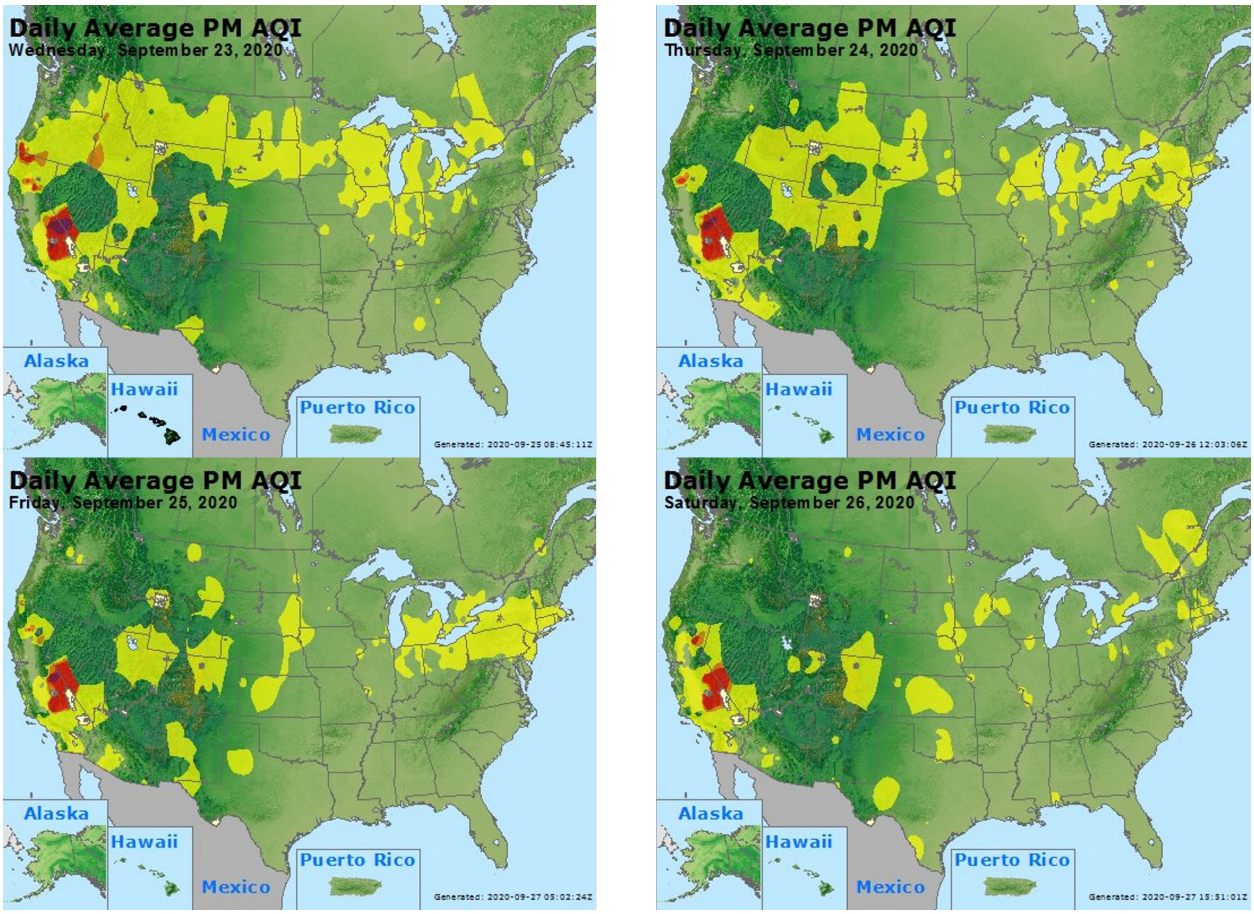

Figure 3-4. Daily $PM_{2.5}$ AQI for the three days before the September 26 event and the day of the event.

HMS Fire Detection Maps

According to EPA's guidance for Tier 1 analysis requirements (U.S. Environmental Protection Agency, 2016), the National Oceanic and Atmospheric Administration (NOAA) Hazard Mapping System (HMS) Fire and Smoke Product can be used to demonstrate the transport of fire emissions to the impacted monitors. The HMS Fire and Smoke Product consists of

1. A daily fire detection product derived from three satellite data products[1] to spatially and temporally map fire locations at 1 km grid resolution, and
2. A daily smoke product derived from visible satellite imagery[2] that consists of polygons showing regions impacted by smoke.

The HMS smoke plume data are based on measurements from several environmental satellites and reviewed by trained NOAA analysts to identify cases where smoke is dispersed by transport. One can download real-time HMS fire detection and smoke products and a six-month archive of the products from the NOAA Satellite and Information Service website (ospo.noaa.gov/Products/land/hms.html).

Figure 3-5 shows HMS smoke and fire detections over the western United States for September 23 to September 26, 2020. As the daily plots indicate, there was concentrated fire activity across California. Nevada was covered in a concentrated smoke plume from the California fires during those days, including the day of the event, even though no fire was observed in Nevada. This is consistent with the increased ozone and $PM_{2.5}$ concentrations observed in the western United States, as shown above in the AQI plots (Figures 3-3 and 3-4).

The HMS smoke plume data for the days leading up to September 26 were obtained and combined with HYSPLIT back trajectories on high ozone concentration days to identify intersections and assess potential smoke impacts (Section 3.1.3). The following sections provide further evidence of smoke transport, based on HYSPLIT trajectories and satellite data, from the California fires (including the SQF Lightning Complex, Blue Jay/Wolf Fires, Creek Fire, Bobcat Fire, and El Dorado Fire) to Clark County.

[1] The HMS fire detection product is developed using data from the Moderate Resolution Imaging Spectroradiometer (MODIS), Geostationary Operational Environmental Satellite system (GOES), Advanced Very High Resolution Radiometer (AVHRR), and Visible Infrared Imaging Radiometer Suite (VIIRS) satellite instruments.
[2] The HMS smoke product is derived from GOES-EAST and GOES-WEST visible satellite imagery.

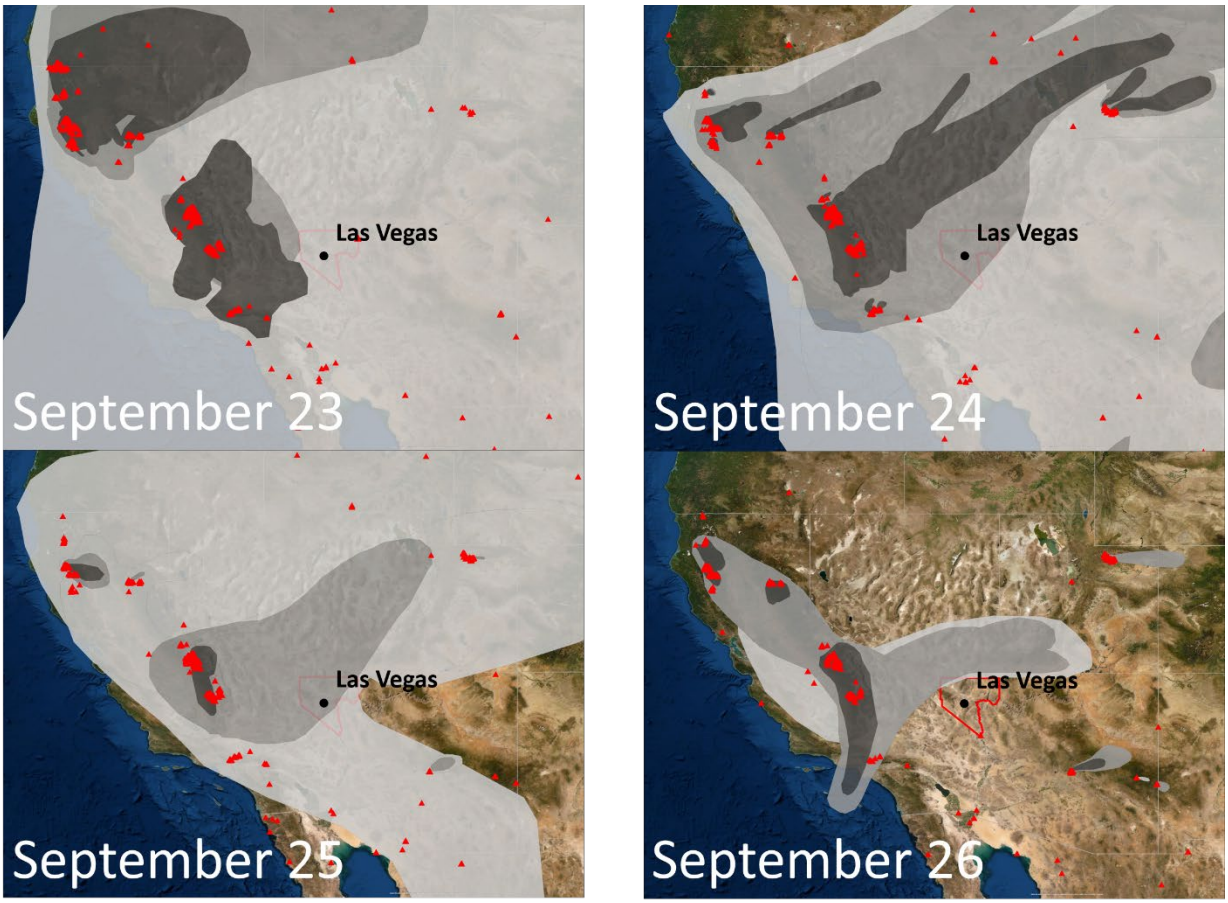

Figure 3-5. Daily HMS smoke over the United States for three days before the September 26 event and the day of the event. Fire detections are shown as red triangles, and smoke is shown in gray.

Visible Satellite Imagery

Visible satellite imagery from the MODIS Aqua and Terra satellites show transport of smoke from the California fires to the western United States, including Nevada, between September 24 and September 26 (**Figures 3-6 through 3-8**). This is consistent with the evidence of smoke over Las Vegas demonstrated by the HMS maps above. A dense smoke plume from fires across California (including the SQF Lightning Complex, Blue Jay/Wolf Fires, Creek Fire, Bobcat Fire, and El Dorado Fire to Clark County) can be observed during the entire 3-day period, travelling northeastward over Nevada; Las Vegas remained in the path of that smoke plume throughout the 3-day period. The movement of this smoke corresponds to the increase in high ozone and $PM_{2.5}$ concentrations in Las Vegas, as shown in the AQI maps above. In addition, the transport of smoke northeastward from California is consistent with transport patterns observed in the HYSPLIT trajectory analysis presented in Section 3.1.3, as well as the satellite and ground-based measurements of smoke-associated species presented in Sections 3.2.3 and 3.2.4.

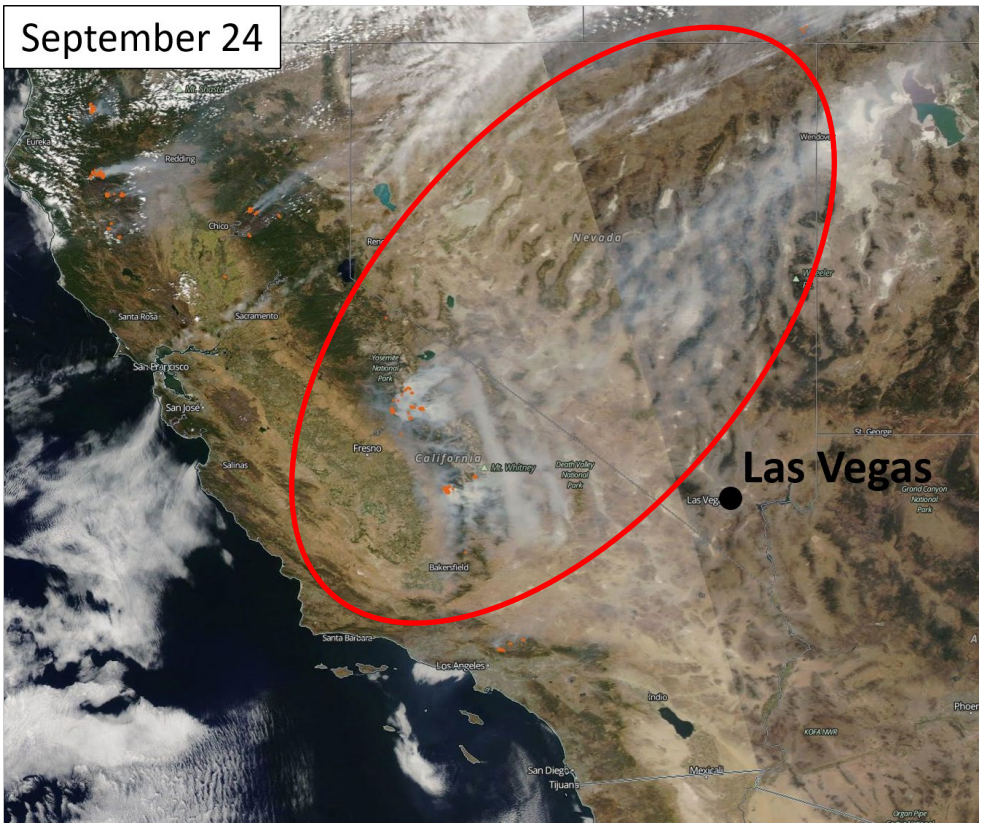

Figure 3-6. Visible satellite imagery from over California and Nevada on September 24, 2020. Source: NASA Worldview.

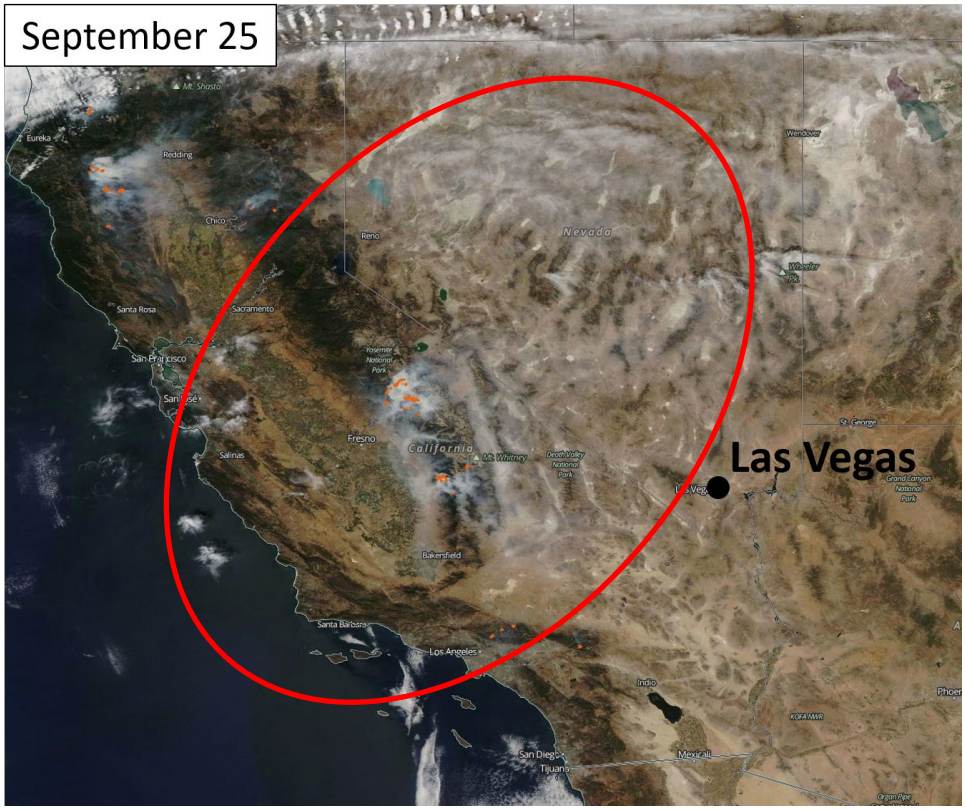

Figure 3-7. Visible satellite imagery from over California and Nevada on September 25, 2020. Source: NASA Worldview.

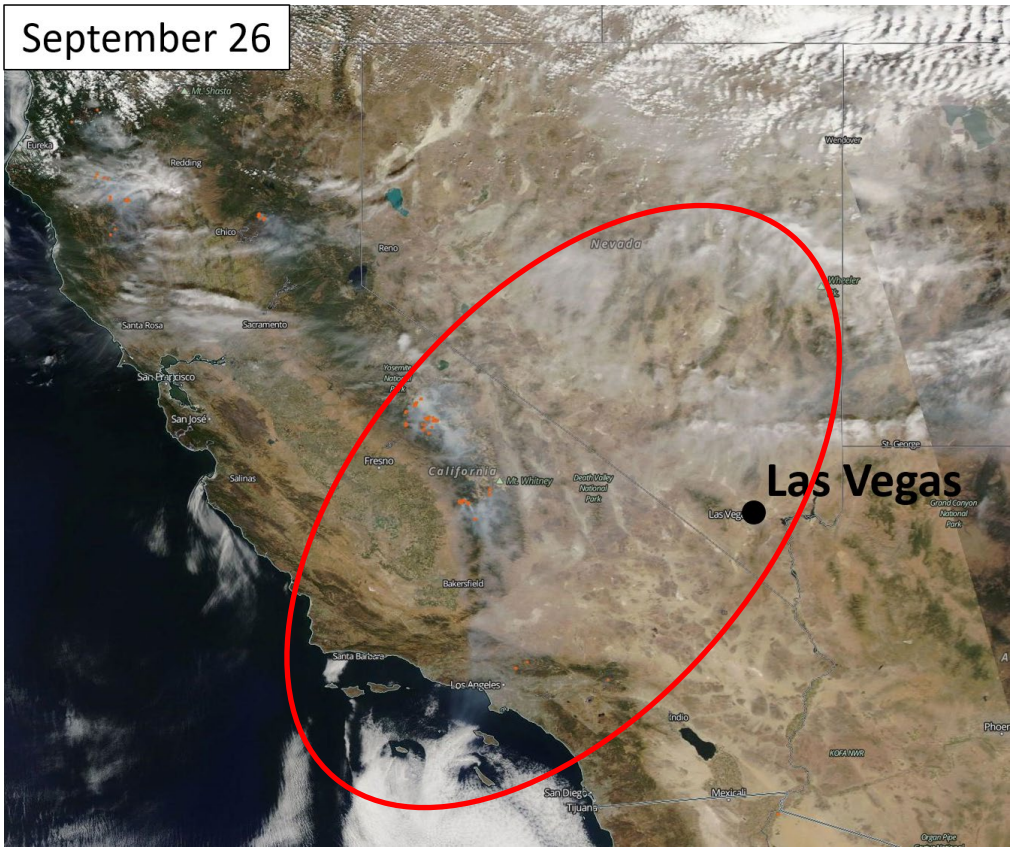

Figure 3-8. Visible satellite imagery from over California and Nevada on September 26, 2020. Source: NASA Worldview.

3.1.3 HYSPLIT Trajectories

HYSPLIT trajectories were run to demonstrate the transport of air parcels to Las Vegas from upwind areas and to show transport of smoke-containing air parcels from wildfires toward the affected monitors. These trajectories show that air was transported from the California fires, including the SQF Lightning Complex, Blue Jay/Wolf Fires, Creek Fire, Bobcat Fire, and El Dorado Fire, to the Clark County area in the days prior to the event and on September 26, 2020. Combined with satellite observations described in Sections 3.1.2 and 3.2.3, the trajectories demonstrate that smoke was transported from California to Las Vegas, Nevada.

NOAA's online HYSPLIT model tool was used for the trajectory modeling (http://ready.arl.noaa.gov/HYSPLIT.php). HYSPLIT is a commonly used model that calculates the path of a single air parcel from a specific location and height above the ground over a period of time. This path is the modeled trajectory. HYSPLIT trajectories can be used as evidence that fire emissions were transported to an air quality monitor. This type of analysis is important for meeting Tier 1 requirements and is required under Tier 3.

The model options used for this study are summarized in Table 3-2. We used meteorological data from the North American Mesoscale Forecast System (NAM, 12-km resolution) and High-Resolution Rapid Refresh (HRRR, 3-km resolution) model (ready.noaa.gov/archives.php). These data are high in spatial resolution, are readily available for HYSPLIT modeling over the desired lengths of time, and are expected to capture fine-scale meteorological variability. All backward trajectory start times were selected to be at noon (20:00 UTC or 12:00 p.m. local standard time (LST) when ozone concentrations peaked at the Walter Johnson station. As suggested in the EPA's EE guidance (U.S. Environmental Protection Agency, 2016), a backward trajectory length of 72 hours was selected to assess whether smoke from the current day or from the previous two days may have been transported over a long distance to the monitoring sites. Trajectories were initiated at 50 m, 500 m, and 1,000 m above ground level to capture transport throughout the mixed boundary layer, as ozone precursors may be transported aloft and influence concentrations at the surface through vertical mixing. Three backward trajectory approaches available in the HYSPLIT model were used in this analysis, including site-specific trajectories, trajectory matrix, and trajectory frequency.

Site-specific back trajectories were run to show direct transport from the wildfire smoke to the affected site(s) – this analysis is useful in linking smoke impacts at a single location (i.e., an air quality monitor) to wildfire smoke. Matrix back trajectories were run to show the general air parcel transport patterns from the Las Vegas area to the wildfire smoke plumes. Similarly, matrix forward trajectories were run to show air parcel transport patterns from the fires to the Las Vegas area. Matrix trajectories are useful in analyzing air transport over areas larger than a single air quality site. Trajectory frequency analysis shows the frequency with which multiple trajectories initiated over multiple hours pass over a grid cell on a map. Trajectory frequencies are useful in estimating the temporal and spatial patterns of air transport from a source region to a specific air quality monitor. Additionally, forward trajectory matrices were run for representative fires (i.e., the Bobcat Fire and the El Dorado Fire) in southern California to show transport in the direction of Clark County. To further model smoke from all fires contributing to the September 26 exceptional event, we initialized forward dispersion modeling from all fires (i.e., the SQF Lightning Complex, Blue Jay/Wolf Fire, Creek Fire, Bobcat Fire, and El Dorado Fire). Dispersion modeling is useful for determining the extent and timing of smoke entering the Clark County area in relation to the September 26 event, especially when smoke from multiple wildfires is mixing in the central and southern California area. Together, these trajectory analyses indicate the transport patterns into Clark County on September 26, 2020.

Site-specific backward trajectories were calculated from the Las Vegas Valley (36.1489°N, 115.2019°W) on September 26, 2020. We chose to model all trajectories for sites within the Las Vegas metropolitan area using the Las Vegas Valley location. The hour of 20:00 UTC (i.e., 12:00 PST) was chosen as the model starting time to coincide with the hour of the highest observed ozone concentration at the Walter Johnson station. The backward trajectories from the Las Vegas Valley with overlayed HMS smoke from September 24 through 26, together with measured ozone (8-hour begin time average), are shown in Figures 3-9 and 3-10. All three trajectories, each at a different height, pass near or directly over the active fires in central and southern California. The figures also

show that back trajectories intersected the smoke plumes originating from these active fires across central and southern California on September 24 and 25, 2020. Additionally, enhanced ozone concentrations were observed at all sites in Las Vegas. **Figure 3-11** shows the high-resolution (3 km) backward trajectories from the Las Vegas Valley on September 26, 2020. The results are consistent in that all three trajectories pass through smoke-laden air in central California, then pass directly over or near the wildfires in southern California (i.e., Bobcat and El Dorado fires).

To identify variations in meteorological patterns of transported air to Las Vegas, we generated a HYSPLIT trajectory matrix. For this approach, trajectories are run in an evenly spaced grid of source locations. **Figure 3-12** shows 72-hour backward trajectory matrices with source locations encompassing Las Vegas. The backward trajectories were both initiated at noon (12:00 p.m. PST/20:00. UTC) at a starting height of 100 m above ground level (AGL). As shown in the plot, the transported air intersecting Las Vegas on September 26, 2020, follows a similar pattern. Consistent with the trajectories depicted in Figures 3-9 and 10, air parcels were transported from the northern California Pacific coast through central and southern California, where wildfires were burning, and progressed northeastward to intersect Las Vegas at 100 m AGL.

A HYSPLIT frequency trajectory was the third trajectory approach used in this analysis. In this option, a trajectory from a single location and height starts every three hours. Using a continuous 0.25-degree grid, the frequency of trajectories passing through each grid cell is totaled and then normalized by the total number of trajectories. **Figure 3-13** shows a 72-hour backward trajectory frequency plot starting from the Las Vegas Valley and 50 m AGL on September 26, 2020. The trajectory frequency plot yields similar results as those from the previous two approaches; transported air impacting the Las Vegas Valley on September 26, 2020, predominately came from central and southern California (near or over the wildfires indicated in Section 3.2.1).

Forward trajectory matrices were run from two fire locations in southern California starting at 20:00 UTC on September 25 (**Figure 3-14 and 3-15**). The heights of 250 m, 500 m, and 1,000 m were chosen to capture transport from locations in the lower troposphere and due to uncertainty in the heights of smoke plumes from the wildfires in southern California. These trajectories, each at different starting heights, show that smoke was transported from the representative fires in southern California (i.e., Bobcat Fire and the El Dorado Fire) to the lower boundary layer over Clark County by noon on September 26, 2020. These forward trajectories, combined with the back trajectories shown above, further support the transport of smoke from California fires to Clark County, Nevada.

Forward dispersion modeling was initiated from all fires (i.e., the SQF Lightning Complex, Blue Jay/Wolf Fire, Creek Fire, Bobcat Fire, and El Dorado Fire) affecting the September 26 exceptional event in Clark County using NAM 12-km meteorology. An equal number of tracer smoke particles were released from each fire based on the conceptual model timeline to help determine the timing and extent of smoke reaching Clark County by September 26. Because an equal number of smoke tracers are released from each fire, the tracer concentration is not relevant to actual smoke concentrations, only the absence or presence of the smoke tracer in a given area should be considered in this analysis. Particles were emitted at 500 m from each fire location on an hourly basis.

Particulate tracer emissions began on September 24 at 00:00 UTC (or September 23 4:00 p.m. PST) and ended on September 27 00:00 UTC (or September 26 4:00 p.m. PST) for a total of 72 hours of emissions. Modeling was resolved to 0.05 degrees, latitude and longitude, grid spacing, and particle dispersion was modeled for September 24 00:00 UTC (September 23 4:00 p.m. PST) through September 27 00:00 UTC (September 26 4:00 p.m. PST) for a total of 72 hours of dispersion. Particles were allowed to dry-deposit and leave the western U.S. domain but were otherwise retained for 5 days representing aged smoke. **Figure 3-16** shows the smoke tracer extent between 0 and 500 m integrated from 12:00 UTC on September 26 (4:00 a.m. PST) to 00:00 UTC on September 27 (September 26 at 4:00 p.m. PST). This figure shows that the smoke from all fires modeled has spread eastward, resulting in widespread smoke coverage which encapsulates Clark County. The modeled smoke coverage is consistent with the visible and HMS smoke products from the same time period shown in Section 3.1.2. The presence of the smoke tracer in the lower boundary layer in Clark County on the EE date reinforces the other analyses presented in this section and indicates that smoke, contributed by all fires listed, affected Clark County on the EE date.

Table 3-2. HYSPLIT run configurations for each analysis type, including meteorology data set, time period of run, starting location(s), trajectory time length, starting height(s), starting time(s), vertical motion methodology, and top of model height.

HYSPLIT Parameter	Backward Trajectory Analysis – Site-Specific	Back Trajectory Analysis – Matrix	Backward Trajectory Analysis – Frequency	Forward Trajectory Analysis – Matrix	Backward Trajectory Analysis – High Resolution	Forward Dispersion Modeling
Meteorology	12-km NAM	12-km NAM	12-km NAM	12-km NAM	3-km HRRR	12-km NAM
Time Period	September 26, 2020	September 26, 2020	September 26, 2020	September 25 –26, 2020	September 26, 2020	September 24-26, 2020
Starting Location	36.2202 N, 115.2507 W	Evenly spaced grid covering Las Vegas, Nevada	36.2202 N, 115.2507 W	Evenly spaced grid covering Bobcat Fire and El Dorado Fire in southern California	36.2202 N, 115.2507 W	Location of the SQF Lightning Complex, Blue Jay/Wolf Fire, Creek Fire, Bobcat Fire, and El Dorado Fire
Trajectory Time Length	72 hours	72 hours	72 hours	30 hours	72 hours	72 hours
Starting Heights (AGL)	50 m, 500 m, 1,000 m	100 m	100 m	100 m, 250 m, 500 m, 1,000 m	50 m, 500 m, 1,000 m	500 m
Starting Times	20:00 UTC	20:00 UTC	20:00 UTC	16:00 UTC, 20:00 UTC	20:00 UTC	00:00 UTC
Vertical Motion Method	Model Vertical Velocity	Model Vertical Velocity	Model Vertical Velocity	Model Vertical Velocity	Model Vertical Velocity	Model Vertical Velocity
Top of Model	10,000 m	10,000 m	10,000 m	10,000 m	10,000 m	10,000 m

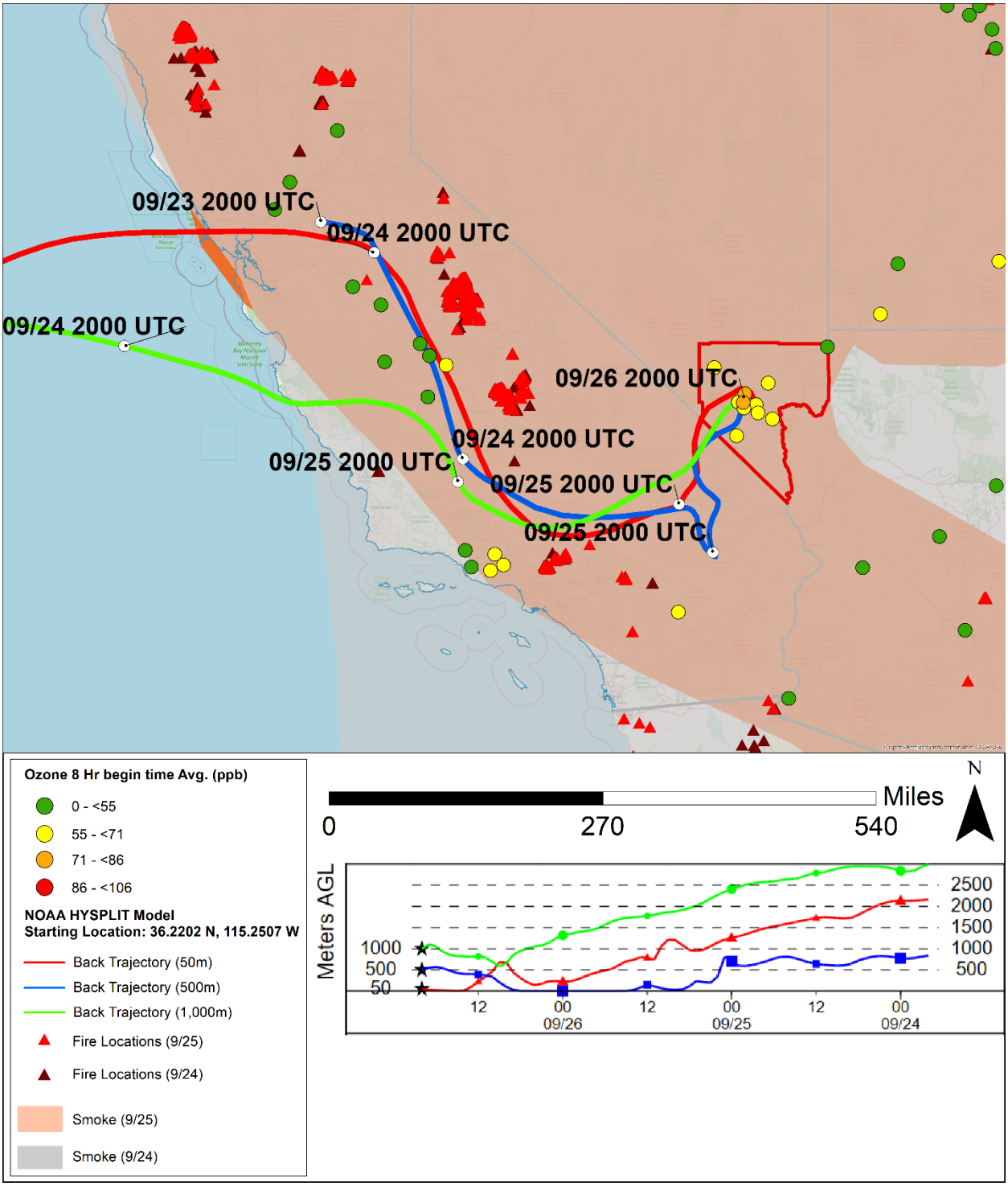

Figure 3-9. 72-hour HYSPLIT back trajectories with the presence of HMS smoke plumes (orange for September 24 and gray for September 25) from downtown Las Vegas, ending on September 26, 2020. NAM back trajectories are shown for 50 m (red), 500 m (green), and 1,000 m (blue) above ground level.

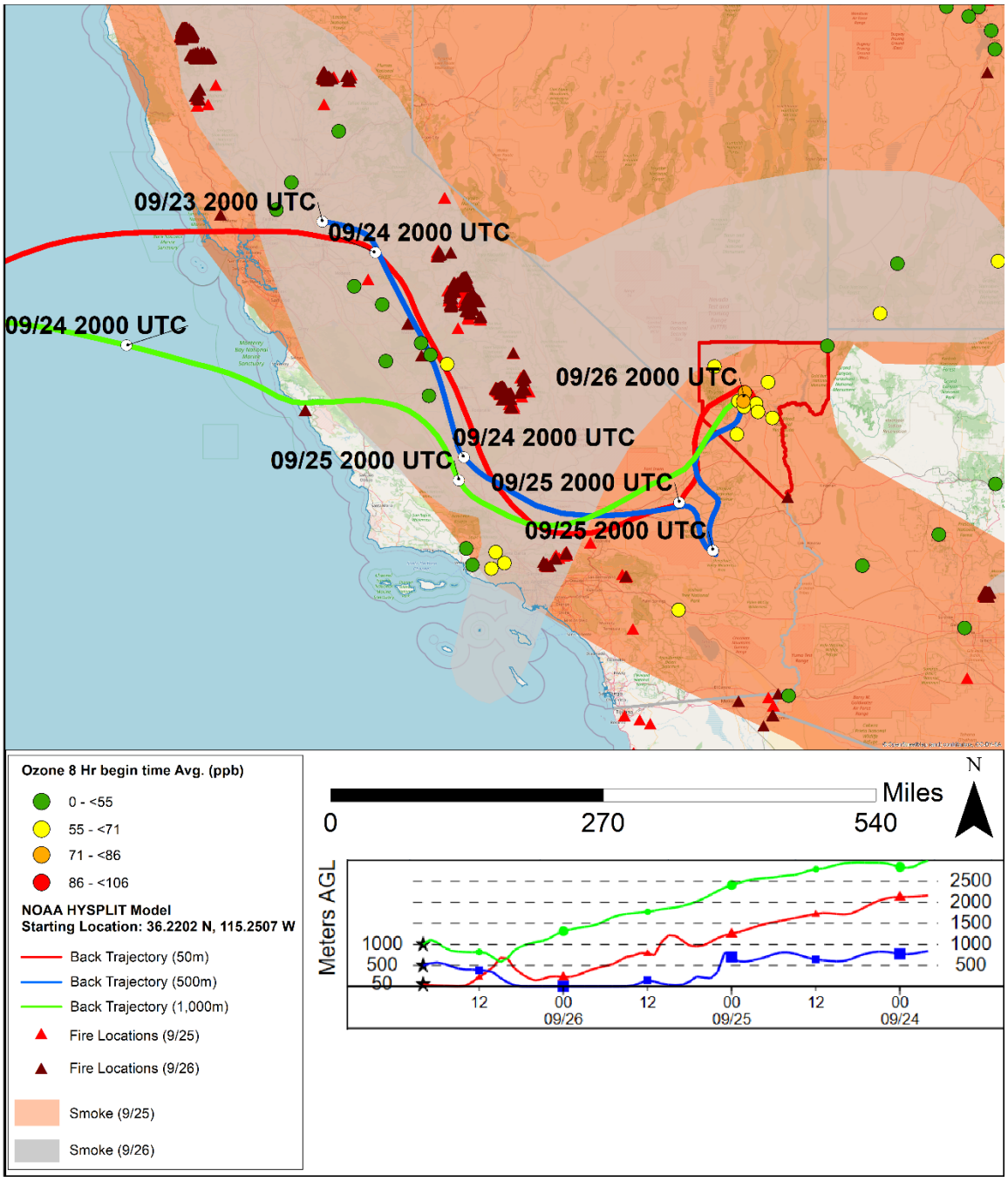

Figure 3-10. 72-hour HYSPLIT back trajectories with the presence of HMS smoke plumes (orange for September 25 and gray for September 26) from downtown Las Vegas, ending on September 26, 2020. NAM back trajectories are shown for 50 m (red), 500 m (green), and 1,000 m (blue) above ground level.

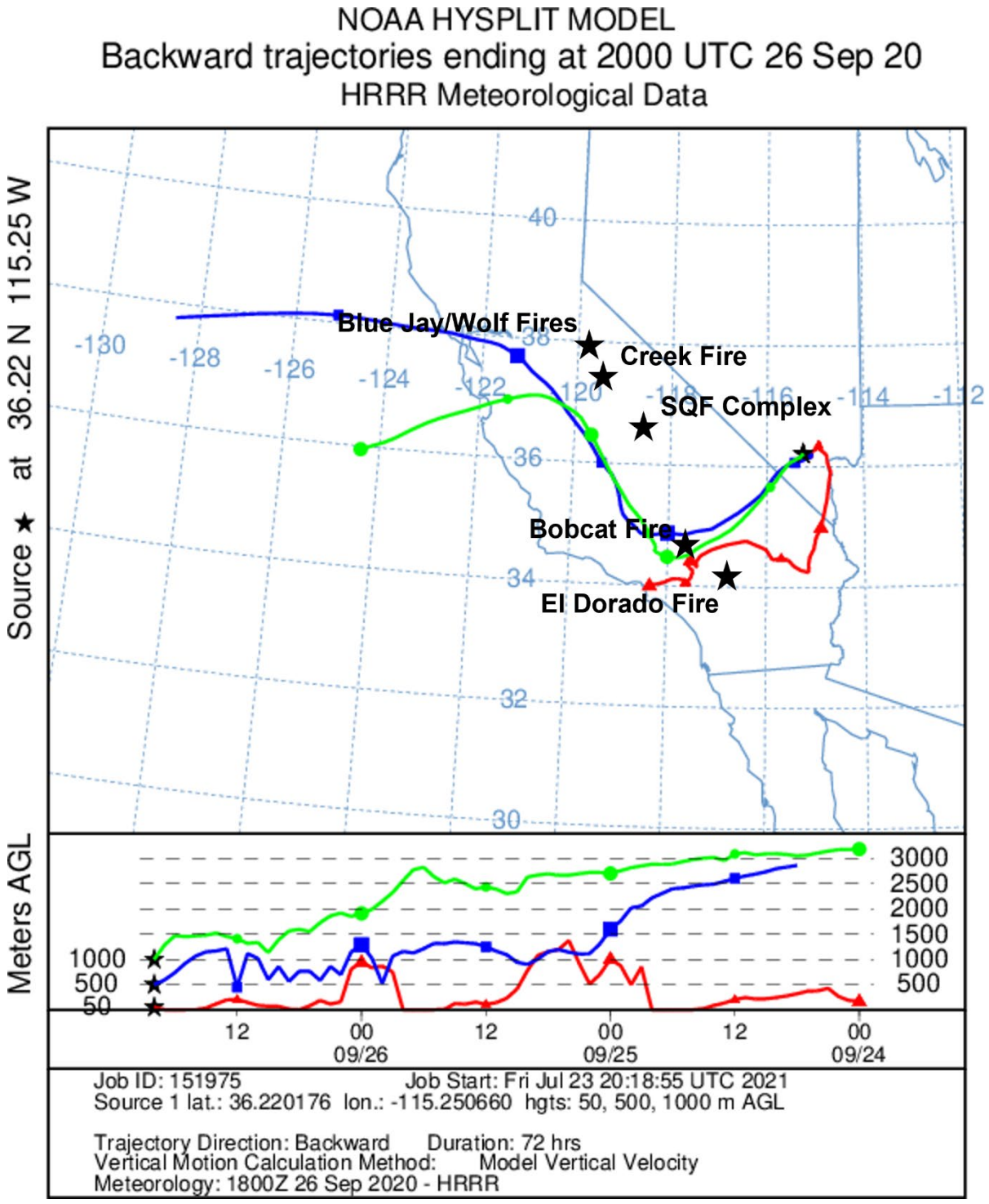

Figure 3-11. High-resolution HYSPLIT back trajectories. 72-hour, HRRR back trajectories initiated on September 26 from downtown Las Vegas are shown for 50 m (red), 500 m (blue), and 1,000 m (green) above ground level.

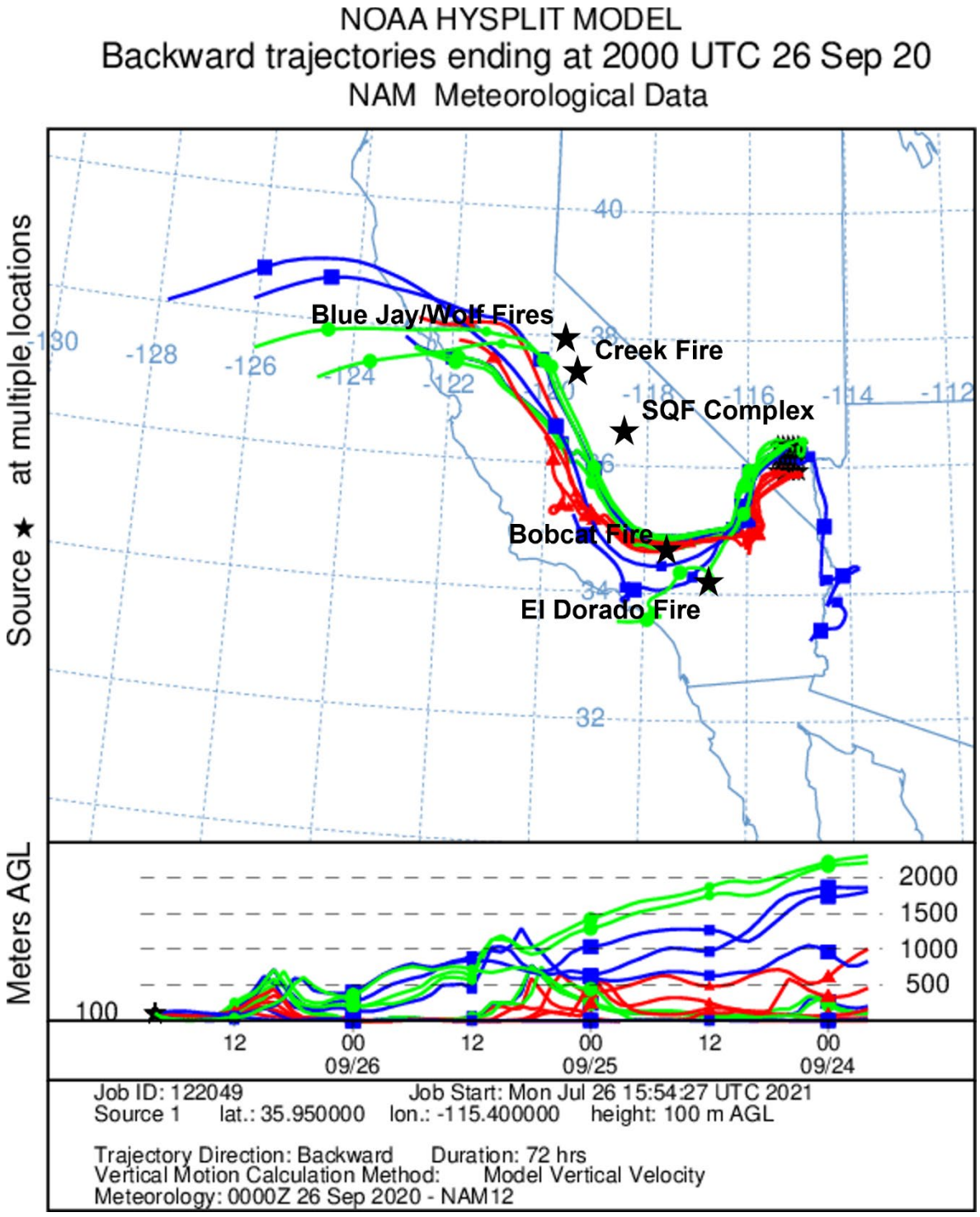

Figure 3-12. HYSPLIT back trajectory matrix. A 72-hour, NAM back trajectory matrix was initiated on September 26 at 20:00 UTC (12:00 p.m. LST) from downtown Las Vegas at 100 m above ground level.

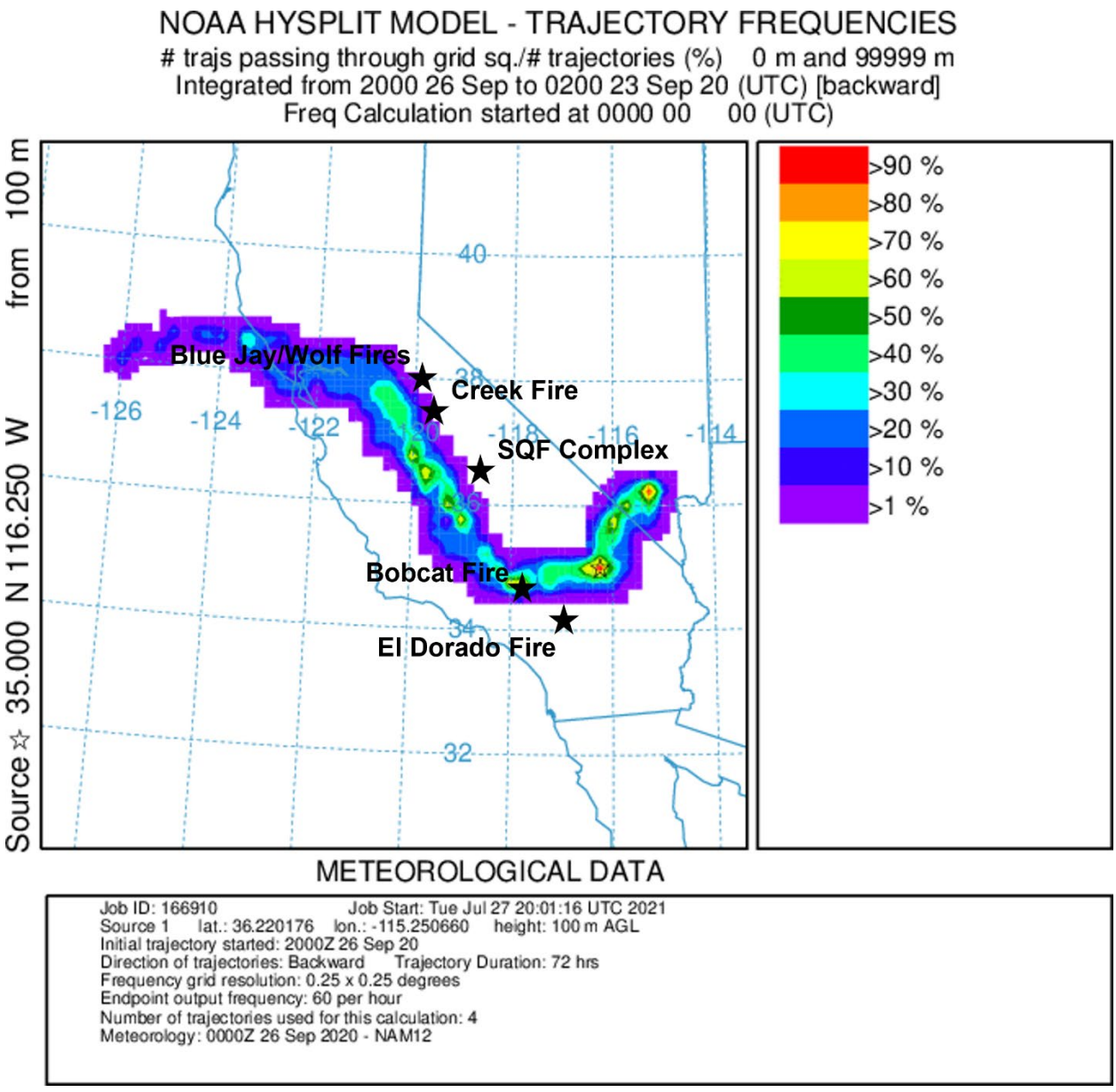

Figure 3-13. HYSPLIT back trajectory frequency. A 72-hour, NAM frequency of back trajectories was initiated on September 26 at 20:00 UTC (12:00 p.m. LST) from downtown Las Vegas at 100 m above ground level. The colors within the frequency plot indicate the percent of trajectories that pass through a grid square.

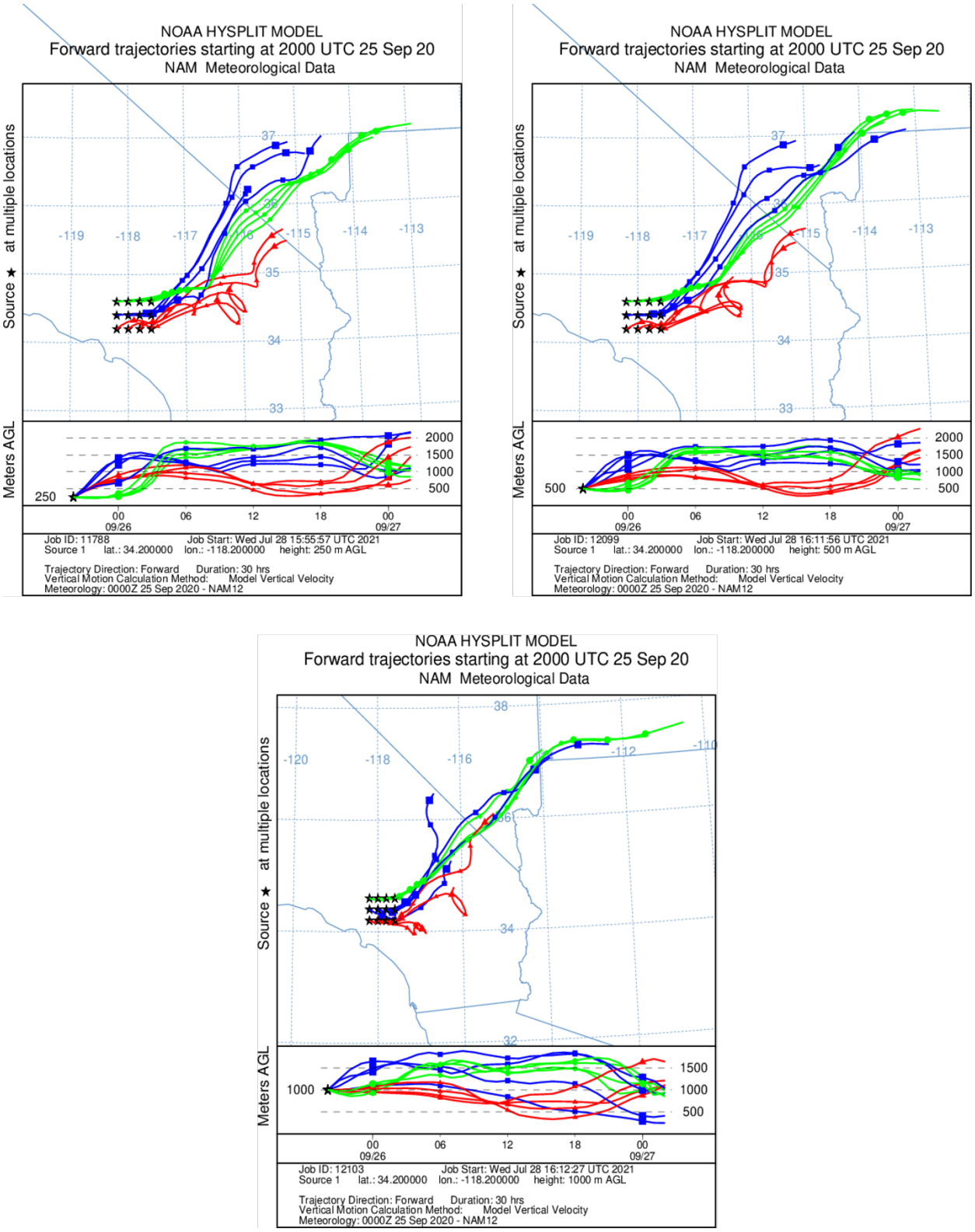

Figure 3-14. HYSPLIT forward trajectory matrices showing transport from the Bobcat Fire. 30-hour, NAM forward trajectory matrices were initiated on September 25 at 20:00 UTC (12:00 p.m. LST) from the Bobcat Fire at 250 m, 500 m, and 1,000 m above ground level.

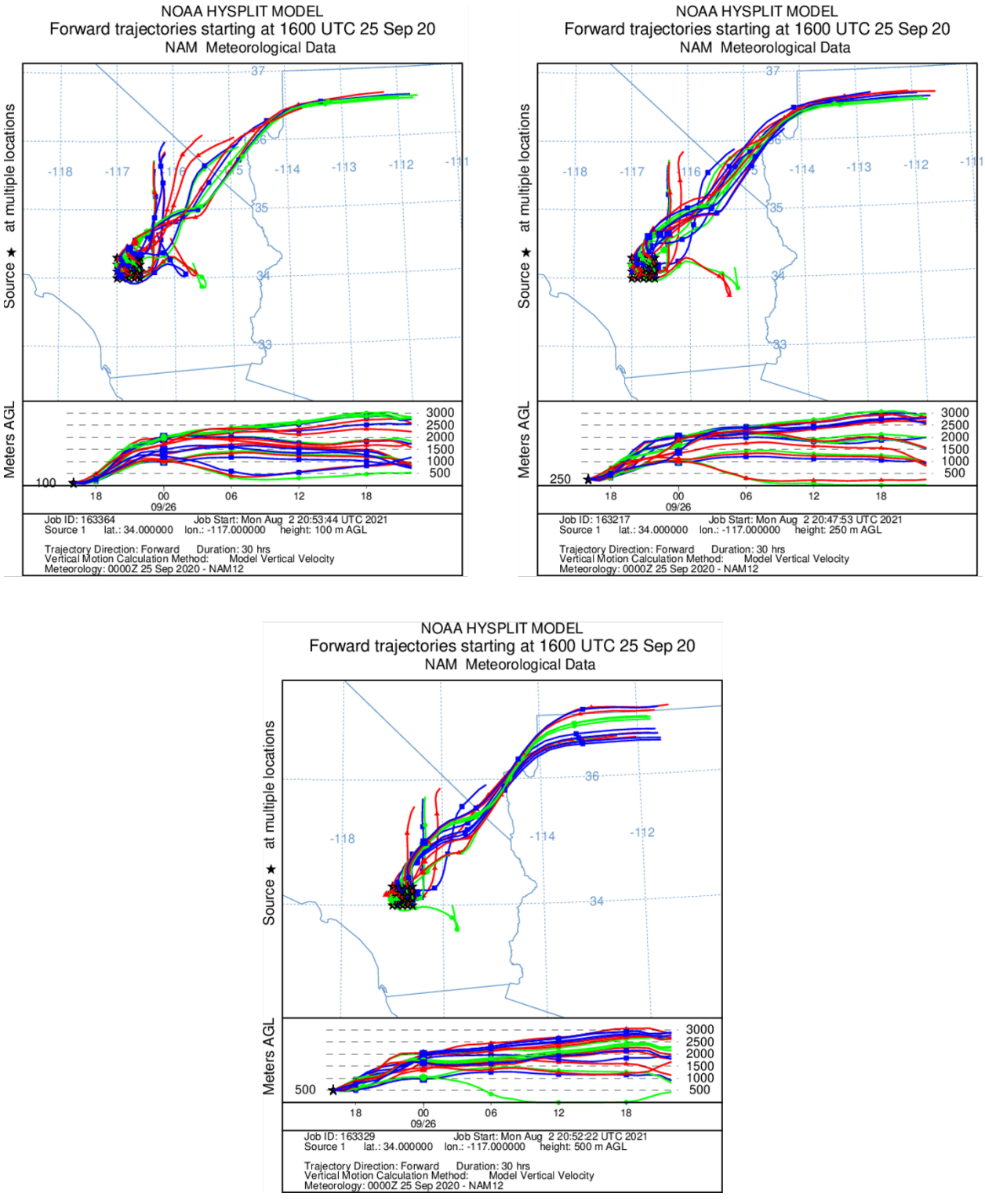

Figure 3-15. HYSPLIT forward trajectory matrices showing transport from the El Dorado Fire. 30-hour, NAM forward trajectory matrices were initiated on September 25 at 20:00 UTC (12:00 p.m. LST) from the El Dorado Fire at 250 m, 500 m, and 1,000 m above ground level.

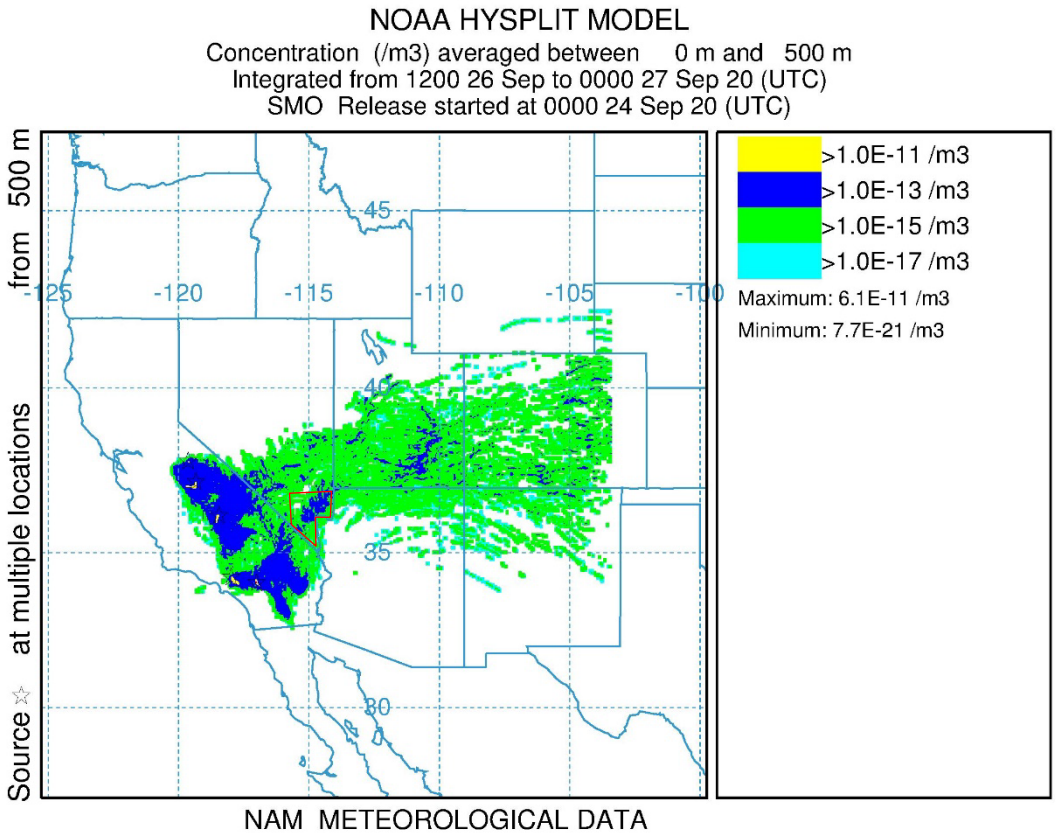

Figure 3-16. HYSPLIT forward dispersion modeling showing transport from all fires (i.e., the SQF Lightning Complex, Blue Jay/Wolf Fire, Creek Fire, Bobcat Fire, and El Dorado Fire). A 72-hour, NAM 12-km emissions and dispersion modeling of smoke tracer particles was initiated on September 24 at 00:00 UTC (4:00 p.m. PST on September 23) at 500 m above ground level. Hourly emission of tracers concluded on September 27 at 00:00 UTC (4:00 p.m. PST on September 26). The particulate smoke tracers shown here are integrated from September 26 at 12:00 UTC (4:00 a.m. PST) to September 27 at 00:00 UTC (4:00 p.m. PST on September 26) and from 0 to 500 m above ground level. The approximate outline of Clark County is shown in red.

3.1.4 Media Coverage and Ground Images

News, weather, and environmental organizations provided widespread coverage of the effects of smoky conditions on air quality in Clark County. The multiple fires west of Las Vegas were cited as contributors to the smoke settling over the area, including the Bobcat Fire. The Clark County Department of Environment and Sustainability (DES) issued a smoke advisory due to wildfire smoke on September 11, and this advisory was extended on four occasions, ultimately lasting through September 28.[3] Figure 3-17 shows a Facebook announcement by Clark County DES reporting the last of these four extensions. Additionally, 40 CFR 50.14(c)(1)(i) requires that air agencies must "notify the

[3] https://www.facebook.com/SustainClarkCounty/posts/1995314223932122

public promptly whenever an event occurs or is reasonably anticipated to occur which may result in the exceedance of an applicable air quality standard" in accordance with the mitigation requirement at 40 CFR 51.930(a)(1). Appendix A provides further details on Clark County Department of Environment and Sustainability's public notification for the potential exceptional event on September 26, 2020.

Figure 3-17 A Facebook post added by the Clark County Department of Environment and Sustainability on September 24, 2020, noting that an existing smoke advisory in the Las Vegas area would extend through September 28, 2020.

On September 24, KNXT and 8 News Now, two Las Vegas news sources, reported on the final extension of this smoke advisory (https://kxnt.radio.com/articles/press-release/smoke-advisory-extended-through-september-28; https://www.8newsnow.com/weather/windy-changes-will-help-clear-our-skies/). 8 News Now also noted that, in addition to the direct effects from wildfire smoke,

temperatures expected over the following two days would fuel elevated ground-level ozone. The *Review Journal*, a local Las Vegas newspaper, also reported on this extended advisory on September 25 stating that "one of the biggest fires in Southern California that is sending smoke toward Las Vegas is the 114,000-acre Bobcat Fire burning in the San Gabriel Canyon northeast of Pasadena" (https://www.reviewjournal.com/local/local-las-vegas/smoke-advisory-for-clark-county-extended-for-the-weekend-2129747/). Other media coverage associated with the September 26 EE can be found in Appendix A.

Ground images from the Clark County Department of Environment and Sustainability, Division of Air Quality's visibility cameras, located on the roof of the M Hotel in Las Vegas, clearly show the smoky conditions that persisted on September 26 (Figure 3-18). When compared to images taken on a clear day (May 21, 2020) (Figure 3-19), the September 26 images show drastically reduced visibility and an opaque gray haze, particularly pronounced in the northern directions, due to wildfire smoke.

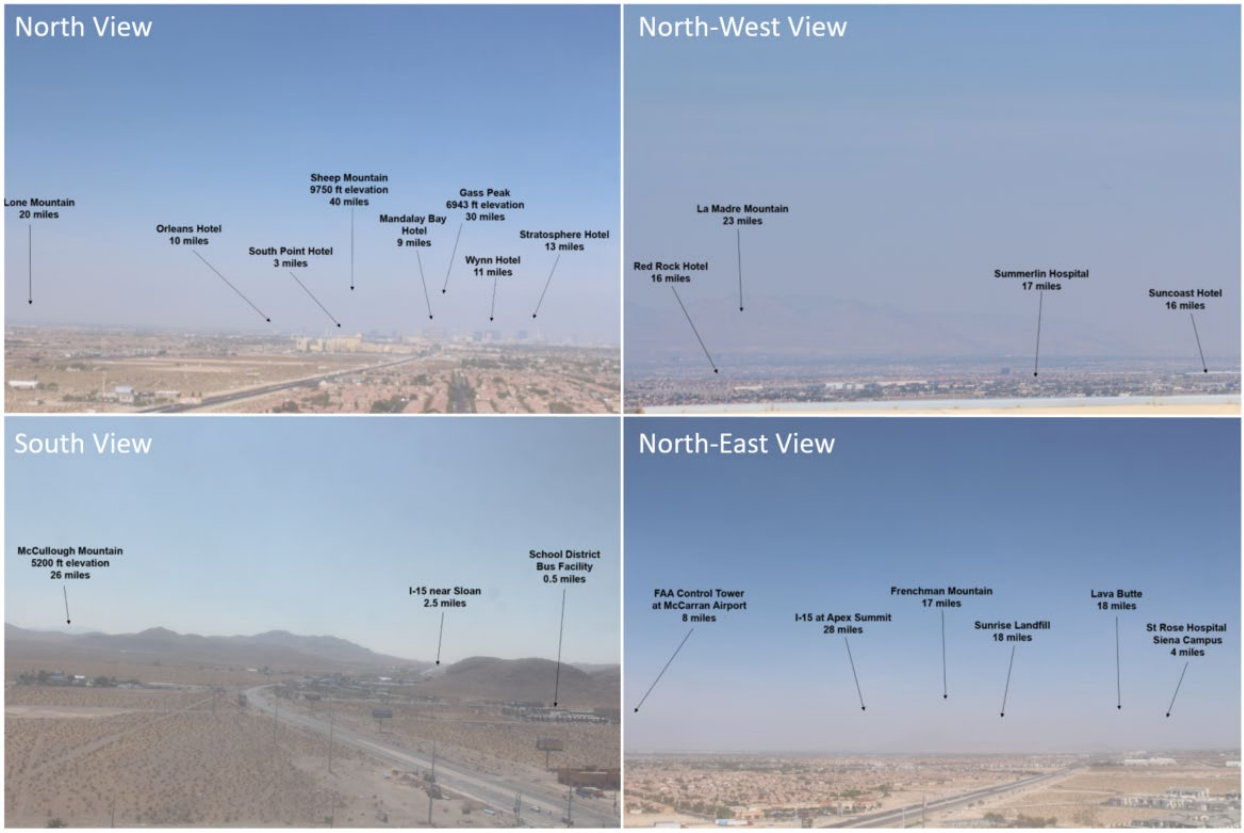

Figure 3-18. Clark County visibility images from September 26, 2020. Images taken from webcams set up in Clark County are shown for the EE on September 26. Each image is labeled with the viewing direction and landmarks.

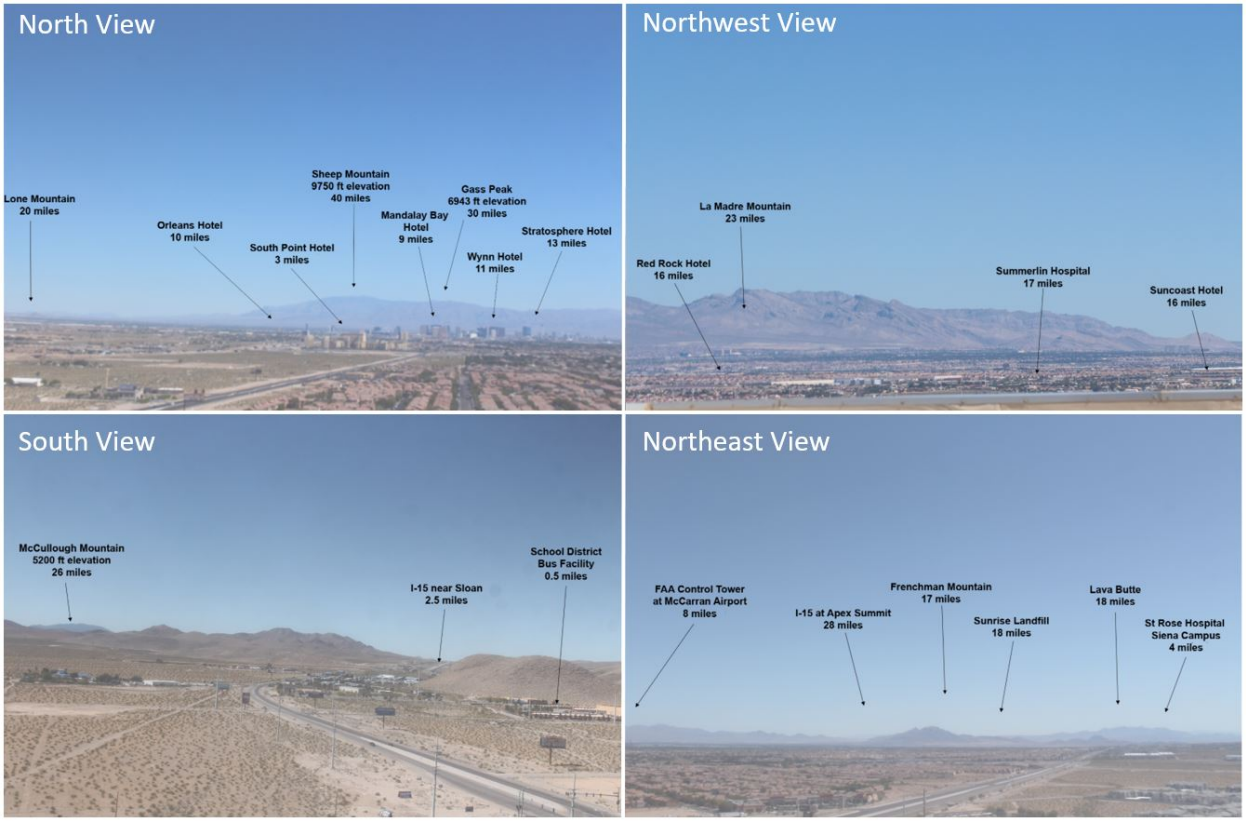

Figure 3-19. Visibility images taken from webcams set up in Clark County are shown for a clear day (May 21, 2020). Each image is labeled with the viewing direction and landmarks.

3.2 Tier 2 Analyses

3.2.1 Key Factor #1: Q/d Analysis

The exceptional event guidance (U.S. Environmental Protection Agency, 2016) describes a method used to relate the quantity of smoke emissions and distance of the fire to an exceeding monitor. The resulting quantity, called Q/d, may be used to screen fires that meet a conservative threshold of air quality impacts.[4] This section provides the results of the Q/d analyses for fires that were likely to have contributed to the September 26 ozone event in Clark County. Based on media coverage, transport analysis, and ground/satellite-based analyses in Section 3.1, the SQF Lightning Complex,

[4] Specifically, fires with a Q/d value meeting the 100 tons/km threshold may qualify for a Tier 2 demonstration of a clear causal relationship. However, this threshold is insufficient to identify all cases where ozone impacts from smoke may have occurred. Pages 16-17 of the guidance state "to determine an appropriate and conservative value for the Q/d threshold (below which the EPA recommends Tier 3 analyses for the clear causal relationship), the EPA conducted a review… The reviews and analyses did not conclude that particular ozone impacts will always occur above a particular value for Q/d. For this reason, a Q/d screening step alone is not sufficient to delineate conditions where sizable ozone impacts are likely to occur." (U.S. Environmental Protection Agency, 2016).

Blue Jay/Wolf Fires, Creek Fire, Bobcat Fire, and El Dorado Fires contributed to smoky conditions and high ozone concentrations in Clark County, Nevada, on September 26, 2020.

Figure 3-20 shows large California fires burning in the vicinity of Clark County on September 26, 2020. Table 3-3 shows agency data available for all fires that are linked through back trajectories with the September 26 exceptional event (as of July 2021). Some of the fires identified were caused by lightning on rugged wildland terrain inaccessible to most firefighting methods:

- SQF Lightning Complex: https://inciweb.nwcg.gov/incident/7048/
- Blue Jay/Wolf Fires: https://inciweb.nwcg.gov/incident/6888/

The other fires that contributed to the September 26 exceedance event include wildfires that began over Labor Day weekend 2020 during a period of very high temperatures, low relative humidity, and low fuel moisture:

- Creek Fire: https://inciweb.nwcg.gov/incident/7147/
- Bobcat Fire: https://inciweb.nwcg.gov/incident/7152/
- El Dorado Fire: https://inciweb.nwcg.gov/incident/7148/

All of these fires burned for a long period of time, and none had a containment date before November 2020. We provide the total acreage burned as of September 26, 2020, in Table 3-3 based on the available agency information. The size of the fires burning on September 26 totaled more than 600,000 acres.

Key factor #1 for a Tier 2 demonstration requires an analysis of wildfire smoke emissions from qualifying fires and the distance from each fire to the affected monitor(s). To identify qualifying fires, the guidance "recommends generating 24-hour back trajectories from the affected ozone monitoring site(s) beginning at each hour of these two or three dates" (U.S. Environmental Protection Agency, 2016). Three dates would be used only if the 8-hour averaging period for the daily maximum 8-hour ozone data include hours falling on two dates (i.e., the 8-hour average includes at least 11 p.m. and midnight on two distinct calendar days). For this demonstration, 24-hour HYSPLIT back trajectories were generated from the monitor location starting on each hour of the day of the exceedance.

The guidance states that "…fires that are close to any of these back trajectories" may be used to calculate Q/d (U.S. Environmental Protection Agency, 2016). To identify fires that fall near the HYSPLIT trajectories, trajectories were buffered by a distance of 25% of the distance traveled by the trajectory, which is consistent with uncertainty reported for HYSPLIT trajectory modeling (Draxler, 1991). Figure 3-21 shows the back trajectories and buffer of uncertainty from Clark County, Nevada. All fires falling within the uncertainty buffer of one or more trajectories were considered candidates for calculating Q/d.

To calculate Q/d for a qualifying fire, daily fire growth was identified using agency reports directly or news reports citing official sources. The daily area growth is first estimated by subtracting the

previous day's total area from the given day's total area. This represents the new area burned on a given day and represents a lower limit to the total area burned on that day. BlueSky Playground Version 3.0.1 (https://tools.airfire.org/playground/v3/) was used to estimate the daily emissions of NO_x and VOCs emissions associated with the daily growth in area burned for Blue Jay/Wolf Fires, Bobcat Fire, Creek Fire, El Dorado Fire, and SQF Complex for September 25 and 26. These emissions estimates underestimate the total daily emissions due to cases when the same area burns for multiple days that are not included in our emissions estimates. These daily emission estimates for NO_x and reactive VOCs (rVOCs) in tons are divided by the distance from each fire to impacted monitors. The fires' location—as reported in InciWeb or by CAL FIRE—was used to identify the distance to the impacted monitors and fuelbed type. Emissions calculations were based on very dry conditions.

EPA guidance recommends that an event may qualify for a Tier 2 demonstration if the Q/d value for a single fire, or the aggregate Q/d across multiple fires, exceeds a conservative value of 100 tons/km. Daily Q/d results indicate that significant emissions of NO_x and rVOCs occurred from most of the candidate fires during the day of the exceedance (**Table 3-4**) and the day prior (**Table 3-5**). However, due to the significant distance between the fire and the monitor location, the emissions were not large enough to reach the Q/d threshold of 100 tons/km for a Tier 2 demonstration, and it was determined that Tier 3 analyses were needed to demonstrate a clear causal relationship.

The results of the Q/d analysis presented in this section agree with and further strengthen the conceptual model and Tier 3 weight of evidence of a clear causal relationship between the identified wildfires smoke emissions and the monitored ozone exceedance identified in this demonstration.

Figure 3-20. Large fires burning on September 26, 2020, in the vicinity of Clark County are shown in red. The Clark County boundary is shown in black.

Table 3-3. Fire data for the California fires associated with the September 26, 2020, EE. Information includes start/containment date, cause of the fire, the agency estimates of the area burned by the EE date (September 26, 2020), and the total reported acres burned. NA means a date has not officially been determined, while '*' means agency data was unavailable so MODIS fire hotspot estimates were used to calculate the burned area.

Fire Name	Start Date	Contained Date	Cause	Area Burned by EE Date (acres)	Total Area Burned (acres)
SQF Lightning Complex	8/19/2020	NA	Lightning	149,888	174,178
Blue Jay Fire	7/24/2020	NA	Lightning	11,504*	6,922
Wolf Fire	8/11/2020	NA	Lightning		2,047
Creek Fire	9/5/2020	12/24/2020	Unknown	302,870	379,895
Bobcat Fire	9/6/2020	NA	Unknown	114,103	115,796
El Dorado Fire	9/5/2020	11/16/2020	Human	22,666	22,744

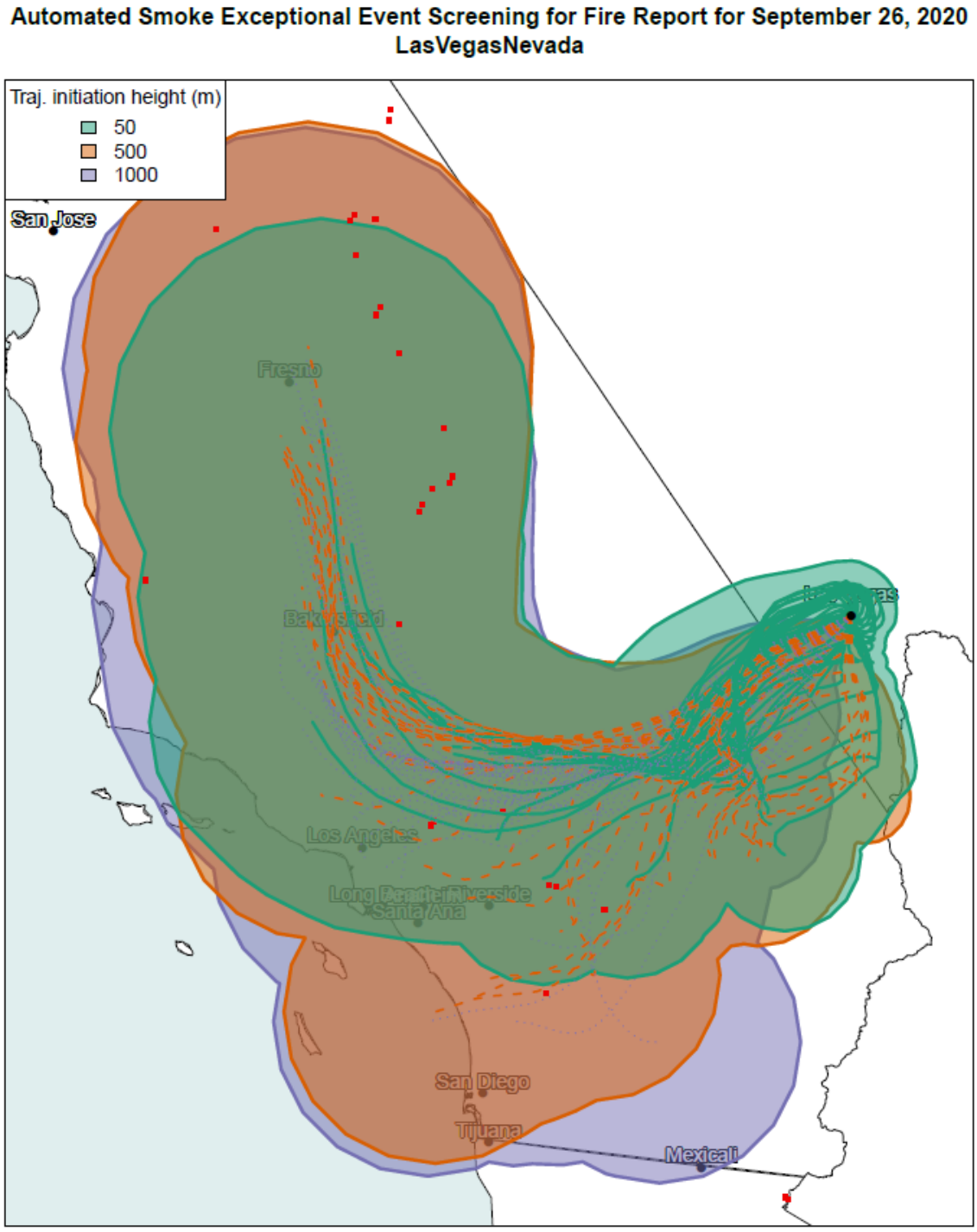

Figure 3-21. Q/d analysis. 24-hour back trajectories are shown as solid or dotted lines. The starting height of the back trajectory is indicated by the color. Uncertainty buffers, calculated as 25% of the distance traveled by the trajectory, are shown in colored polygons. Active fires on September 26 are shown as red squares. Fires falling within one or more uncertainty buffer(s) were used to calculate individual and aggregate Q/d values.

Table 3-4. Daily growth, daily emissions associated with the daily growth in area burned, and Q/d for the fires with potential smoke contribution on September 26, 2020. Total area burned represents the cumulative area burned across the entire history of the fire up to and including September 26. Growth for all dates shown were obtained from agency estimates available from the Incident Information System (InciWeb) or from news sources citing official reports. Aggregate Q/d calculated for all fires shown is 29.8. Column "E (Tons)" represents the sum of NO_x and rVOC emissions.

Fire Name	Total Area Burned (Acres)	Daily Growth (Acres)	NO_x (Tons)	VOCs (Tons)	Reactive VOCs (Tons)	E (Tons)	Distance (Km)	Q/d (Tons/km)	Fuel Loading	Fire size data source
SQF Complex	149,888	1,038	46.27	1,689.8	1,014	1,060	296	3.6	Red fir forest	https://inciweb.nwcg.gov/incident/7048/
Blue Jay Fire	4,598	90	4.01	146.5	88	92	436	0.2	Red fir forest	https://goldrushcam.com/sierrasuntimes/index.php/news/local-news/25648-cal-fire-california-statewide-fire-summary-for-sunday-morning-september-27-2020
Wolf Fire	1,087	0	0	0	0	0	438	0.0	Red fir forest	https://goldrushcam.com/sierrasuntimes/index.php/news/local-news/25648-cal-fire-california-statewide-fire-summary-for-sunday-morning-september-27-2020
Creek Fire	302,716	11,668	422.42	15,865.3	9,519	9,942	381	26.1	Douglas-fir-sugar pine-tanoak forest	https://inciweb.nwcg.gov/incident/7147/
Bobcat Fire	114,103	99	3.2	16.8	10	13	322	0.0	Scrub oak chaparral shrubland	https://inciweb.nwcg.gov/incident/7152/

Table 3-5. Daily growth, daily emissions associated with the daily growth in area burned, and Q/d for the fires with potential smoke contribution on September 25, 2020. Total area burned represents the cumulative area burned across the entire history of the fire up to and including September 25. Growth for all dates shown were obtained from agency estimates available from the Incident Information System (InciWeb) or from news sources citing official reports. Aggregate Q/d calculated for all fires shown is 14.5. Column "E (Tons)" represents the sum of NO_x and rVOC emissions.

Fire Name	Total Area Burned (Acres)	Daily Growth (Acres)	NO_x (Tons)	VOCs (Tons)	Reactive VOCs (Tons)	E (Tons)	Distance (Km)	Q/d (Tons/km)	Fuel Loading	Fire size data source
SQF Complex	148,850	4,073	181.54	6,630.7	3,978	4,160	296	14.1	Red fir forest	https://inciweb.nwcg.gov/incident/7048/
Blue Jay Fire	4,508	10	0.45	16.28	10	10	436	0.0	Red fir forest	https://goldrushcam.com/sierrasuntimes/index.php/news/local-news/25629-cal-fire-california-statewide-fire-summary-for-saturday-morning-september-26-2020
Wolf Fire	1,087	0	0	0	0	0	438	0.0	Red fir forest	https://goldrushcam.com/sierrasuntimes/index.php/news/local-news/25629-cal-fire-california-statewide-fire-summary-for-saturday-morning-september-26-2020
Creek Fire	291,048	211	7.64	286.9	172.1	180	381	0.47	Douglas-fir-sugar pine-tanoak forest	https://inciweb.nwcg.gov/incident/7147/
Bobcat Fire	114,004	18	0.58	3.1	1.83	2	322	0.01	Scrub oak chaparral shrubland	https://inciweb.nwcg.gov/incident/7152/

3.2.2 Key Factor #2: Comparison of Event Concentrations with Non-Event Concentrations

Another key factor in determining whether the September 26, 2020, exceedance event is exceptional is to compare event ozone concentrations with non-event concentrations via percentile and rank-order analysis. Table 3-6 shows September 26, 2020, concentrations as a percentile in comparison with the last six years of data (2015 to 2020; with and without the other proposed 2018 and 2020 EE days included) at each site in Clark County. For the two monitoring sites (Walter Johnson and Joe Neal) that show a NAAQS standard exceedance on September 26, all of the exceedances are greater than or equal to the 98th percentile when compared to the last six years of data, even with all other proposed 2018 and 2020 EE days included. Without the other EE days included, the percentiles are slightly higher (≥99th percentile). To confirm that the calculated percentiles are not biased by non-ozone season data, Table 3-7 shows the September 26 percentile ranks for all monitoring sites around Clark County in comparison with the last six years of ozone season (May to September) data. At Joe Neal, the September 26 percentile ranks in the 98th percentile (with all proposed 2018 and 2020 EE days included), while Walter Johnson ranks in the 95th percentile when compared with the last six ozone seasons. When the other possible EE days are excluded, the percentile ranks for Joe Neal and Walter Johnson increase to ≥97th percentile. Although not all of the sites showed a >99th percentile rank for September 26 compared with the last six ozone seasons, this analysis confirms that the September 26 EE had unusually high concentrations of ozone when compared with the last six years of data and the last six ozone seasons.

We also compared the rank-ordered concentrations at each site for 2020. As shown in Figures 2-3 and 2-4, 2020 ozone concentrations were not atypically low, which might bias our rank-ordered analysis for September 26, 2020. Tables 3-8 and 3-9 show the rank-ordered ozone concentrations for 2018 through 2020 and the design values for 2020, with the proposed 2018 and 2020 EEs included. For the monitoring sites that showed an exceedance of the NAAQS standard, September 26 was not in the top four highest ozone concentrations for 2020. However, without the other proposed EE event in 2020 included, all affected sites rank September 26 as the second highest ozone event in 2020.

For further comparison with non-event ozone concentrations, Table 3-10 shows 5-year (2015-2019) MDA8 ozone statistics for the week before and after September 26. This two-week window analysis shows that each affected monitoring site shows MDA8 ozone concentrations on September 26, 2020, to be well above the average and in the 95th percentile of the last five years of data.

The percentile, rank-ordered analyses, and the two-week window analysis, indicate that all affected monitoring sites on September 26, 2020, showed unusually high ozone concentrations compared with non-event concentrations. This conclusion supports a key factor, suggesting that September 26 was an EE in Clark County, Nevada.

Table 3-6. Six-year percentile ozone. The September 26 EE ozone concentration at each site is calculated as a percentile of the last six years with and without other 2018 and 2020 EEs included in the historical record.

AQS Site Code	Site Name	6-Year Percentile	6-Year Percentile w/o EE Dates
320030071	Walter Johnson	97.9	*98.7*
320030075	Joe Neal	99.1	*99.5*

Table 3-7. Six-year, ozone-season percentile ozone. The September 26 EE ozone concentration at each site is calculated as a percentile of the last six years' ozone season (May-September) with and without other 2018 and 2020 EEs included in the historical record.

AQS Site Code	Site Name	6-Year Percentile	6-Year Percentile w/o EE Dates
320030071	Walter Johnson	95.2	*97.1*
320030075	Joe Neal	98.0	*98.9*

Table 3-8. Site-specific ozone design values for the Joe Neal monitoring site. The top five highest ozone concentrations for 2018-2020 at Joe Neal are shown, and proposed EE days in 2018 and 2020 are included.

Joe Neal Rank	2018	2019	2020
Highest	80	74	81
Second Highest	78	70	78
Third Highest	76	69	78
Fourth Highest	76	68	78
Fifth Highest	74	67	76
Design Value		74	

Table 3-9. Site-specific ozone design values for the Walter Johnson monitoring site. The top five highest ozone concentrations for 2018-2020 at Walter Johnson are shown, and proposed EE days in 2018 and 2020 are included.

Walter Johnson Rank	2018	2019	2020
Highest	79	77	82
Second Highest	77	69	82
Third Highest	77	69	78
Fourth Highest	76	68	77
Fifth Highest	76	68	75
Design Value		73	

Table 3-10. Two-week non-event comparison. September 2, 2020, MDA8 ozone concentrations for each affected site are shown in the top row. Five-year (2015-2019) average MDA8 ozone statistics for September 19 through October 3 are shown for each affected site around Clark County to compare with the event ozone concentrations.

	Joe Neal 320030075	Walter Johnson 320030071
Sep. 26	75	71
Mean	48	49
Median	47	48
Mode	45	47
St. Dev	9	9
Minimum	32	33
95 %ile	62	65
99 %ile	70	69
Maximum	75	71
Range	43	38
Count	92	92

3.2.3 Satellite Retrievals of Pollutant Concentrations

Satellite retrievals of pollutants associated with wildfire smoke, such as AOD, CO, and NO_x can provide evidence that smoke was present at a monitoring site. We examined maps of Multi-Angle Implementation of Atmospheric Correction (MAIAC) AOD from the Moderate Resolution Imaging Spectroradiometer (MODIS) instrument onboard the Aqua and Terra satellites, CO retrievals from the Atmospheric Infrared Sounder (AIRS) instrument onboard the Aqua satellite, and NO_2 retrievals from the Ozone Monitoring Instrument (OMI). OMI NO_2 retrievals were inconclusive for September 26, but are shown in **Appendix B** for completeness. These maps provide evidence to support the transport of smoke from the fires in California, including the SQF Lightning Complex, Blue Jay/Wolf Fires, Creek Fire, Bobcat Fire, and El Dorado Fire to Clark County, Nevada, as already demonstrated with visual imagery and trajectories in Sections 3.1 and 3.2. MODIS AOD measurements indicate the concentration of light-absorbing aerosols, including those emitted by wildfires, in the total atmospheric column. Between September 23 and September 26, AOD measurements show areas of widespread enhanced aerosols over California and Nevada, especially over the Creek Fire and SQF Complex in eastern California (**Figure 3-22**). Areas of enhanced aerosols persist over the California Fires and are transported to the Clark County area by September 25. MODIS AOD retrievals also indicate increased aerosols on the northern edge of Clark County on September 26 (**Figure 3-23**).

CO measurements at 500 hPa from AIRS show a similar pattern of wildfire emission plumes seen in the MODIS AOD data noted above. The map shows widespread enhanced CO at 500 hPa throughout eastern California and central Nevada by September 25 (**Figure 3-24**). Unfortunately, CO measurements from AIRS were unavailable over much of Clark County on September 26. On September 25, relatively small CO concentration enhancements in the Clark County area (<100 ppbv at 500 hPa) extended from the eastern CA fires to the northern edge of Clark County (see **Figure 3-25** for a zoomed-in view of Clark County). Although small upper-level CO enhancements were observed in Clark County, this does not rule out the enhancements of CO at surface level due to the wildfire emission plume transport.

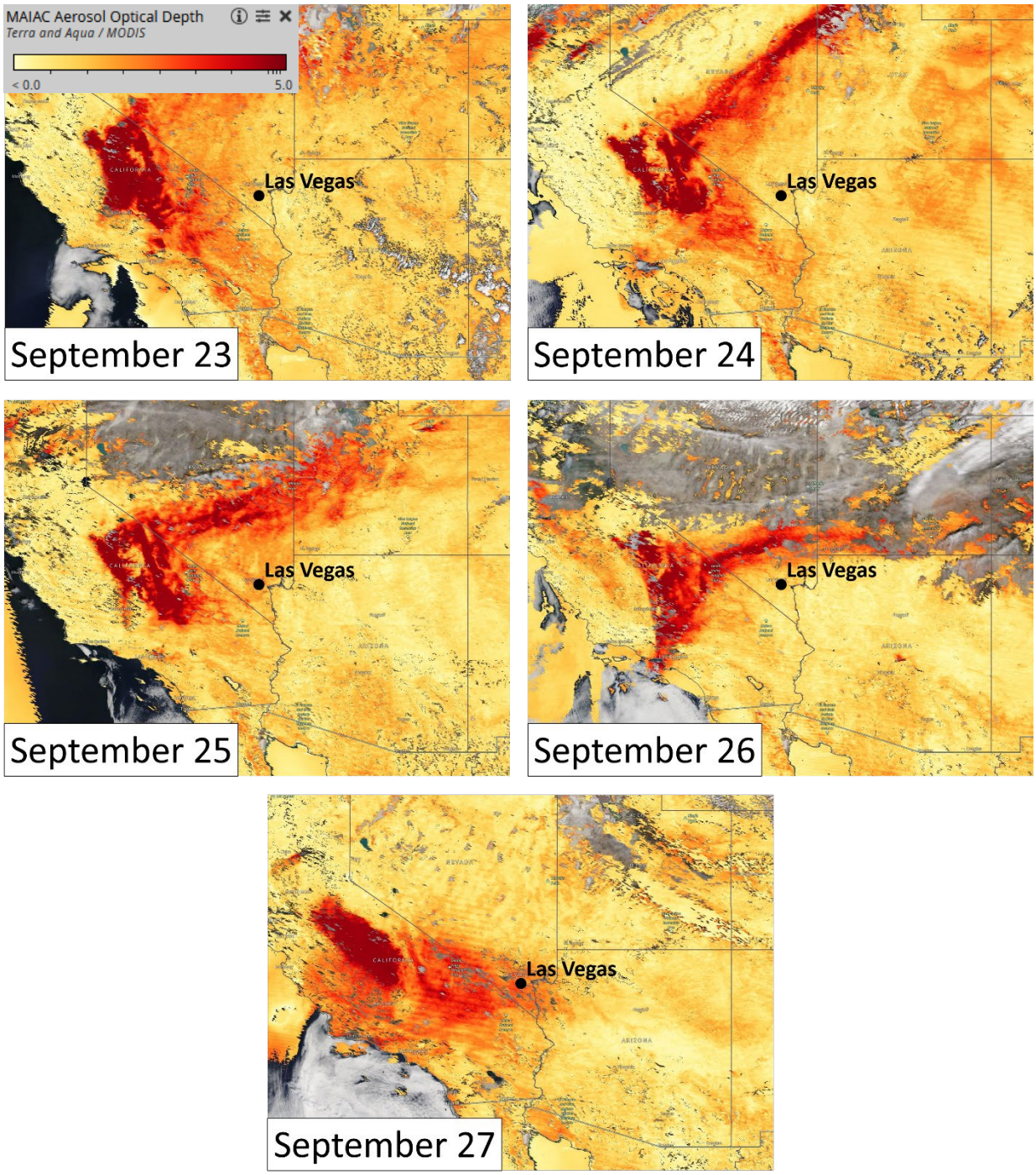

Figure 3-22 MAIAC MODIS Aqua/Terra combined AOD retrievals for the three days before the EE, during the EE on September 26, and the day after the EE are shown.

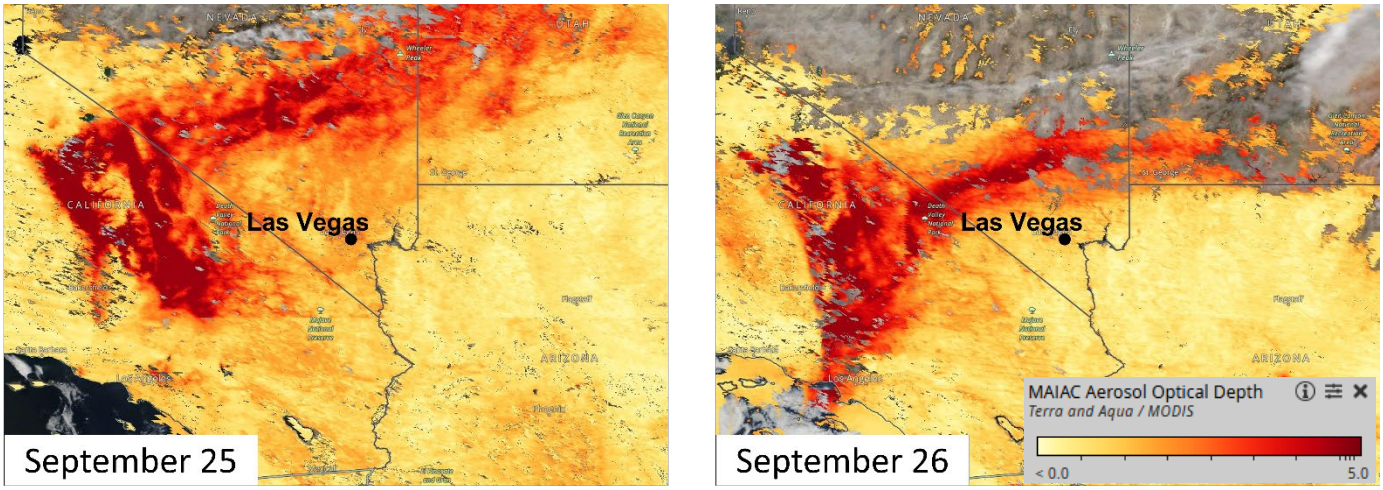

Figure 3-23. A zoomed-in view (over Clark County and wildfires in southern California) of the MAIAC MODIS Aqua/Terra combined AOD retrieval before the EE and during the EE on September 26, 2020.

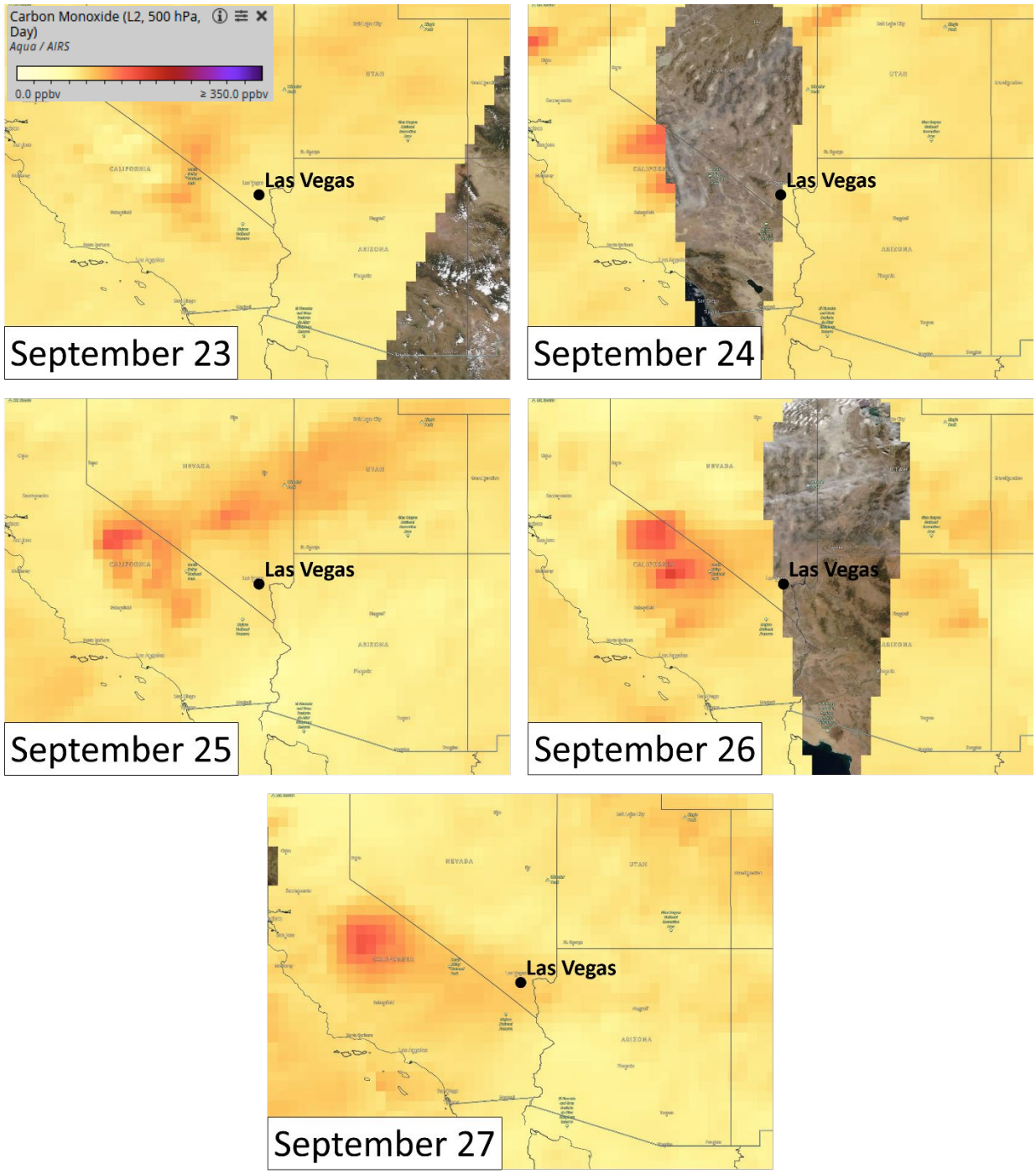

Figure 3-24. MODIS Aqua AIRS CO retrievals for the three days before the EE, during the EE on September 26, 2020, and the day after the EE.

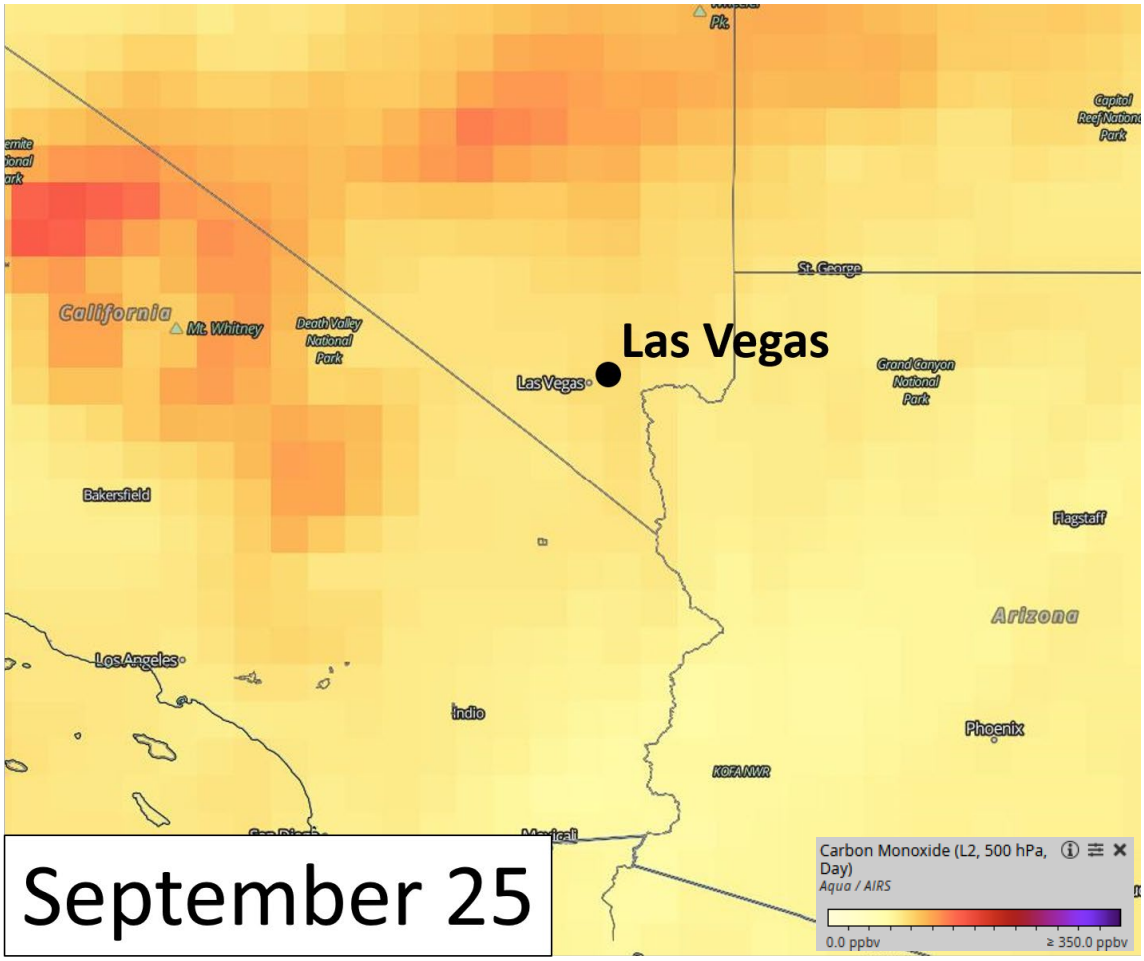

Figure 3-25. A zoomed-in view (over Clark County and wildfires in southern California) of the Aqua AIRS CO retrieval immediately before the EE on September 26, 2020.

3.2.4 Supporting Pollutant Trends and Diurnal Patterns

Ground measurements of wildfire plume components (e.g., $PM_{2.5}$, CO, NO_x, and VOCs) can be used to further demonstrate that smoke impacts ground-level air quality if enhanced concentrations or unusual diurnal patterns are observed. We examined concentrations of $PM_{2.5}$, CO, NO, NO_2, and TNMOC measured at all exceedance sites, as well as other nearby sites in Clark County. If $PM_{2.5}$, CO, NO_x, and VOCs were enhanced at the time the smoke plume arrived in Clark County, these measurements would provide additional supporting evidence of smoke impacts in Clark County.

Figure 3-26 shows an overall view of pollutants measured around Clark County in the week before and after the September 26 event (up to September 30, 2020, the end of the ozone season). The peak daily concentration of $PM_{2.5}$ at exceedance-affected monitoring sites and nearby sites is not

remarkably higher than on days surrounding the event. Similarly, although spikes in NO, NO_2, and TNMOC also occurred on September 26, these increases are similar in magnitude to increases observed on nearby dates. However, as noted in Section 3.1.4, wildfire impact affected the Clark County region throughout this 2-week period. Therefore, these pollutants are potentially elevated above normal levels throughout the window seen in Figure 3-26. The following figures in this section will explore the diurnal trend and concentration of supporting pollutants on September 26 compared to the seasonal average to give a better comparison to expected concentrations.

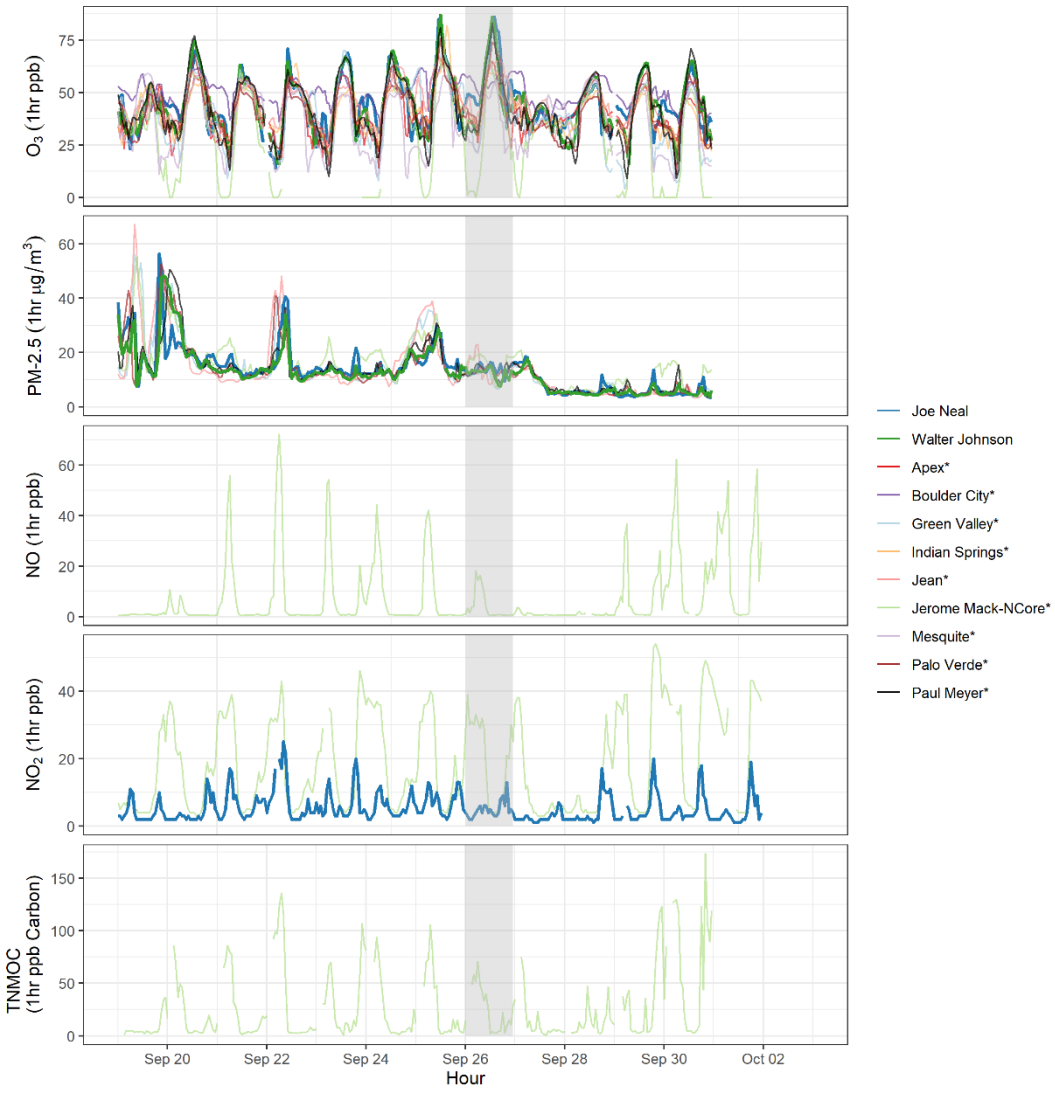

Figure 3-26. Hourly concentrations of ozone, $PM_{2.5}$, and NO_x. Colored lines represent sites in exceedance on September 26. Gray lines represent supporting sites in Clark County. The gray bar represents September 26.

Unusual diurnal patterns of supporting measurements can provide evidence that smoke impacted Clark County air quality. Figure 3-27 shows the diurnal profile for ozone and $PM_{2.5}$ at exceedance-affected sites in Clark County alongside the seasonal (May to September) average ozone and $PM_{2.5}$ diurnal profiles. One year of $PM_{2.5}$ data is available at Walter Johnson and three years of data is available at Joe Neal. On a typical day, the diurnal profile of ozone peaks around midday and shows an overnight trough, while the diurnal profile of $PM_{2.5}$ exhibits slight troughs during the afternoon and near midnight. Both ozone and $PM_{2.5}$ concentrations were elevated well above average at both sites during the daytime on September 26. Plots of $PM_{10}/PM_{2.5}$ are included in Appendix C, and indicate that the contribution of dust to abnormalities in $PM_{2.5}$ concentration are minimal. These coincident observations of elevated ozone and $PM_{2.5}$ concentrations at each exceedance site provide supporting evidence of an abnormal surface-level $PM_{2.5}$ source potentially associated with wildfire smoke.

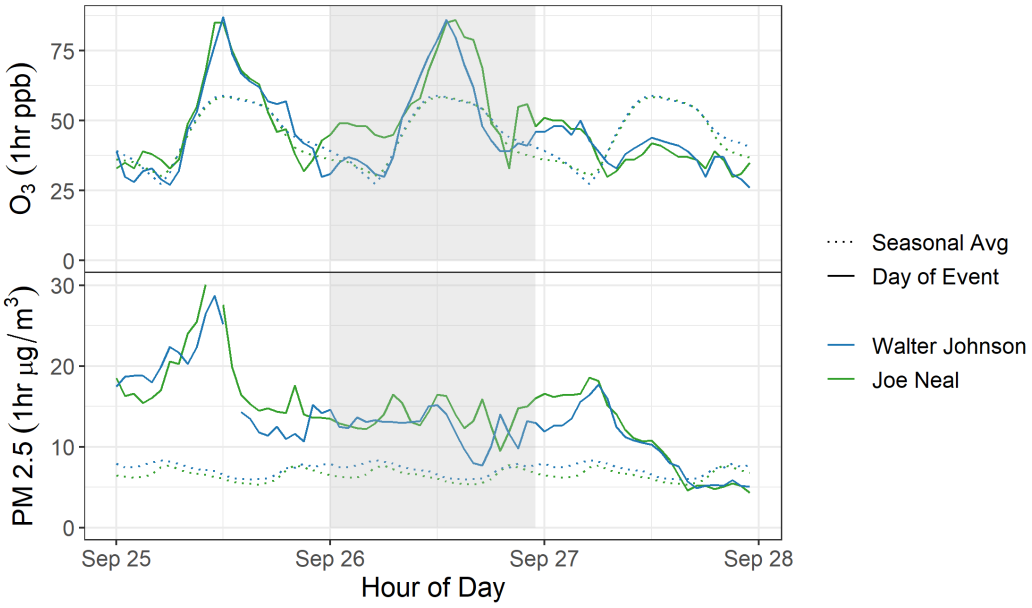

Figure 3-27. September 26 diurnal profile of ozone and $PM_{2.5}$ (solid), and the seasonal (May-Sept.) average (dotted) at sites in exceedance on September 26. 2020.

Figures 3-28 and 3-29 further display the diurnal profile and average seasonal diurnal profile of ozone and $PM_{2.5}$ for each event-affected monitoring site separately, along with the 5th to 95th percentile range of the seasonal diurnal profiles. On September 26, concentrations of ozone at both sites rose above the 95th percentile at their peak value for the day. At both sites, $PM_{2.5}$ concentrations were elevated above average throughout the event day and the prior day (September 25). Furthermore, $PM_{2.5}$ concentrations rose above the 95th percentile at both sites on September 25, and reached a concentration comparable to the 95th percentile value at Joel Neal on September 26.

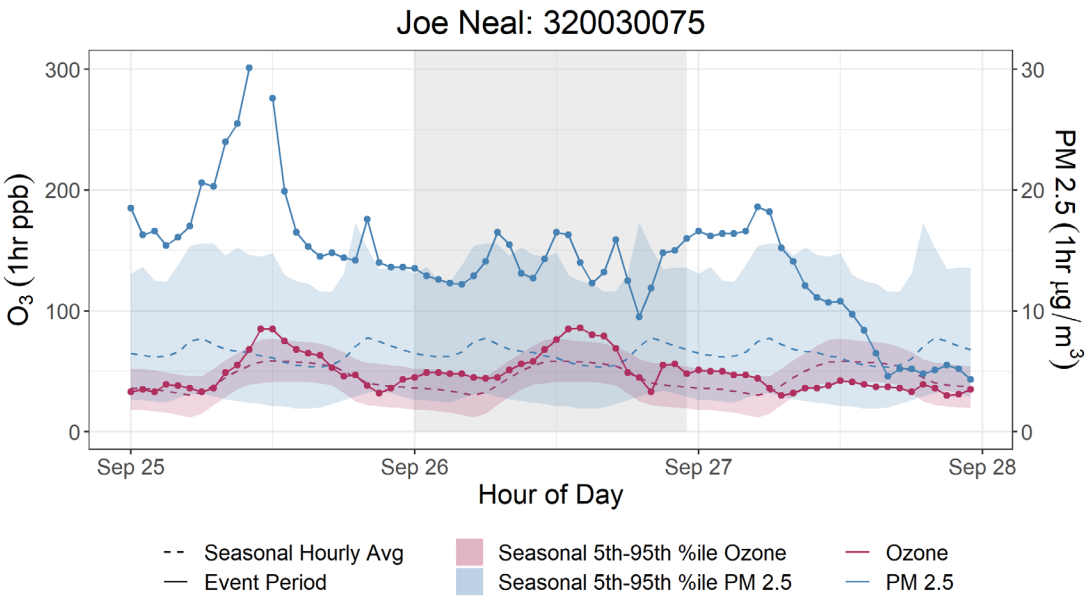

Figure 3-28. Diurnal profile of ozone (red) and $PM_{2.5}$ (blue) concentrations at Joe Neal, including concentrations on September 26 (solid) and the seasonal (May-Sept.) average (dotted). Data from Jerome Mack are plotted for seasonal average $PM_{2.5}$. Shaded ribbons represent the 5th-95th percentile range.

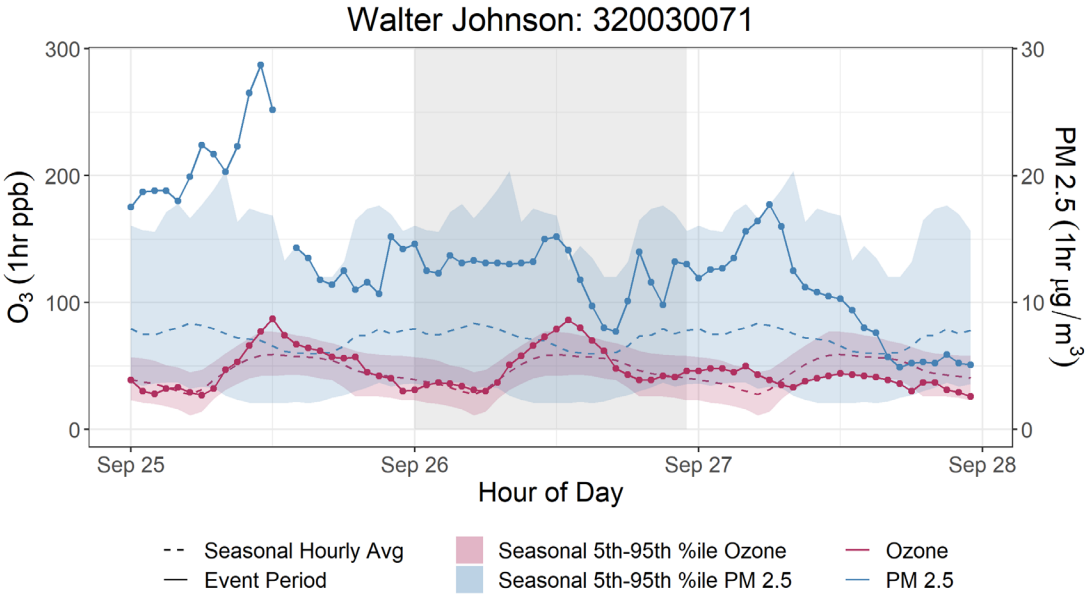

Figure 3-29. Diurnal profile of ozone (red) and $PM_{2.5}$ (blue) concentrations at Walter Johnson, including concentrations on September 26 (solid) and the seasonal (May-Sept.) average (dotted). Data from Jerome Mack are plotted for seasonal average $PM_{2.5}$. Shaded ribbons represent the 5th-95th percentile range.

Two years of CO data are available from Joe Neal, and CO data are not available from Walter Johnson. The diurnal profiles of ozone and CO, along with their seasonal profiles on September 26, are displayed in Figure 3-30. CO levels at Joe Neal were higher than average on the day before and during the afternoon on the event date. During the afternoon on September 26, CO concentrations remained well above average when a minimum CO concentration is expected. The abnormal diurnal pattern of CO throughout the event period lends evidence to an unusual source of CO in the area, supporting the assertion that smoke was present at the surface in Clark County on September 26, 2020.

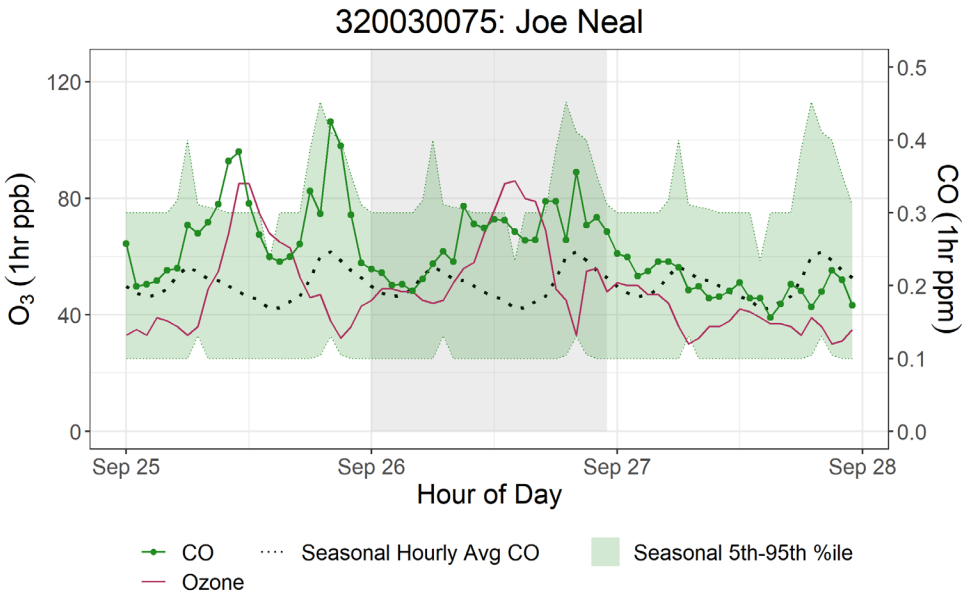

Figure 3-30. Ozone (red) and CO (green) concentrations for Joe Neal on September 26. The dashed line shows the seasonal (May to Sept.) average CO diurnal profile. The green shaded area indicates the seasonal 5th to 95th percentile values for statistical reference. September 26, 2020, is highlighted in gray.

Lastly, concentrations of NO and NO_2 were examined for the September 26 event in Clark County. NO data is available only at the NCore reference site Jerome Mack (five years of data), and this profile is displayed in Figure 3-31. This reference is included to demonstrate any regional abnormalities in NO concentrations during the event period, but should not be considered a proxy for any single event site. The 5-year diurnal NO trend shows a peak in the morning that quickly drops to near-zero values before noon. NO observations on the event date closely followed the diurnal pattern to peak values, but then remained enhanced into the mid-morning, even exceeding the 5-year 95th percentile between 9:00 and 10:00 a.m.

Figures 3-32 and 3-33 show the 5-year diurnal average of NO_2 concentrations at Joe Neal and reference site Jerome Mack, the only sites for which NO_2 data are available. Five years of NO_2 data

are available from Joe Neal, and four years of NO_2 data are available from Jerome Mack. NO_2 concentrations at Joe Neal were elevated well above average during the morning of September 25, the night before the event date, as well as during the evening of the event date. These deviations from the typical diurnal pattern are mirrored at the reference site Jerome Mack, where NO_2 concentrations exceeded the 95th percentile value during all three of these periods. These instances of abnormally high NO_x concentrations during the September 26, 2020, event period in Clark County lend evidence to wildfire emission plume influence at the surface.

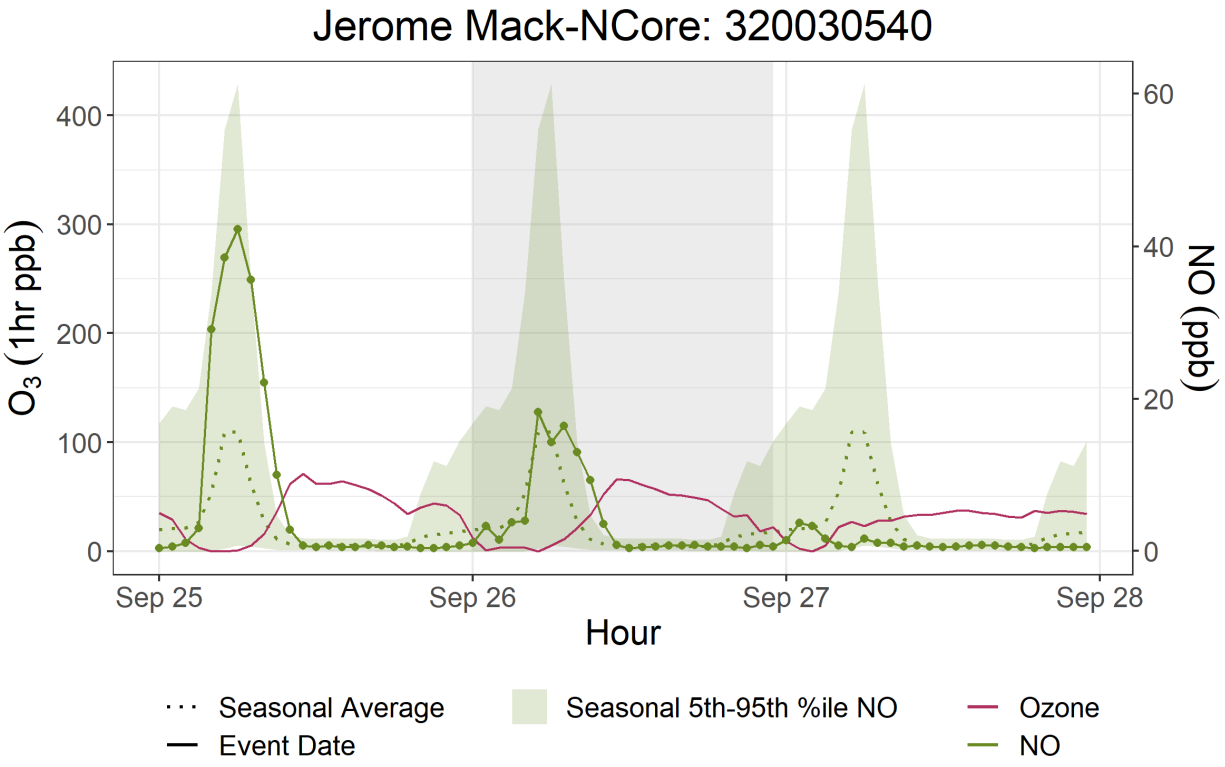

Figure 3-31. Ozone (red) and NO (green) concentrations during the September 26 exceptional event at the Jerome Mack NCore monitoring site. The 5-year seasonal (dotted line) and 5th-95th percentile range (shaded area) is also shown. September 26 is highlighted by the gray shaded area.

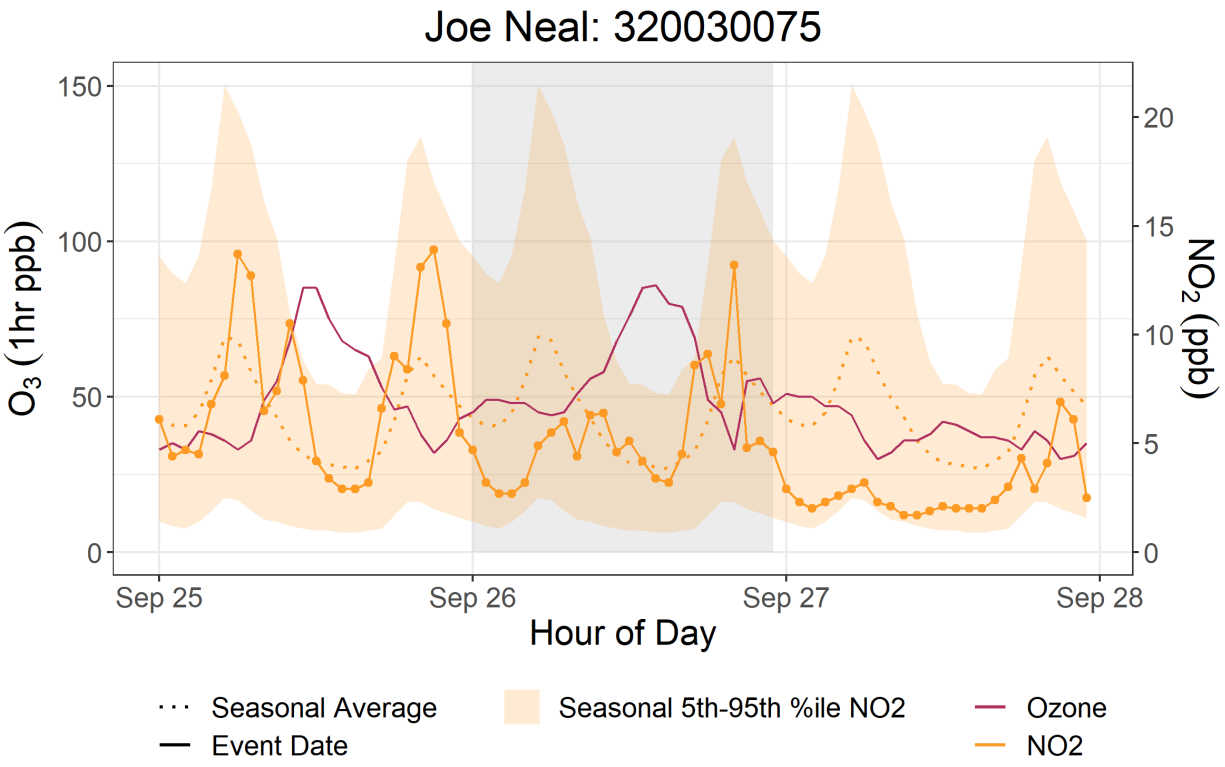

Figure 3-32. Ozone (red) and NO_2 (yellow) concentrations during the September 26 exceptional event at the Joe Neal monitoring site. The 5-year seasonal (dotted line) and 5th-95th percentile range (shaded area) is also shown. September 26 is highlighted by the gray shaded area.

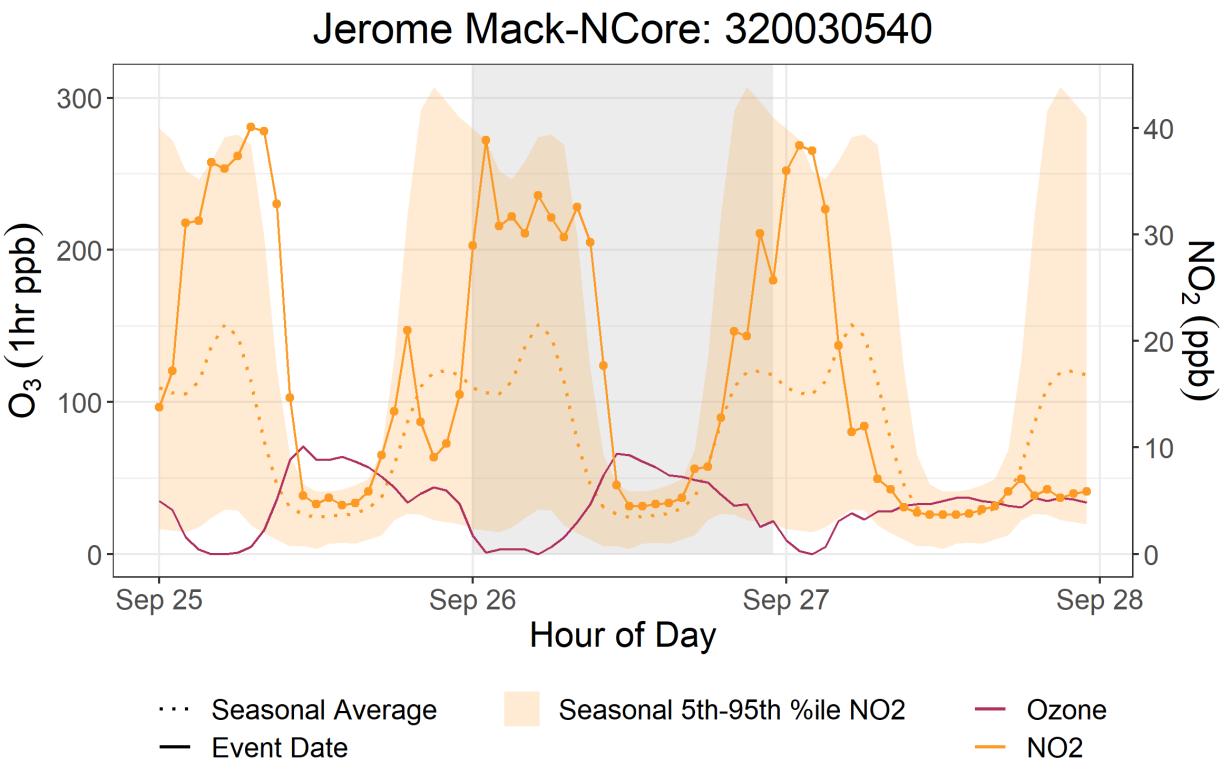

Figure 3-33. Ozone (red) and NO_2 (yellow) concentrations during the September 26 exceptional event at the Jerome Mack NCore monitoring site. The 4-year seasonal (dotted line) and 5th-95th percentile range (shaded area) is also shown. September 26 is highlighted by the gray shaded area.

The supporting pollutant trends and diurnal patterns, showing $PM_{2.5}$, CO, NO_x, and ozone concentrations outside of their normal seasonal or yearly historical averages, provide additional proof of wildfire emission plume impacts on the Clark County area on September 25 and 26, 2020. Wildfires can generate the precursors needed to create ozone, CO, NO_x, and VOCs. While ozone concentrations can be suppressed very near a fire due to NO_x titration, downwind areas are likely to see an increase in ozone concentrations due to the presence of both precursor gases and sufficient UV radiation (i.e., when an air mass leaves an area of very thick smoke that inhibited solar radiation) (Finlayson-Pitts and Pitts Jr, 1997; Jaffe et al., 2008; Bytnerowicz et al., 2010). Ozone precursors from wildfire smoke can also be transported a significant distance downwind, and if these compounds are mixed into an urban area (such as Las Vegas), the resulting ozone concentrations can be significantly higher than they would be from either the smoke plume or the urban area alone (Jaffe et al., 2013; Wigder et al., 2013; Lu et al., 2016; Brey and Fischer, 2016). Since we find evidence of smoke impacts on September 26 in Clark County via supporting pollutant measurements and other analyses in Sections 3.1 and 3.2, we suggest that both the direct transport of ozone and the transport of ozone precursor gases likely caused the ozone exceedance.

Filter samples were also taken at the Jerome Mack (including a collocated sample) monitoring site in Clark County every three days during 2020. From these filter samples, concentrations of levoglucosan (a wildfire smoke tracer) were analyzed by the Desert Research Institute (DRI) via gas chromatography-mass spectroscopy (GC-MS). Levoglucosan is produced by the combustion of cellulose and is emitted during large wildfire events, which can then be transported downwind (Simoneit et al., 1999; Simoneit, 2002; Bhattarai et al., 2019). Levoglucosan has an atmospheric lifetime of one to four days before it is lost due to atmospheric oxidation, and can therefore be used as a tracer of biomass burning (wildfires) far downwind from its source (Hoffmann et al., 2009; Hennigan et al., 2010; Bhattarai et al., 2019; Lai et al., 2014). In the Las Vegas region, residential wood combustion has historically not been a significant contributor to levoglucosan concentrations during the late summer time frame (Kimbrough et al., 2016). Table 3-11 shows levoglucosan concentration, uncertainty, and positive/negative detection certainty on a non-smoke day and on September 27 (used as a proxy for the September 26 EE event). Table 3-11 also shows the average levoglucosan concentration from 19 2018-2019 background days together with its standard deviation, and propagated uncertainty at the Jerome Mack site for comparison. On these background days, no ozone exceedance was observed, and fire/smoke influence was minimal according to HMS. Immediately after the September 26 EE event however, non-zero levoglucosan concentrations and positive detections are seen after smoke is transported to Clark County from the California fires. The 30 ng/m^3 detection of levoglucosan in Clark County at the Jerome Mack monitoring site is significantly higher than the background average of 2±3 ng/m^3, providing certain evidence that wildfire smoke was affecting the area near the time period of the September 26 ozone exceedance.

Table 3-11. Levoglucosan concentrations at monitoring sites around Clark County, Nevada, before and after the September 26 ozone event. Positive or negative detection is also shown.

Sample Date	Sampling Site	Levoglucosan (ng/m^3)	Levoglucosan Uncertainty (ng/m^3)	Levoglucosan Detected?
Background days (2018-2019)	Jerome Mack	2±3	1	N/A
9/27/2020	Jerome Mack	30	3	Positive

3.3 Tier 3 Analyses

3.3.1 Total Column & Meteorological Conditions

Satellite analyses and HYSPLIT trajectories shown in Section 3.1 provide strong evidence that smoke was present over Clark County at the time of the EE on September 26, 2020. However, the visible true color, AOD, and CO satellite data do not provide information about the vertical distribution of visible or measured smoke components. We examined satellite-retrieved aerosol vertical profiles and ceilometer mixing height measurements to determine whether the smoke plume was present at or near the surface on September 26.

The Cloud-Aerosol Light Detection and Ranging (LIDAR) and Infrared Pathfinder Satellite Observation (CALIPSO) system is a remote sensing instrument mounted on the CloudSat satellite that provides vertical profile measurements of atmospheric aerosols and clouds. Detected aerosols are classified into marine, marine mixture, dust, dust mixture, clean/background, polluted continental, smoke, and volcanic aerosol types.

The best CALIPSO aerosol retrieval over Clark County for the September 26 ozone event is available at approximately 2:40 a.m. LST on September 25 (**Figure 3-34 and 3-35**). The CALIPSO vertical profile captures information immediately north of Clark County during the early morning of the day preceding the event. Increased backscatter between the altitudes of approximately 1,000 to 3,000 m AGL provides evidence of increased aerosols at low levels in the vertical columns near Clark County (**Figures 3-36 and 3-37**). Based on the back-scatter profiles, the aerosol type for this backscatter feature is approximated from CALIPSO retrievals to be smoke, indicating the presence of smoke in the mixed layer immediately north of Clark County on September 25.

The mesoscale and local meteorological conditions from September 23 to September 26 provide evidence for the transport of smoke from the fires in eastern and southern California to Clark County, Nevada, and subsequent vertical mixing of smoke from aloft to the surface. Upper-level wind barbs at 500 hPa over southern California and Nevada indicate a weak westerly and northwesterly wind direction facilitating the transport of any upper-level wildfire emission plumes eastward towards Clark County (**Figure 3-38**).

Local observations of mixing heights in the Las Vegas area on September 25 and September 26 suggest that smoke was likely mixed into the lower levels of the atmosphere. Ceilometer data from the Jerome Mack site indicate mixing heights on September 25 and September 26 between approximately 1,725 m and 2,250 m for several hours during each day (**Figure 3-39**). Furthermore, a surface low-pressure system was centered over the border of Nevada and California between September 23 and September 26. Low pressure at the surface is often associated with enhanced vertical mixing in the lower troposphere (**Figure 3-40**). Mixing height data from the ceilometer and the surface weather maps provide evidence of enhanced vertical mixing in the lower troposphere when smoke was present over Clark County.

In addition to the ceilometer-based measurements, vertical temperature profiles (Skew-T diagrams) can be used to estimate mixing heights. The vertical temperature profile at Las Vegas from September 23 and September 26 shows the vertical atmospheric profile becoming drier in the lower troposphere—as exhibited by the widening between the temperature profile and the dewpoint profile—with surface wind directions consistently from the north, northwest, and southwest (Figures 3-41 and 3-42), indicating the potential for smoke transport from the California fires into the mixed layer in Clark County. Enhanced vertical mixing from September 23 and September 26 can be seen from a pronounced, very large mixed layer—as indicated by temperatures decreasing with height roughly along the dry adiabat up to at least 600 hPa—with associated warm temperatures and very dry air. The CALIPSO vertical profile of aerosols over Clark County in the morning of September 25, the upper-level and surface weather maps, the ceilometer data, and the vertical temperature and wind profile suggest the existence of smoke within the mixed layer, the transport of smoke from the fires in California to Clark County, and subsequent mixing in the lower troposphere.

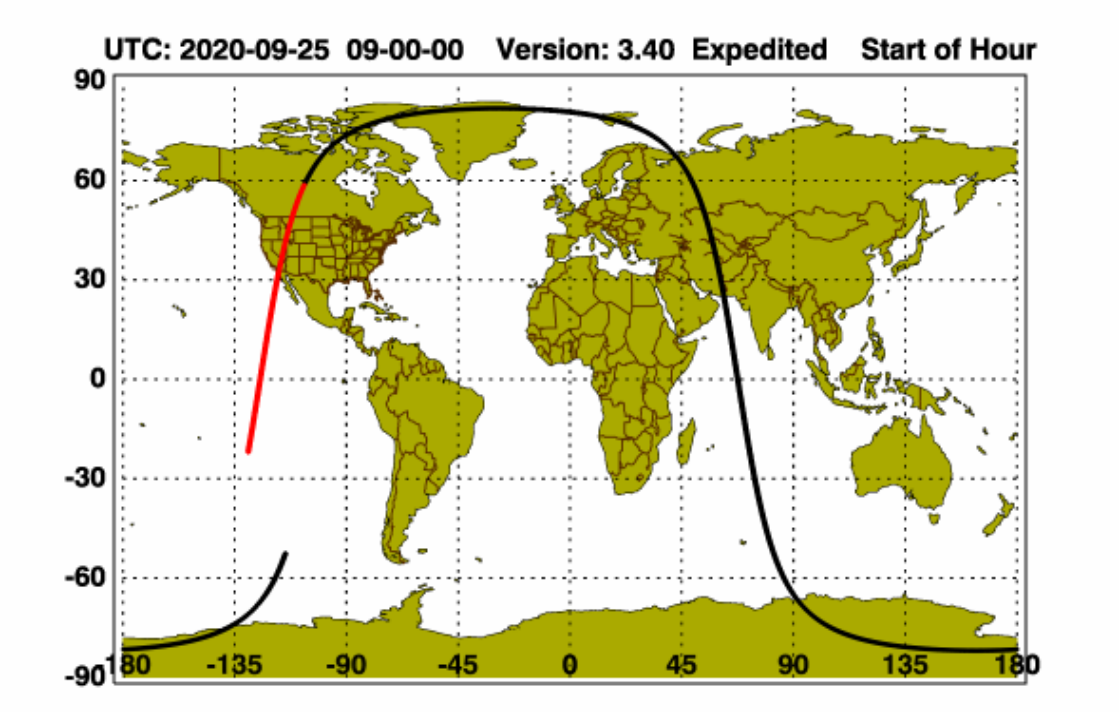

Figure 3-34. The CALIPSO retrieval path for September 25, 2020. This overpass was the closest to Clark County and the nearest in time.

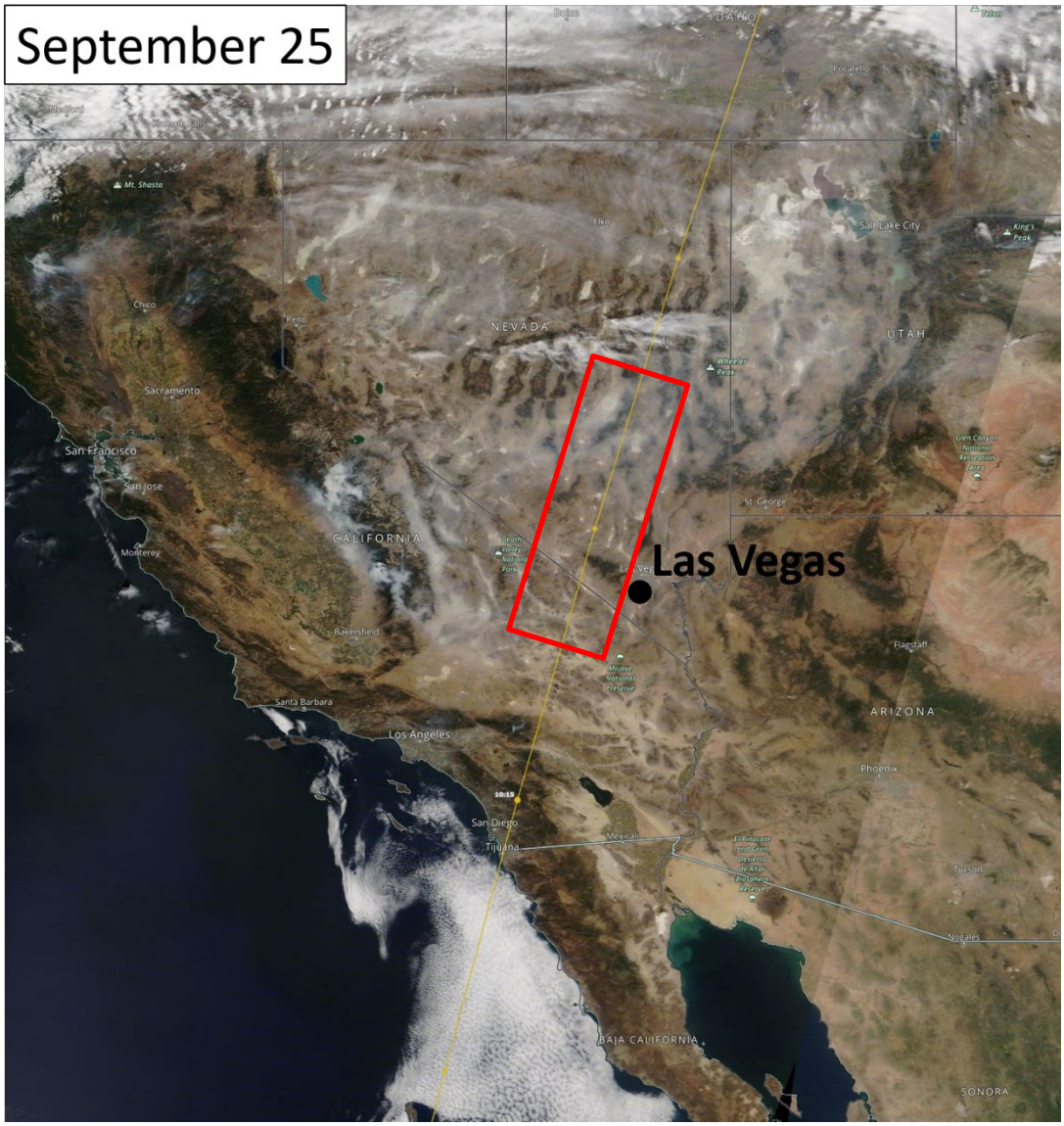

Figure 3-35. The CALIPSO retrieval path for September 25, 2020. This overpass was the closest to Clark County and the nearest in time.

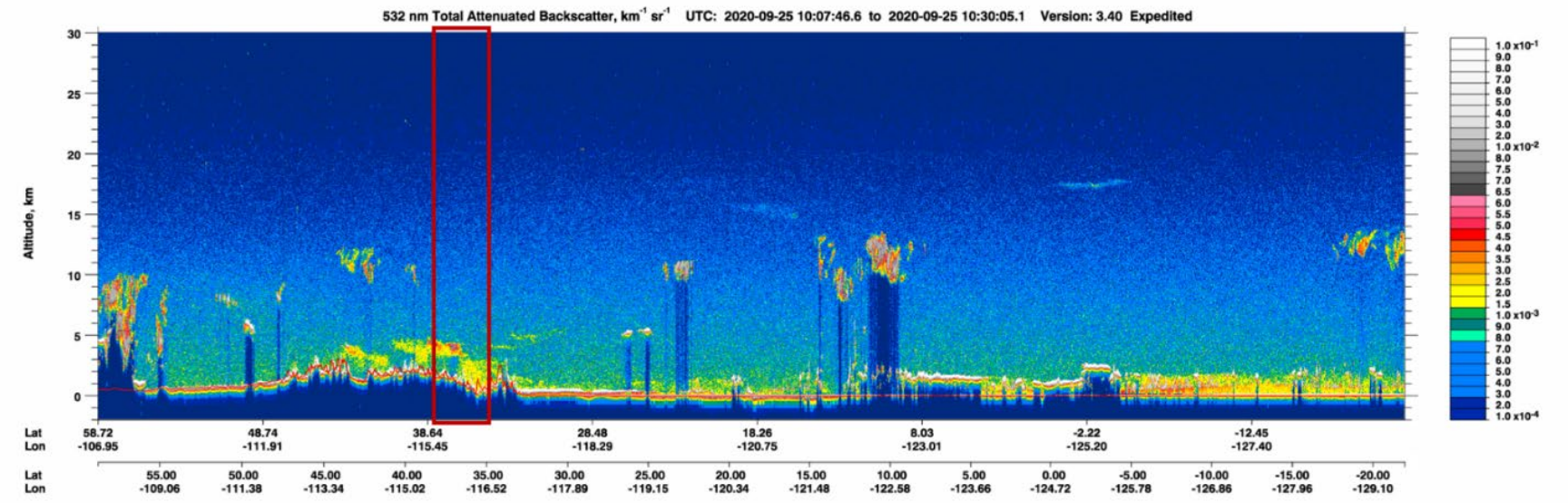

Figure 3-36. CALIPSO total column profile backscatter information for the September 25, 2020, overpass over Clark County, Nevada (approximate areas indicated by a red box).

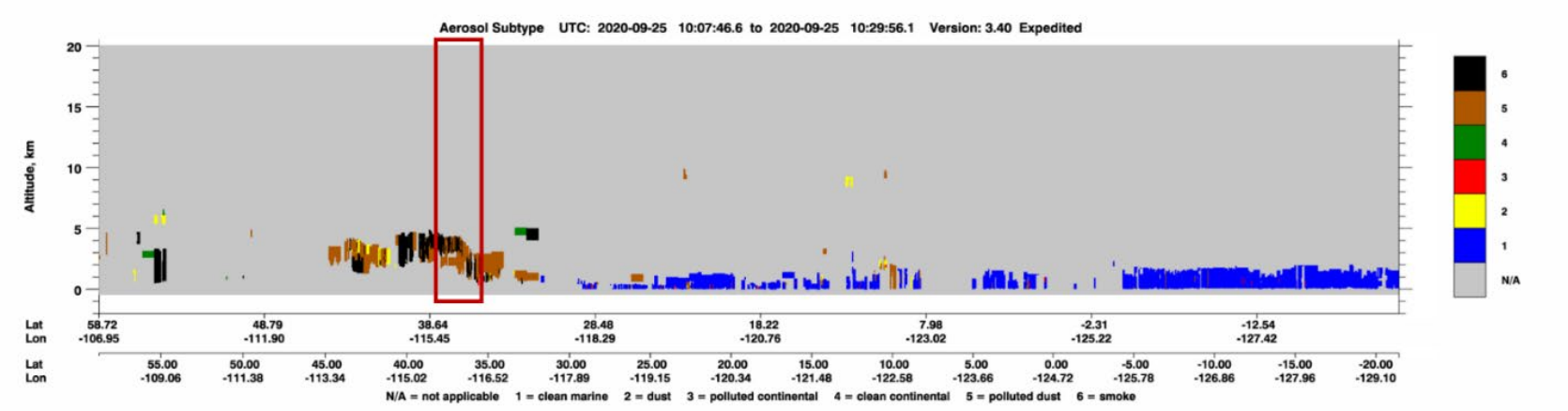

Figure 3-37. CALIPSO total column profile aerosol subtype information for the September 25, 2020, overpass over Clark County, Nevada (approximate areas indicated by a red box).

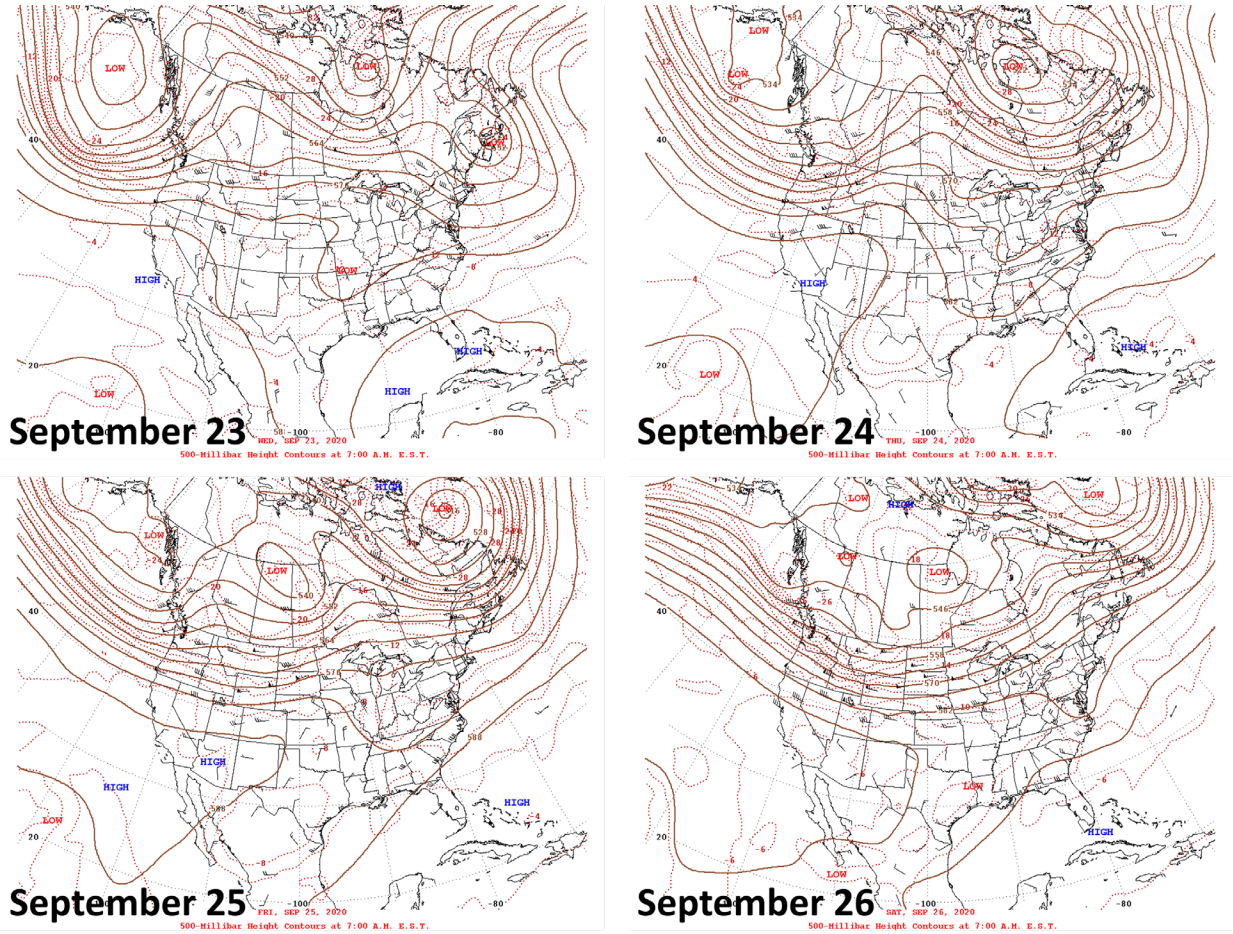

Figure 3-38. Daily upper-level meteorological maps for the three days leading up to the EE and during the September 26 EE.

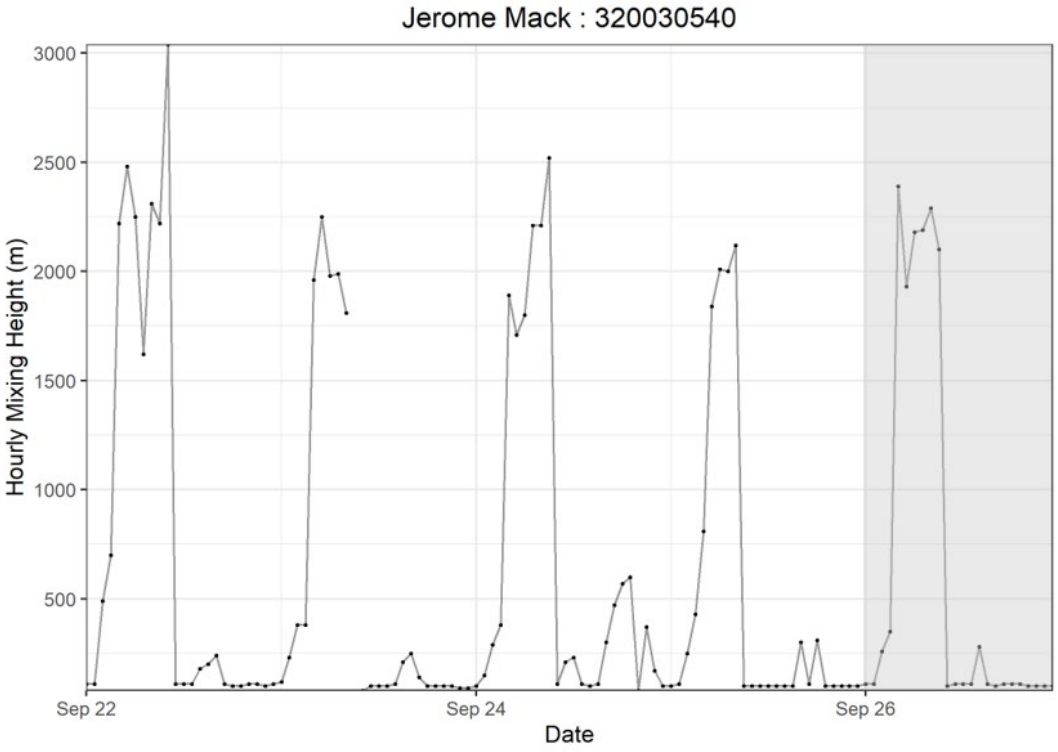

Figure 3-39. Time series of mixing heights taken from Jerome Mack (NCore Site) for two weeks before and after the September 26 EE day. The grey shaded area highlights September 26, 2020.

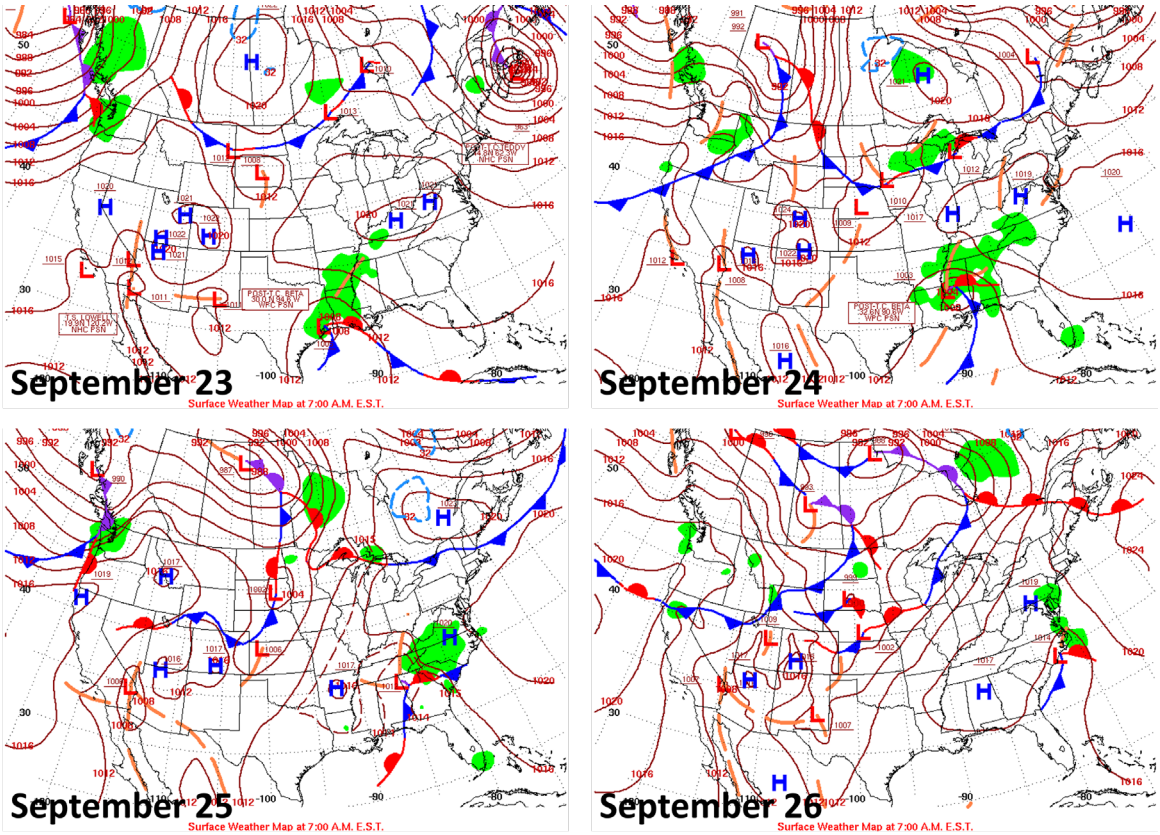

Figure 3-40. Daily surface meteorological maps for the three days leading up to the EE and during the September 26 EE.

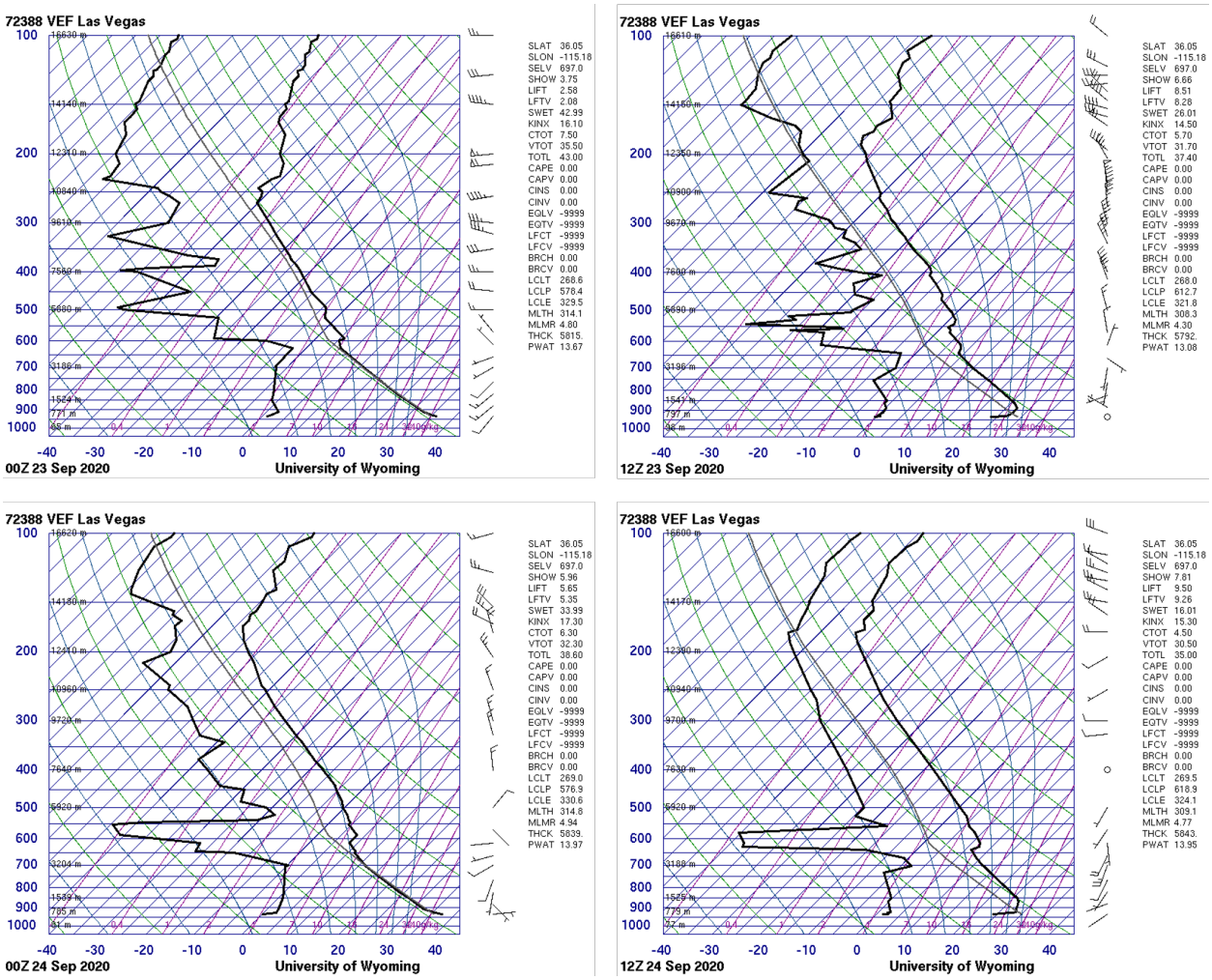

Figure 3-41. Skew-T diagrams from September 23 and 24, 2020, in Las Vegas, Nevada.

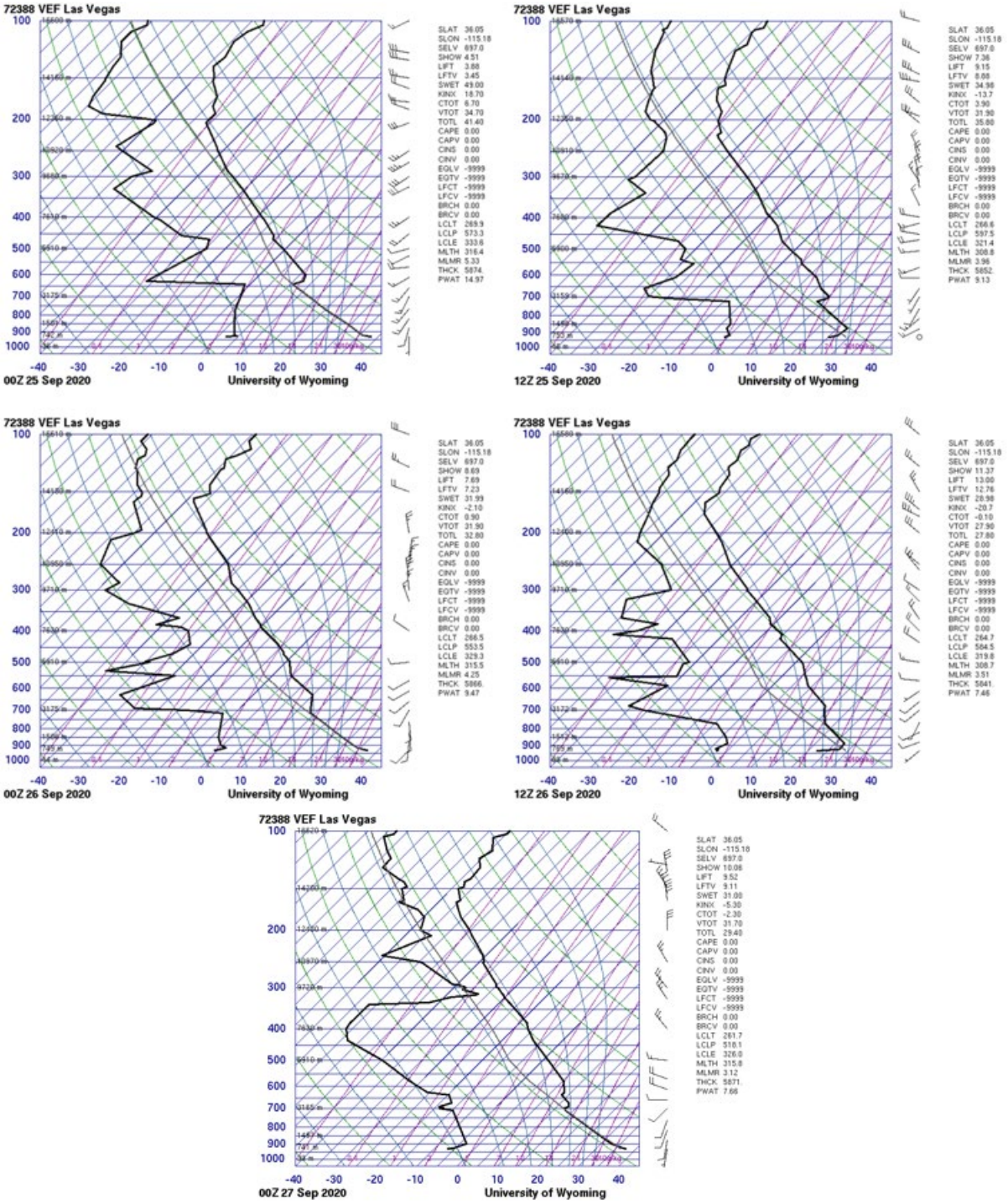

Figure 3-42. Skew-T diagrams from September 25 and 26, 2020, in Las Vegas, Nevada.

3.3.2 Matching Day Analysis

In order to identify the best matching meteorological days, both synoptic and local conditions were examined from ozone-season days (April 1 through September 30) between 2014 and 2020. Excluded from this set are days with suspected EEs in the 2018 and 2020 seasons, as well as dates within five days of the event date, to ensure that lingering effects of smoke transport or stratospheric intrusion did not appear in the data.

To best represent similar air transport, twice daily HYSPLIT trajectories (initiated at 18:00 and 22:00 UTC) from Clark County for 2014-2020 were clustered by total spatial variance. The calculation, based on the difference between each point along a trajectory, provides seven distinct pathways of airflow into Clark County (see Section 3.3.3 for more details). The cluster that best represents the trajectory on the EE day was chosen, and ozone-season days within the cluster were then subset for regional meteorological comparison to the EE day.

For the meteorological comparison, a correlation score was assigned to each day from the cluster subset. The National Centers for Environmental Prediction (NCEP) reanalysis data were compiled for the ozone seasons in 2014-2020. Daily average wind speed, geopotential height, relative humidity, and temperature were considered at 1,000 mb and 500 mb. At the surface, daily average atmospheric pressure, maximum temperature, and minimum temperature were utilized. Pearson product-moment coefficient of linear correlation (pattern correlation) was calculated between the EE date and each cluster-subset ozone-season day in 2014-2020 for each parameter. The pattern correlation calculates the similarity between two mapped variables at corresponding grid locations within the domain. The statistic was calculated using a regional domain of 30°N-45°N latitude and 125°W-105°W longitude. The correlation score for each day was defined as the average pattern correlation of all parameters at each height. The correlation scores were then ranked by the highest correlation for 1,000 mb, surface, and 500 mb. Dates within five days of the EE were removed from the similar day analysis to ensure the data are mutually exclusive. The 50 dates with the highest rank correlation scores were then chosen as candidate matching days for further analysis.

Local meteorological conditions for the subset of candidate matching days were then compared to conditions on September 26, 2020, and filtered to identify five or more days that best matched the event date. Meteorological maps at the surface and 500 mb, and local meteorological data describing temperature, wind, moisture, instability, mixing layer height, and cloud cover were examined. The data source for each parameter is summarized in Table 3-12.

Table 3-12. Local meteorological parameters and their data sources.

Meteorological Parameter	Data Source
Maximum daily temperature	Jerome Mack - NCore Monitoring Site
Average daily temperature	Jerome Mack - NCore Monitoring Site
Resultant daily wind direction	Jerome Mack - NCore Monitoring Site (calculated vector average)
Resultant daily wind speed	Jerome Mack - NCore Monitoring Site (calculated vector average)
Average daily wind speed	Jerome Mack - NCore Monitoring Site
Average daily relative humidity (RH)	Jerome Mack - NCore Monitoring Site
Precipitation	Jerome Mack - NCore Monitoring Site
Total daily global horizontal irradiance (GHI)	UNLV Measurement and Instrumentation Data Center (MIDC) in partnership with NREL (https://midcdmz.nrel.gov/apps/daily.pl?site=UNLV&start=20060318&yr=2021&mo=4&dy=29)
4:00 p.m. local standard time (LST) mixing layer mixing ratio	Upper air soundings from KVEF (http://weather.uwyo.edu/upperair/sounding.html)
4:00 p.m. LST lifted condensation level (LCL)	Upper air soundings from KVEF (http://weather.uwyo.edu/upperair/sounding.html)
4:00 p.m. LST convective available potential energy (CAPE)	Upper air soundings from KVEF (http://weather.uwyo.edu/upperair/sounding.html)
4:00 p.m. LST 1000-500 mb thickness	Upper air soundings from KVEF (http://weather.uwyo.edu/upperair/sounding.html)
Daily surface meteorological map	NOAA's Weather Prediction Center Daily Weather Maps (https://www.wpc.ncep.noaa.gov/dailywxmap/index.html)
Daily 500 mb meteorological map	NOAA's Weather Prediction Center Daily Weather Maps (https://www.wpc.ncep.noaa.gov/dailywxmap/index.html)

Matching Day Analysis

The meteorological conditions on September 26, 2020, were fairly normal for the region at this time of year. Table 3-13 displays that the percentile ranking of each examined meteorological parameter other than relative humidity at the Jerome Mack-NCore site falls within the 5th to 95th percentile range among seven years of observations for the 30-day period surrounding September 26 (September 11 through October 11) with the exception of 500-1,000 mb thickness, which was unusually high (99th percentile). Measurement summaries over this 30-day period best represent the expected conditions on the event date. The maximum temperature on September 26 was above the median for this time of year, which is reflected in the low relative humidity. The relative humidity is at the 8th percentile. As is typical for Clark County during this period, there was no precipitation.

Table 3-13. Percentile rank of meteorological parameters on September 26, 2020, compared to the 30-day period surrounding September 26 over seven years (September 11 through October 11, 2014-2020). The percentile ranking of precipitation is marked NA because a vast majority of examined days recorded 0 inches. The percentile ranking of a directional degree value is irrelevant and has been marked NA.

Date	Max Temp (°F)	Avg Temp (°F)	Resultant Wind Direction (°)	Resultant Wind Speed (mph)	Avg Wind Speed (mph)	Avg RH (%)	Precip (in)	Total GHI (kWh/m^2)	Mixing Layer Mixing Ratio (g/kg)	LCL (mb)	CAPE (J/kg)	500-1,000 mb Thickness (m)
2020-09-26	82	72	NA	31	33	8	NA	62	18	2	76	99

The subset of synoptically similar days identified according to the methodology above was further filtered based on parameters listed in Table 3-12 to match local meteorological conditions that existed on the event date. Table 3-14 shows the 11 days that best match the meteorological conditions that existed on September 26, 2020, as well as the MDA8 ozone concentration at each site that experienced an ozone exceedance on September 26, 2020. June 14, 2017, was identified as a meteorologically similar day, however the FAST-LVOS study that occurred from late spring through early summer in 2017 identified that a stratospheric intrusion significantly contributed to the ozone exceedance in Clark County on June 14, 2017. Therefore, this date has been excluded from the analysis (Langford and Senff, 2019). Weather maps for September 26, 2020, and each date listed in Table 3-14, show highly consistent conditions, with a surface low-pressure system and an upper-level region of either low-gradient or relatively high pressure over Clark County. Most dates also had a surface high to the east. Surface and upper-level maps are included in Appendix D.

Table 3-14 shows the average MDA8 ozone concentration across these 11 days with a range defined by one standard deviation, a conservative estimate given the small sample size. The expected MDA8 ozone concentration, given similar meteorological conditions to those on the event date, is below the 70-ppb ozone standard at each site, ranging from 65 to 66 ppb. Further, the upper end of the provided range at each site does not exceed the ozone standard. Only one date out of the 11, June 8, 2018, exceeds the 70-ppb ozone standard on a day when morning transport came directly from the Los Angeles basin and the HRRR model showed effects of smoke on this day (see Appendix D). However, because the HYSPLIT model did not intersect smoke and there were no fires immediately upwind, this date was not excluded from the analysis. Several similar dates with higher photochemical potential than September 26 (lower wind speeds, higher average temperatures, and greater solar irradiance) did not exceed the ozone standard. Thus, an ozone exceedance on September 26, 2020, was unexpected based on meteorological conditions alone. If meteorology were the sole cause of the ozone exceedance on September 26, 2020, we would expect to see similarly high ozone levels on each of the similar days listed in Table 3-14, especially those with even warmer average temperatures than experienced on September 26, alongside other similar conditions.

Table 3-14. Top 11 matching meteorological days to September 26, 2020. WJ and JN refer to monitoring sites Walter Johnson and Joe Neal, respectively. Average MDA8 ozone concentration of meteorologically similar days is shown plus-or-minus one standard deviation rounded to the nearest ppb.

Date	Max Temp (°F)	Avg Temp (°F)	Resultant Wind Direction (°)	Resultant Wind Speed (mph)	Avg Wind Speed (mph)	Avg RH (%)	Precip (in)	Total GHI (kWh/m^2)	Mixing Layer Mixing Ratio (g/kg)	LCL (mb)	CAPE (J/kg)	500-1,000 mb Thickness (m)	MDA8 Ozone Concentration (ppb)	
													WJ	JN
2020-09-26	100	85.83	118.36	1.17	2.25	13.71	0	6.01	3.12	518.14	0	5871	71	75
2014-08-31	106	94	158.13	1.82	2.81	13.38	0	7.15	4.99	560.81	0	5896	59	NA
2017-06-02	101	86.92	132.47	0.18	1.18	12.83	0	8.76	3.58	549.62	0	5804	68	65
2017-06-29	108	96.12	147.42	2.85	3.69	7.96	0	8.95	3.5	510.18	0	5878	67	70
2018-06-08	103	90.62	140.86	1.4	3.1	8.83	0	8.83	4.58	564.05	0	5828	74	71
2018-09-01	103	89.67	57.17	0.35	1.79	11.46	0	6.69	4.11	542.95	0	5848	65	66
2019-08-12	105	91.71	113.79	0.96	2.59	13.75	0	7.99	5.17	566.09	0	5855	57	57
2020-06-15	100	88.92	171.55	3.74	4.82	12.12	0	8.56	4.1	557.15	0	5845	60	61
2020-06-21	108	96.38	125.64	2.14	2.84	8.42	0	8.76	4.73	538.65	0	5898	63	67
2020-07-10	110	97.29	115.69	1.14	2.44	6.46	0	8.62	6.13	565.7	0	5917	68	66
2020-08-04	107	96.25	143.24	3.1	4.29	5	0	8.03	5.21	550.72	0	5896	64	67
2020-09-25	101	87.46	148.59	1.53	3.12	13.96	0	5.82	4.25	553.54	0	5866	69	70
Average MDA8 Ozone Concentration of Meteorologically Similar Days													**65 ± 5**	**66 ± 4**

These findings show that an external source of ozone contributed to the ozone exceedance on September 26, 2020. All examined meteorological parameters besides 500-1,000 mb thickness fall between the 5th and 95th percentile. Our analysis expanded on methods shown in the EPA guidance and a previously concurred EE to identify 11 days that are meteorologically similar to September 26, 2020 (Arizona Department of Environmental Quality, 2018). The expected MDA8 ozone concentration at each site is over 5 ppb below the concentrations measured at each site on September 26, 2020. Based on this evidence, it is unlikely that meteorology alone enhanced photochemical production of ozone enough to cause an exceedance on September 26, 2020. This validates the existence of an extrinsic ozone source on September 26, 2020.

3.3.3 GAM Statistical Modeling

Generalized additive models (GAM) are a type of statistical model that allows the user to predict a response based on linear and non-linear effects from multiple variables (Wood, 2017). These models tend to provide a more robust prediction than Eulerian photochemical models or simple comparisons of similar events (Simon et al., 2012; Jaffe et al., 2013; U.S. Environmental Protection Agency, 2016). Camalier et al. (2007) successfully used GAM modeling to predict ozone concentrations across the eastern United States using meteorological variables with r^2 values of up to 0.8. Additionally, previous concurred exceptional event demonstrations and associated literature, i.e., Sacramento Metropolitan Air Quality Management District (2011), Alvarado et al. (2015), Louisiana Department of Environmental Quality (2018), Arizona Department of Environmental Quality (2016), and Pernak et al. (2019) used GAM modeling to predict ozone events that exceed the NAAQS standards, some in EE cases. By comparing the GAM-predicted ozone values to the actual measured ozone concentrations (i.e., residuals), we can determine the effect of outside influences, such as wildfires or stratospheric intrusions, on ozone concentrations each day (Jaffe et al., 2004). High, positive residuals suggest a non-typical source of ozone in the area but cannot specifically identify a source. Gong et al. (2017) and McClure and Jaffe (2018) used GAM modeling, in addition to ground and satellite measurements of wildfire pollutants, to estimate the enhancement of ozone during wildfire smoke events. Similar to other concurred EE demonstrations, we used GAM modeling of meteorological and transport variables to estimate the MDA8 ozone concentrations at multiple sites across Clark County for 2014-2020. To estimate the effect of wildfire smoke on ozone concentrations, we can couple the GAM residual results (observed MDA8 ozone–GAM-predicted MDA8 ozone) with the other analyses to confirm that the non-typical enhancement of ozone is due to wildfires on September 26, 2020.

Using the same GAM methodology as prior concurred EE demonstrations and the studies mentioned above, we examined more than 30 meteorological and transport predictor variables, and through testing, compiled the 16 most important variables to estimate MDA8 ozone each day at eight monitoring sites across Clark County, Nevada (Paul Meyer, Walter Johnson, Joe Neal, Green Valley, Boulder City, Jean, Indian Springs, and Jerome Mack). As suggested by EPA guidance (U.S. Environmental Protection Agency, 2016), we used meteorological variables measured at each station

(the previous day's MDA8 ozone, daily min/max temperature, average temperature, temperature range, wind speed, wind direction, or pressure), if available (see Table 2-1). If meteorological variables were not available at a specific site, we supplemented the data with National Centers for Environmental Prediction (NCEP) reanalysis meteorological data to fill any data gaps. We also tested filling data gaps with Jerome Mack meteorological data and found results had no statistical difference. We used sounding data from KVEF (Las Vegas Airport) to provide vertical meteorological components; soundings are released at 00:00 and 12:00 UTC daily. Variables such as temperature, relative humidity, wind speed, and wind direction were averaged over the first 1000 m above the surface to provide near-surface, vertical meteorological parameters. Other sounding variables, such as Convective Available Potential Energy (CAPE), Lifting Condensation Level (LCL) pressure, mixing layer potential temperature, mixed layer mixing ratio, and 500-1,000 hPa thickness provided additional meteorological information about the vertical column above Clark County. We also initiated HYSPLIT GDAS 1°x1° 24-hour back trajectories from downtown Las Vegas (36.173° N, -115.155° W, 500 m agl) at 18:00 and 22:00 UTC (10:00 a.m. and 2:00 p.m. local standard time) each day to provide information on morning and afternoon transport during critical ozone production hours. We clustered the twice-per-day back trajectories from 2014-2020 into seven clusters. **Figure 3-43** shows the clusters, percentage of trajectories per cluster, and heights of each trajectory cluster. We identified a general source region for each cluster: (1) Northwest U.S., (2) Stagnant Las Vegas, (3) Central California, (4) Long-Range Transport, (5) Northern California, (6) Southern California, and (7) Baja Mexico. Within the GAM, we use the cluster value to provide a factor for the distance traveled by each back trajectory. Additionally, day of year (DOY) was used in the GAM to provide information on season and weekly processes. The year (2014, 2015, etc.) was used a factor for the DOY parameter to distinguish interannual variability.

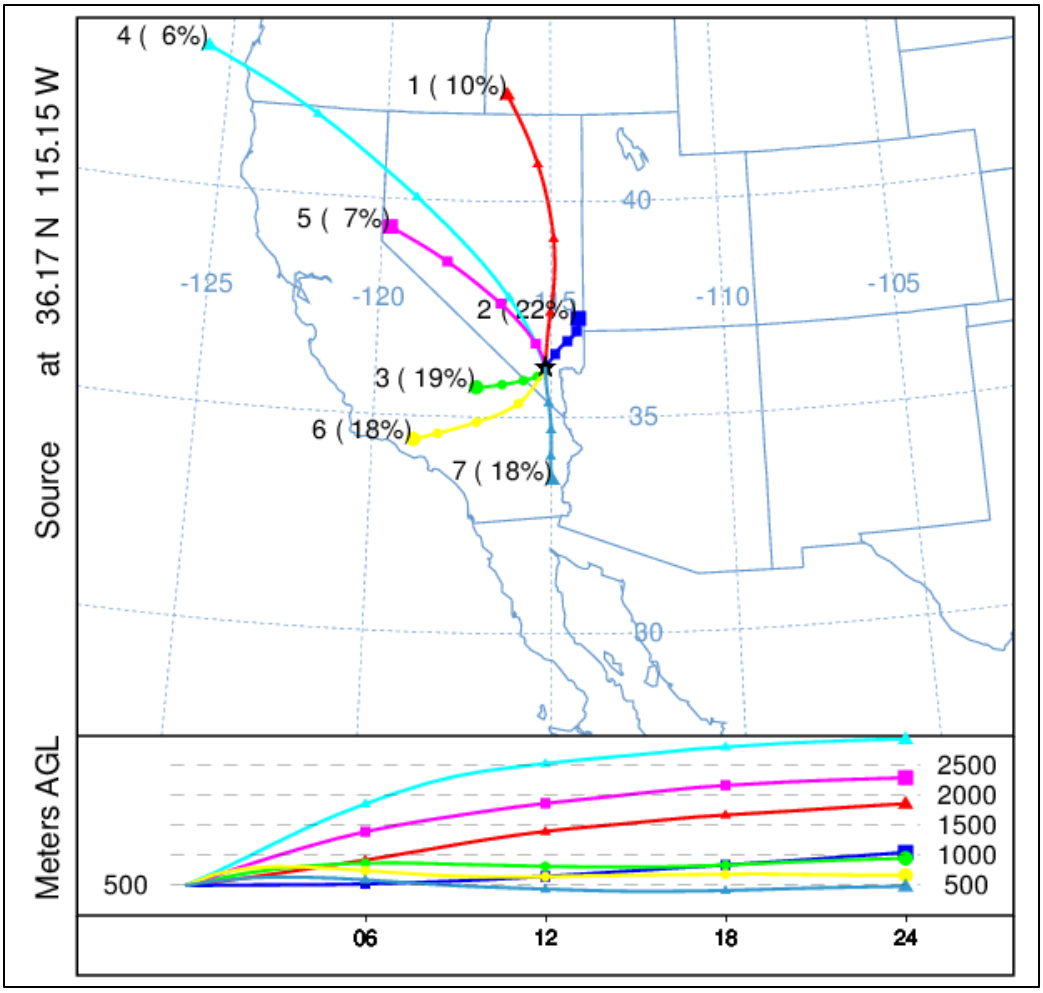

Figure 3-43 Clusters for 2014-2020 back trajectories. Seven unique clusters were identified for the twice daily (18:00 and 22:00 UTC) back-trajectories for 2014-2020 initiated in the middle of the Las Vegas Valley. The percentage of trajectories per cluster is shown next to the cluster number, and the height of each cluster is shown below the map.

Once all the meteorological and transport variables were compiled, we inserted them into the GAM equation to predict MDA8 ozone:

$$g(MDA8\ O_{3,i}) = f_1(V1_i) + f_2(V2_i) + f_3(V3_i) + \cdots + residual_i$$

where f_i are fit functions calculated from penalized cubic regression splines of observations (allowing non-linearity in the fit), Vi are the variables, and i is the daily observation. All variables were given a cubic spline basis except for wind direction, which used a cyclic cubic regression spline basis. For DOY and back trajectory distances, we used year factors (i.e., 2014-2020) and cluster factors (i.e., 1-7) to distinguish interannual variability and source region differences. The factors provide a different smooth function for each category (Wood, 2017). For example, the GAM smooth of DOY for 2014 can

be different than 2015, 2016, etc. In order to optimize the GAM, we first must adjust knots or remove any variables that are over-fitting or under-performing. We used the "mgcv" R package to summarize and check each variable for each monitoring site (Wood, 2020). A single GAM equation (using the same variables) was used for each monitoring site for consistency. During the initial optimization process, we removed the proposed 2018 and 2020 EE days from the dataset. We also ran 10 cross-validation tests by randomly splitting data 80/20 between training/testing for each monitoring site to ensure consistent results. All cross-validation tests showed statistically similar results with no large deviations for different data splits. We used data from each site during the April -September ozone seasons for 2014 through 2020, which is consistent with other papers modeling urban ozone (e.g., Pernak et al., 2019; McClure and Jaffe, 2018; Solberg et al., 2019; Solberg et al., 2018) and ozone concentrations during the periods with exceptional events are within the representative range of ozone in the GAM model.

Table 3-15 shows the variables used in the GAM and their F-value. The F-value suggests how important each variable is (higher value = more important) when predicting MDA8 ozone. Any bolded F-values had a statistically significant correlation ($p < 0.05$). R^2, the positive 95th quantile of residuals, and normalized mean square residual values for each monitoring site are listed at the bottom of the table.

Table 3-15. GAM variable results. F-values per parameter used in the GAM model are shown for each site. Units and data sources for each parameter in the GAM model are shown on the right of the table. The 95th quantile, R^2, and normalized mean square residual information are shown at the bottom of the table.

Parameters	Paul Meyer	Walter Johnson	Joe Neal	Green Valley	Jerome Mack	Boulder City	Jean	Indian Springs	Unit	Source
Day of Year (DOY) factored by Year (2014-2020)	**8.11**	**7.09**	**7.65**	**11.8**	**7.94**	**7.11**	**8.68**	**7.53**	--	--
Previous Day MDA8 Ozone	**37.9**	**22.7**	**41.5**	**18.1**	**27.9**	**31.3**	**105.5**	**123.8**	ppb	Monitor Data
Average Daily Temperature	1.92	**2.90**	**4.80**	0.05	1.83	2.13	0.12	1.83	K	Monitor Data/NCEP Reanalysis
Maximum Daily Temperature	1.37	**2.74**	**2.48**	0.16	0.38	0.02	1.30	1.52	K	
Temperature Range (TMax - TMin)	**4.12**	2.13	1.38	1.74	1.77	1.51	0.50	0.54	K	
Average Daily Pressure	**5.54**	**6.42**	**6.74**	**4.64**	**2.94**	0.22	2.17	0.24	hPa	
Average Daily Wind Speed	**11.1**	**5.03**	**7.49**	**5.02**	**15.3**	0.07	0.49	2.19	knots	
Average Daily Wind Direction	0.47	**1.04**	0.24	**1.35**	**2.43**	0.69	0.11	**2.48**	deg	
18 UTC HYSPLIT Distance factored by Cluster	1.70	1.82	1.69	0.92	2.52	2.97	1.66	1.03	km	HYSPLIT Back-Trajectories
22 UTC HYSPLIT Distance factored by Cluster	1.03	0.74	1.47	1.47	1.20	1.26	1.19	0.50	km	
00 UTC Convective Available Potential Energy	3.50	0.13	0.37	1.17	1.16	0.57	**5.71**	**6.49**	J/kg	Sounding Data
00 UTC Lifting Condensation Level Pressure	1.36	**2.78**	2.29	2.41	**3.76**	0.38	1.43	0.38	hPa	
00 UTC Mixing Layer Potential Temperature	0.65	0.79	1.72	0.10	1.23	0.97	1.09	2.53	K	
00 UTC Mixed Layer Mixing Ratio	**2.10**	**2.76**	**2.85**	**3.09**	**3.07**	**2.42**	0.69	1.04	g/kg	
00 UTC 500-1000 hPa Thickness	**2.91**	0.43	1.70	1.60	1.69	**4.11**	**2.18**	1.83	m	
12 UTC 1km Average Relative Humidity	**12.4**	**14.6**	**17.8**	**21.3**	**37.5**	**26.0**	**11.1**	2.18	%	
95th Quantile of Positive Residuals (ppb)	10	10	10	10	9	9	9	10		
R^2	0.55	0.58	0.60	0.58	0.61	0.58	0.57	0.55		
Normalized Mean Square Residual	3.6E-06	7.3E-04	6.1E-05	1.3E-04	3.1E-05	1.3E-04	1.2E-04	1.5E-04		

Table 3-16 provides GAM residual and fit results for all sites for the ozone seasons of 2014 through 2020. Overall, the residuals are low for all data points, and similarly low for all non-EE days. However, the 2018 and 2020 EE day residuals are significantly higher than the non-EE day results, meaning there are large, atypical influences on these days. Figure 3-44 shows non-EE vs EE median residuals with the 95th confidence intervals denoted as notches in the boxplots. We show the data in both ways to provide specific values, as well as illustrate the difference in non-EE vs EE residuals. Since the 95th confidence intervals for median EE residuals are above and do not overlap with those for non-EE residuals at any site in Clark County, we can state that the median residuals are higher and statistically different ($p<0.025$). The R^2 for each site ranged between 0.55 and 0.61, suggesting a good fit for each monitoring site, and similar to the results in prior studies and EE demonstrations mentioned previously (r^2 range of 0.4-0.8). We also provide the positive 95th quantile MDA8 ozone concentration, which is used to estimate a "No Fire" MDA8 ozone value based on the EPA guidance (U.S. Environmental Protection Agency, 2016). We also provide the median residuals (and confidence interval) for all non-EE days with observed MDA8 at or above 60 ppb; this threshold was needed to build a sufficient sample size with a representative distribution, and derive the median and 95% confidence interval. It should be noted that four out of the seven years modeled by the GAM were high wildfire years, and these values likely include a significant amount of wildfire days. We were not able to systematically remove wildfire influence by subsetting the Clark County ozone data based on HMS smoke, HMS smoke and $PM_{2.5}$ concentrations, and low wildfire years. These methods produced a significant number of false positives and negatives, and yielded datasets that were still affected by wildfire smoke. Therefore, these values should be considered an upper estimate of residuals for high ozone days. We see that the median residuals for 2018 and 2020 EE days are significantly higher than those on non-EE high observed ozone days since their confidence intervals do not overlap (or are comparable for the Jerome Mack station). The non-EE day residuals on days where observed MDA8 was at or above 60 ppb were determined to be normally distributed with a slight positive skew (median skewness = 0.39).

Table 3-16. Overall 2014-2020 GAM median residuals and 95% confidence interval range in square brackets for each site modeled. Sample size is shown in parentheses below the residual statistics. For sample sizes of less than ten, we include a range of residuals in square brackets instead of the 95% confidence interval. Residual results are split by non-EE days and the 2018 and 2020 EE days. R^2 for each site is also shown along with the positive 95th quantile result.

Site Name	All Residuals (ppb)	Non-EE Day Residuals (ppb)	2018 & 2020 EE Day Residuals (ppb)	R^2	Positive 95th Quantile (ppb)	Non-EE Day Residuals when MDA8 ≥ 60 ppb (ppb)
Boulder City	0.22 [-0.04, 0.48] (1,132)	0.22 [-0.04, 0.48] (1,130)	12.05 [10.38-13.72] (2)	0.58	9	4.05 [3.55, 4.55] (200)
Green Valley	0.17 [-0.15, 0.48] (948)	0.10 [-0.21, 0.41] (934)	7.38 [5.40, 9.36] (14)	0.58	10	3.76 [3.28, 4.23] (271)
Indian Springs	0.13 [-0.18, 0.44] (1,014)	0.08 [-0.22, 0.38] (1,010)	12.30 [9.37-17.19] (4)	0.55	10	4.79 [4.26, 5.32] (201)
Jean	0.21 [-0.06, 0.48] (1,149)	0.20 [-0.07, 0.47] (1,146)	12.57 [9.59-13.90] (3)	0.57	9	3.40 [2.94, 3.85] (290)
Jerome Mack	0.09 [-0.19, 0.36] (1,152)	0.05 [-0.22, 0.32] (1,141)	6.83 [4.21, 9.45] (11)	0.61	9	3.83 [3.32, 4.33] (242)
Joe Neal	0.23 [-0.08, 0.54] (1,113)	0.17 [-0.13, 0.47] (1,097)	7.77 [5.79, 9.75] (16)	0.60	10	3.32 [2.92, 3.71] (377)
Paul Meyer	0.21 [-0.08, 0.50] (1,159)	0.10 [-0.19, 0.39] (1,137)	8.11 [6.34, 9.88] (22)	0.55	10	3.58 [3.19, 3.97] (388)
Walter Johnson	0.27 [-0.03, 0.57] (1,163)	0.19 [-0.10, 0.48] (1,141)	7.16 [5.11, 9.21] (22)	0.58	10	3.53 [3.13, 3.93] (379)

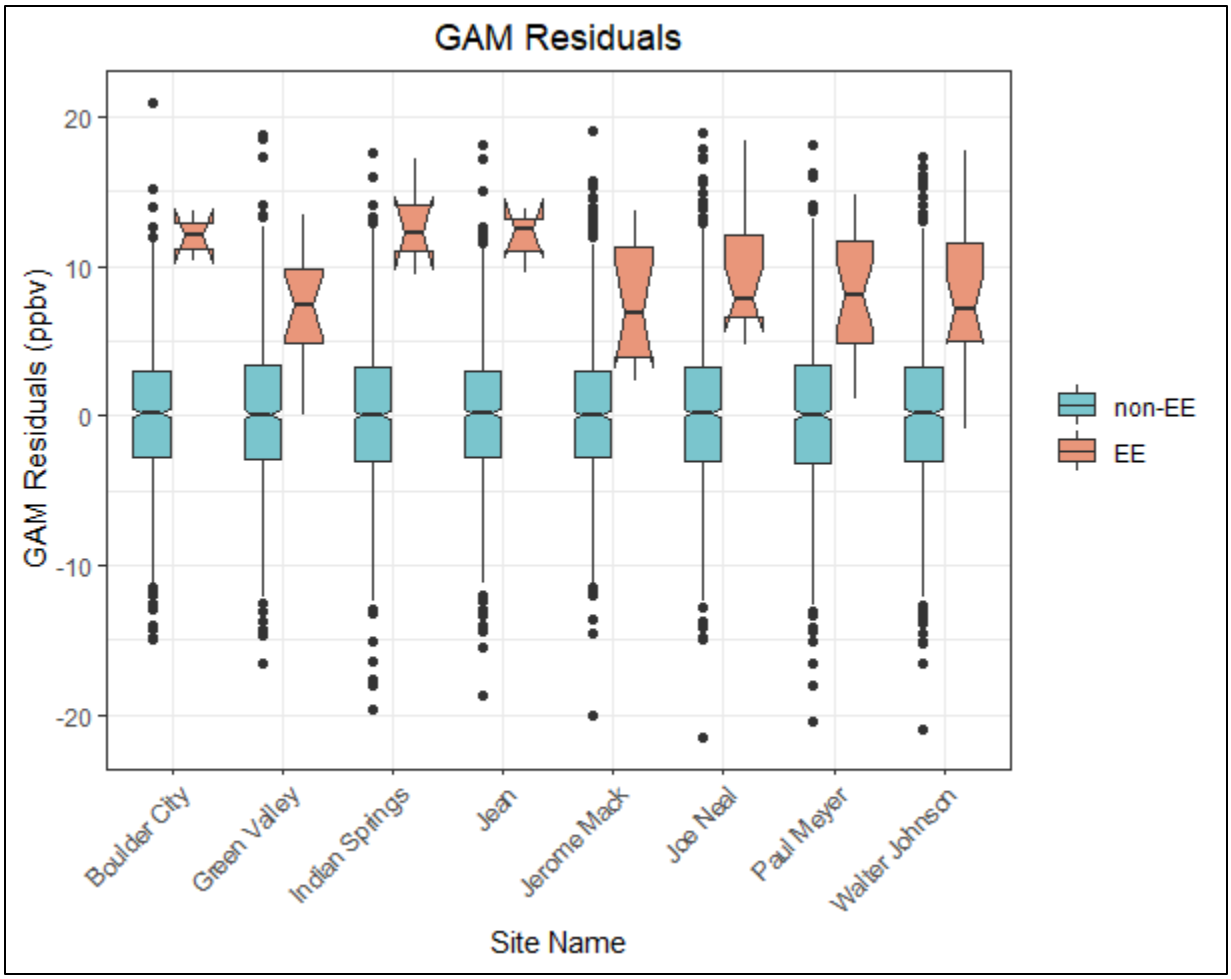

Figure 3-44. Exceptional event vs. non-exceptional event residuals. Non-exceptional events (non-EE in blue) and exceptional events (EE in orange) residuals are shown for each site modeled in Clark County. The notches for each box represent the 95th confidence interval. This figure illustrates the information in Table 3-16.

Overall, the GAM results show low bias and consistently significantly higher residuals on EE days compared with non-EE days. We also evaluated the GAM performance on verified high ozone, non-smoke days by looking at specific case studies. This was done to assess whether high-ozone days, such as the EE days, have a consistent bias that is not evident in the overall or high ozone day GAM performance. Out of the seven years used in the GAM model, four were high wildfire years in California (2015, 2017, 2018, and 2020). Since summer winds in Clark County are typically out of California (44% of trajectories originate in California according to the cluster analysis [not including transport through California in the Baja Mexico cluster]), wildfire smoke is likely to affect a large portion of summer days and influence ozone concentrations in Clark County. We identified specific case studies where most monitoring sites in Clark County had an MDA8 ozone concentration greater than or equal to 60 ppb and had no wildfire influence; "no wildfire influence" was determined by

inspecting HMS smoke plumes and HYSPLIT back trajectories for each day and confirming no smoke was over, near, or transported to Clark County. We found one to two examples from each year used in the GAM modeling, and required that at least half of the case study days needed to include an exceedance of the ozone NAAQS. **Table 3-17** shows the results of these case studies. Most case study days, including NAAQS exceedance days, show positive and negative residuals even when median ozone is greater than or equal to 65 ppb in Clark County, similar to the results for the entire multi-year dataset. GAM residuals on non-EE days when MDA8 is at or above 60 ppb have a median of 3.69 [95% confidence interval: 3.47, 3.88] (see Table 3-16). The high ozone, non-smoke case study days all show median residuals within or below the confidence interval of the high ozone residuals (from Table 3-16), meaning that the GAM model is able to accurately predict high ozone, non-smoke days within a reasonable range of error. Two additional factors indicate the GAM has good performance on normal, high ozone days: (1) the median residuals for the case studies are mostly lower than the 95% confidence interval of high ozone residuals (i.e., includes non-EE wildfire days), and (2) the case study days were verified as non-smoke days, Thus, residuals above the 95th confidence interval of the median residuals, such as those on the EE days, are statistically higher than on days with comparable high ozone concentrations, and not biased high because of the high ozone concentrations on these days.

Table 3-17. GAM high ozone, non-smoke case study results. Median GAM residuals for ten days in 2014-2020 are shown where most monitoring sites had MDA8 ozone concentrations of 60 ppb or greater. Sites used to calculate the MDA8 and GAM residual median/range are listed in the Clark County AQS Site Number column by site number.

Date	Clark County AQS Site Number	Median (Range) of Observed MDA8 Ozone (ppb)	Median (Range) GAM Residual (ppb)
5/17/2014	0601, 0075, 1019, 0540, 0043, 0071	66 (64-71)	1.66 (-0.53-4.28)
6/4/2014	0601, 0075, 0540, 1019, 0043, 0071	69 (66-72)	3.46 (1.70-4.80)
6/3/2015	1019, 0043, 0075, 0540, 7772, 0601, 0071	71 (65-72)	3.01 (-0.34-5.77)
6/20/2015	0601, 0298, 7772, 1019, 0540, 0075, 0043, 0071	65 (63-70)	1.40 (-6.20-5.28)
6/3/2016	0298, 1019, 0075, 0540, 0043, 0071	65 (63-71)	3.89 (1.89-5.26)
7/28/2016	0075, 0071, 0298, 0540, 0043	70 (63-72)	0.24 (-5.95-3.67)
6/17/2017	0601, 0075, 0071, 1019, 0540, 0298, 0043	66 (63-72)	1.85 (-1.94-7.01)
6/4/2018	0601, 0298, 7772, 1019, 0540, 0075, 0043, 0071	65 (60-67)	3.06 (-0.91-3.60)
5/5/2019	0601, 0298, 7772, 1019, 0540, 0075, 0043, 0071	65 (62-67)	1.28 (-2.00-3.42)
5/15/2020	0298, 0043, 0075, 0071	63 (63-65)	1.52 (1.09-3.49)

We also evaluate the bias of GAM residuals versus predicted MDA8 ozone concentrations in Figure 3-45. Residuals (i.e., observed ozone minus GAM-predicted MDA8 ozone) should be independent of the GAM-predicted ozone value, meaning that the difference between the actual ozone concentration on a given day and the GAM output should be due to outside influences and not well described by meteorological or seasonal values (i.e., variables used in the GAM prediction). Therefore, in a well-fit model, positive and negative residuals should be evenly distributed across all

GAM-predicted ozone concentrations and on average zero. In Figure 3-45, we see daily GAM residuals at all eight monitoring sites in Clark County from 2014-2020, the residuals are evenly distributed across all GAM-predicted ozone concentrations, with no pattern or bias at high or low MDA8 fit concentrations. This evaluation of bias in the model is consistent with established literature and other EE demonstrations (Gong et al., 2018; McVey et al., 2018; Texas Commission on Environmental Quality, 2021; Pernak et al., 2019), and indicate a well-fit model. In Figure 3-46, we also provide a histogram of the residuals at each monitoring site modeled in Clark County. This analysis shows that residuals at each site are distributed normally around a median near zero, and none of the distributions shows significant tails at high or low residuals (median skew = 0.05 with 95% confidence interval [-0.03, 0.12]). This analysis of error in the model and our results are consistent with previously concurred EE demonstrations (Arizona Department of Environmental Quality, 2016) and previous literature (Jaffe et al., 2013; Alvarado et al., 2015; Gong et al., 2017; McClure and Jaffe, 2018; Pernak et al., 2019). Appendix E provides GAM residual analysis from the concurred ADEQ and submitted TCEQ demonstrations that compare well with our GAM residual results. Based on these analysis methods, bias in the model is low throughout the range of MDA8 prediction values and confirms that the GAM can be used to predict MDA8 ozone concentrations in Clark County.

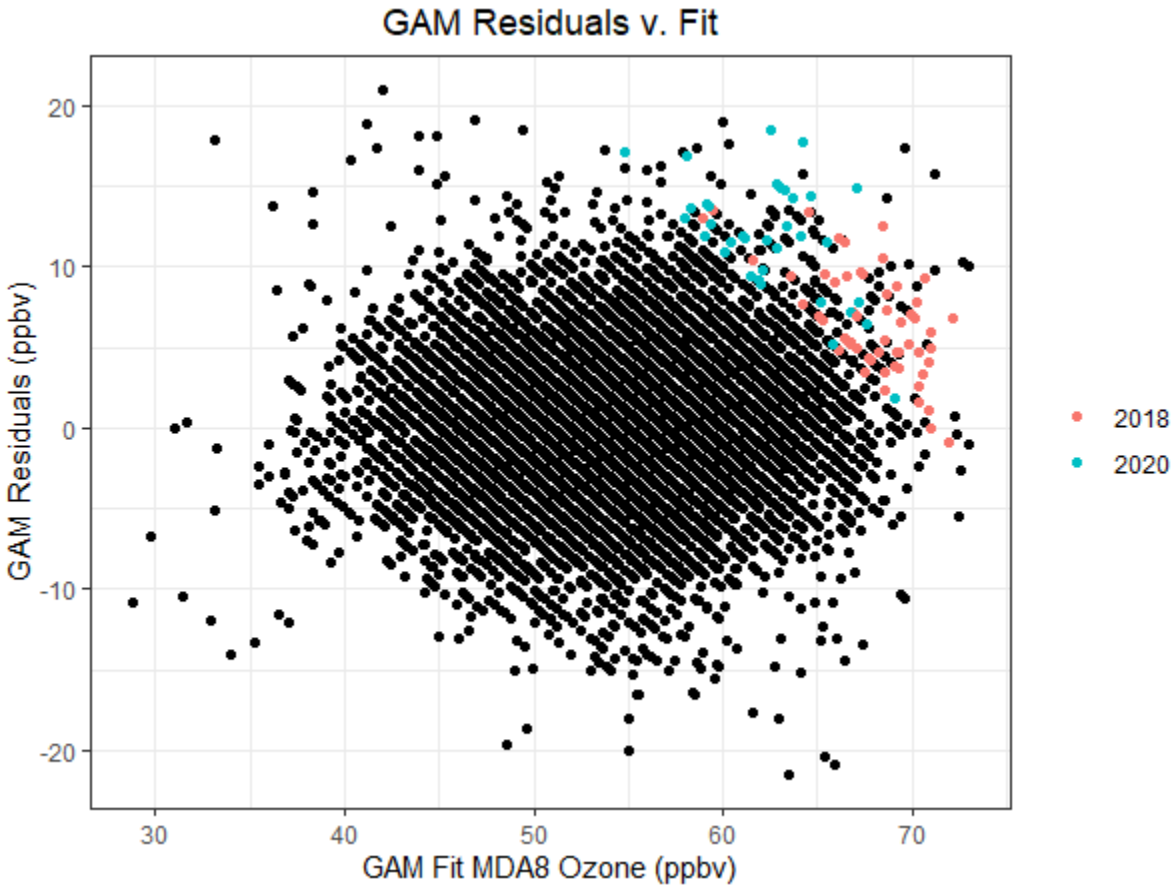

Figure 3-45. Daily GAM residuals for 2014-2020 vs GAM Fit (Predicted) MDA8 Ozone values. 2018 and 2020 exceptional events residuals are shown in red and blue.

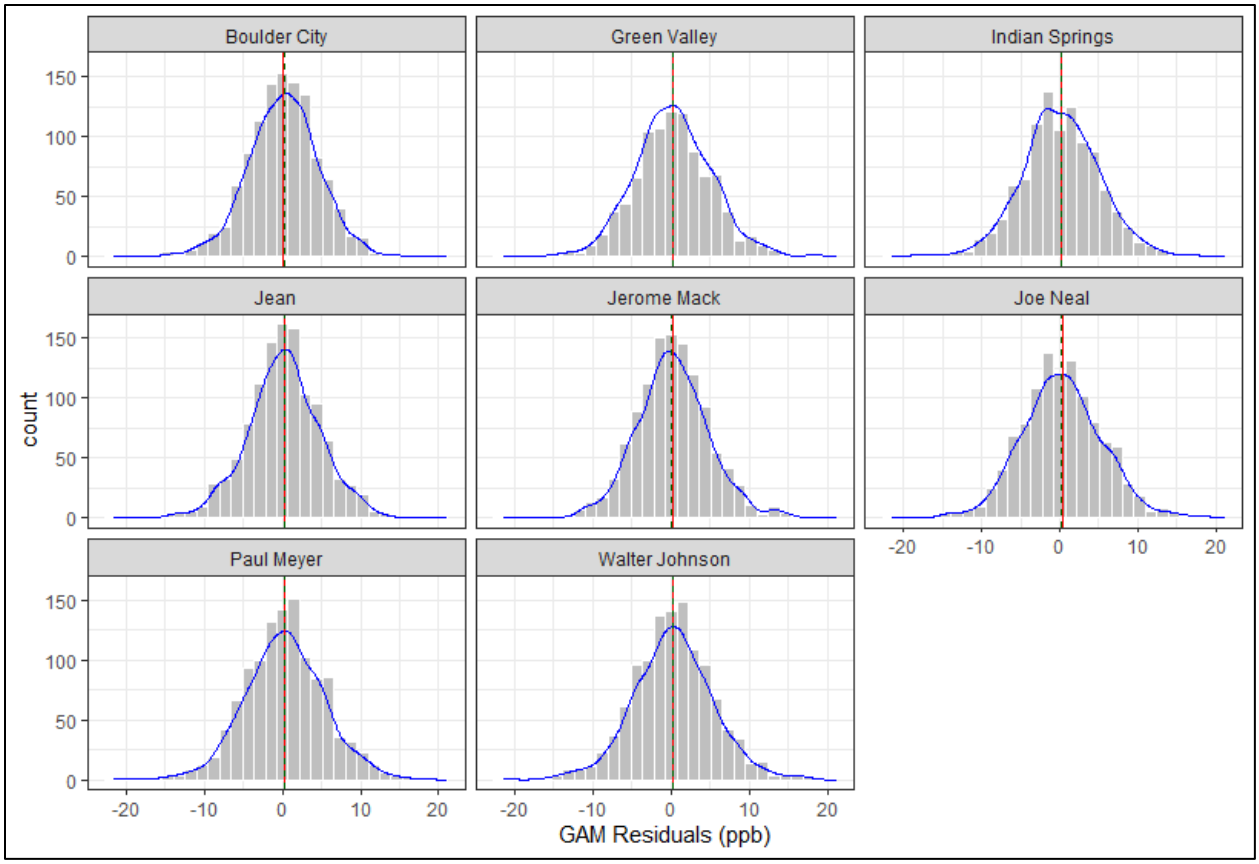

Figure 3-46. Histogram of GAM residuals at all modeled Clark County monitoring sites. The red line indicates the mean and the green dashed line indicates the median. The blue line provides the density distribution.

Within the GAM model, we include HYSPLIT 24-hour distance values, which are factored by cluster, to provide source region and stagnation information into the algorithm. A major upwind pollution source for Las Vegas is the Los Angeles Basin (see the Southern California cluster), which is around 400 km away. Since the GAM model uses source region and distance traveled information to help predict daily MDA8 ozone concentrations, contributions from LA should be accounted for in the algorithm. Based on this, we can assess whether GAM residuals on LA-source region days were significantly different from other source regions. In **Figures 3-47 and 3-48**, we subset the GAM results by removing any potential EE days. From these results, we find that both morning (18:00 UTC) and afternoon (22:00 UTC) trajectory data have similar distributions for all clusters. The notches in the box plots (representing the 95th confidence interval) provide an estimate of statistical difference, and show that the median of residuals is near zero for all clusters. The Northwest U.S. cluster at 18:00 UTC shows slightly negative residuals, while the Long-Range Transport cluster shows slightly positive residuals for both 18:00 and 22:00 UTC. The Southern California cluster shows a median residual of around zero for both 18:00 and 22:00 UTC trajectories, with significant overlap between the 95th confidence intervals of most other clusters (not statistically different). Additionally, the number of data points per cluster (bottom of each figure) corresponds well with transport from California being

dominant for the April through September time frame. Overall, this analysis provides evidence that even when the Los Angeles Basin (Southern California cluster) is upwind of Las Vegas, the GAM model performs well (low median residuals), and the results are statistically similar to most of the other clusters. This implies that when residuals are large, the Los Angeles Basin's influence is unlikely to be the only contributor to enhancements in MDA8 ozone.

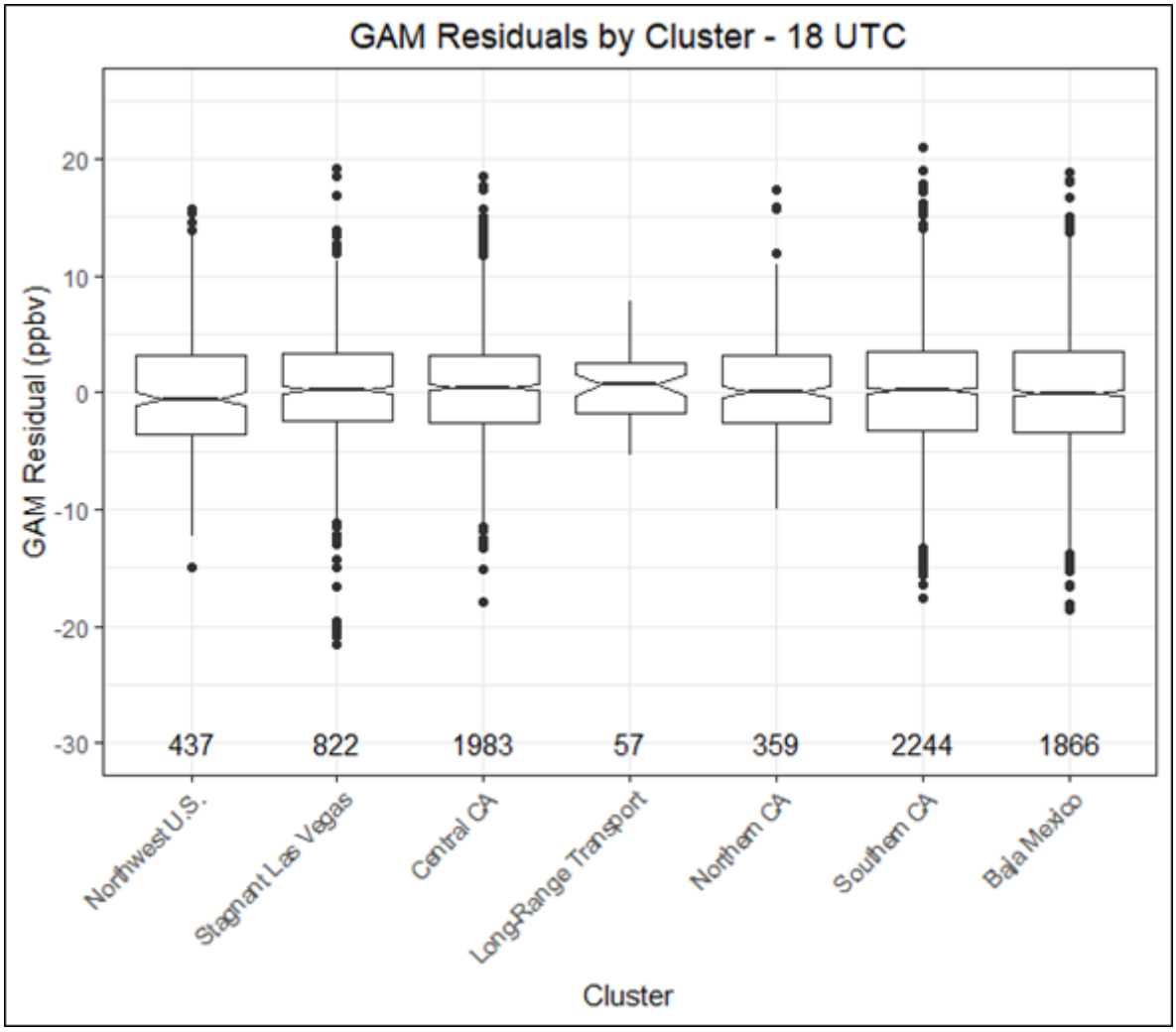

Figure 3-47. GAM cluster residual results for 18:00 UTC. The cluster is determined by grouping 24-hour back trajectories from Las Vegas based on their path. Clusters were created by using back trajectory results from Clark County between 2014 and 2020 (EE days were removed).

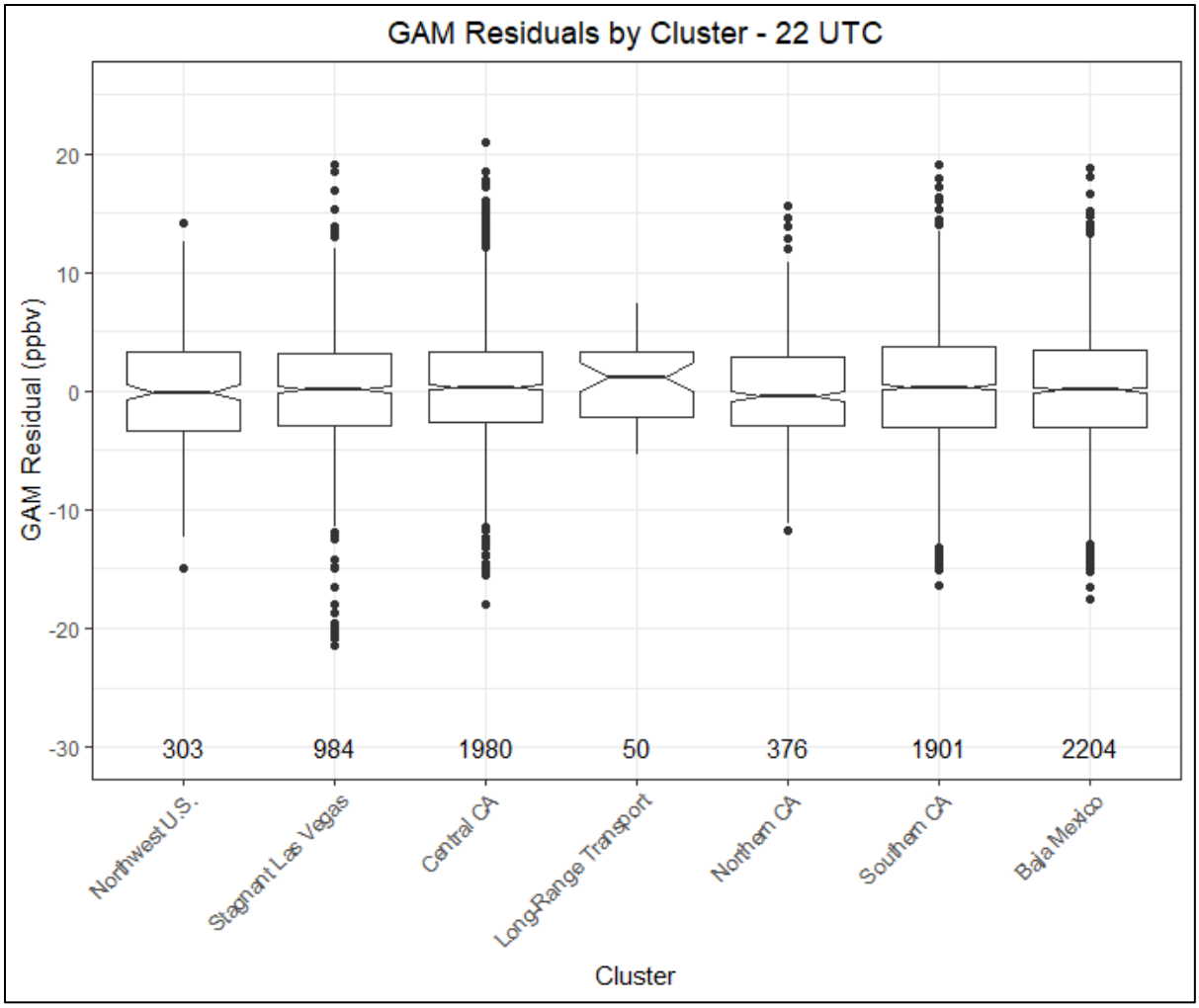

Figure 3-48. GAM cluster residual results for 22:00 UTC. The cluster is determined by grouping 24-hour back trajectories from Las Vegas based on their path. Clusters were created by using back trajectory results from Clark County between 2014 and 2020 (EE days were removed).

Mobile emissions sources decreased throughout the U.S. after COVID restrictions went into place in March 2020. Based on emission inventories from Las Vegas, on-road emissions make up a significant portion of the NO_x emissions inventory (see Section 2.3 for more details). Based on traffic data from the Nevada Department of Transportation, on-road traffic in Clark County in 2020 was significantly different than 2019 through early to mid-June (depending on the area where traffic volume was measured; see **Appendix F** for more details). **Figure 3-49** provides a scatter plot of MDA8 ozone observed versus GAM fit for all eight monitoring sites, separated by year. The linear regression fit, slope, and intercept do not show large difference between 2020 and other modeled years. **Figure 3-50** provides a more in-depth look at the most heavily affected months due to COVID restrictions and traffic changes (April – May 2020). The 95th confidence interval (shown as a notch in the box plots) show overlap between 2020 and most other years (except 2015 and 2016). The May 6, 9, and 28 EE days are included in the 2020 box. This analysis shows that there was not a statistically

different GAM response in 2020 compared with other years; this is confirmed in the COVID analysis section (Appendix F), where we show that MDA8 ozone during April – May 2020 in Las Vegas was not statistically different from previous years. While the reduction in traffic emissions due to COVID restrictions did not affect the September 26 event, we thought it was important to address the effects of COVID restrictions on the 2020 GAM results. Overall, ozone in Clark County did not change significantly and, similarly, GAM results were not significantly affected.

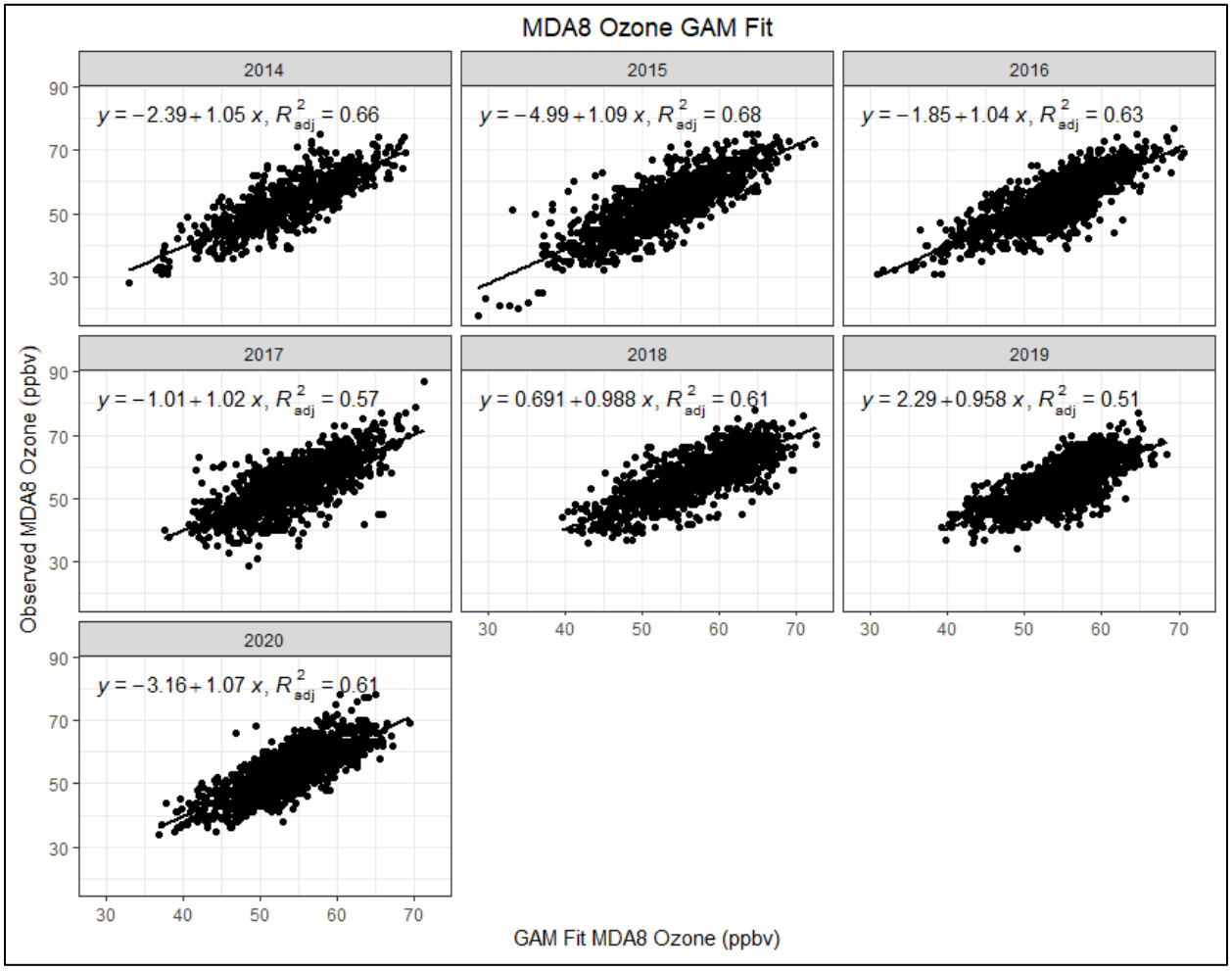

Figure 3-49. Observed MDA8 ozone vs. GAM fit ozone by year. The relationship between observed MDA8 ozone and GAM fit ozone at all eight modeled monitoring sites in Clark County is broken out by year, with linear regression and fit statistics shown (slope, intercept, and r^2). EE days are not included in the regression equations.

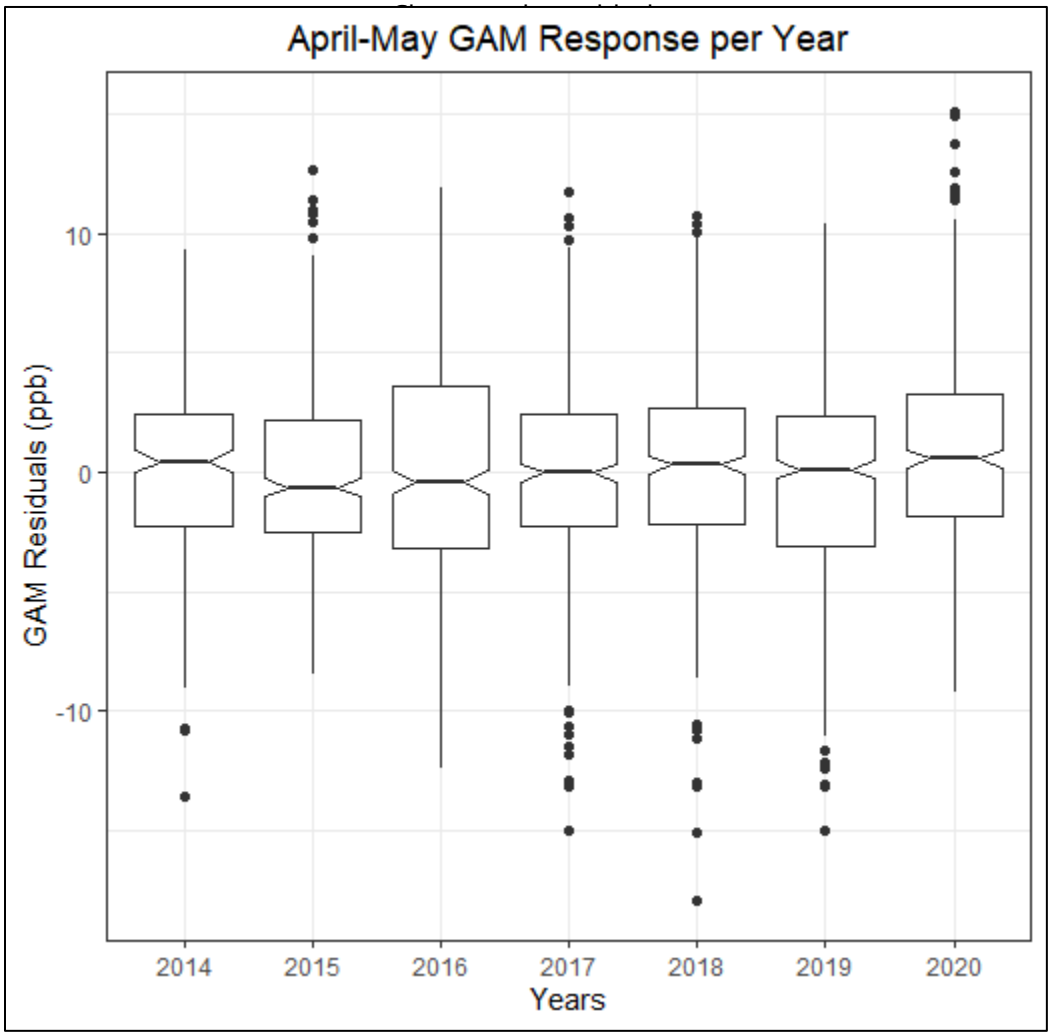

Figure 3-50. April–May Interannual GAM Response. April–May residuals per year from 2014–2020 are plotted for all eight modeled monitoring sites in Clark County. The potential EE days of May 6, 9, and 28 are included.

Figure 3-51 provides the observed MDA8 ozone versus GAM Fit MDA8 from 2014 through 2020 for the sites affected on September 26 (Joe Neal and Walter Johnson). We marked the possible 2020 (red), 2018 (blue), and other (purple) EE days to show that observed MDA8 ozone on these days is higher than those predicted by the GAM. The other (purple) points are from 2014–2016, and are suspected wildfire events, as indicated in EPA AQS record. We also highlight the September 26, 2020, EE day as a large red triangle in each figure. Linear regression statistics (slope, intercept, and r^2) are also provided for context. All linear regressions show a slope near unity, and a low intercept value (around 4 ppb) with a good fit r^2 value.

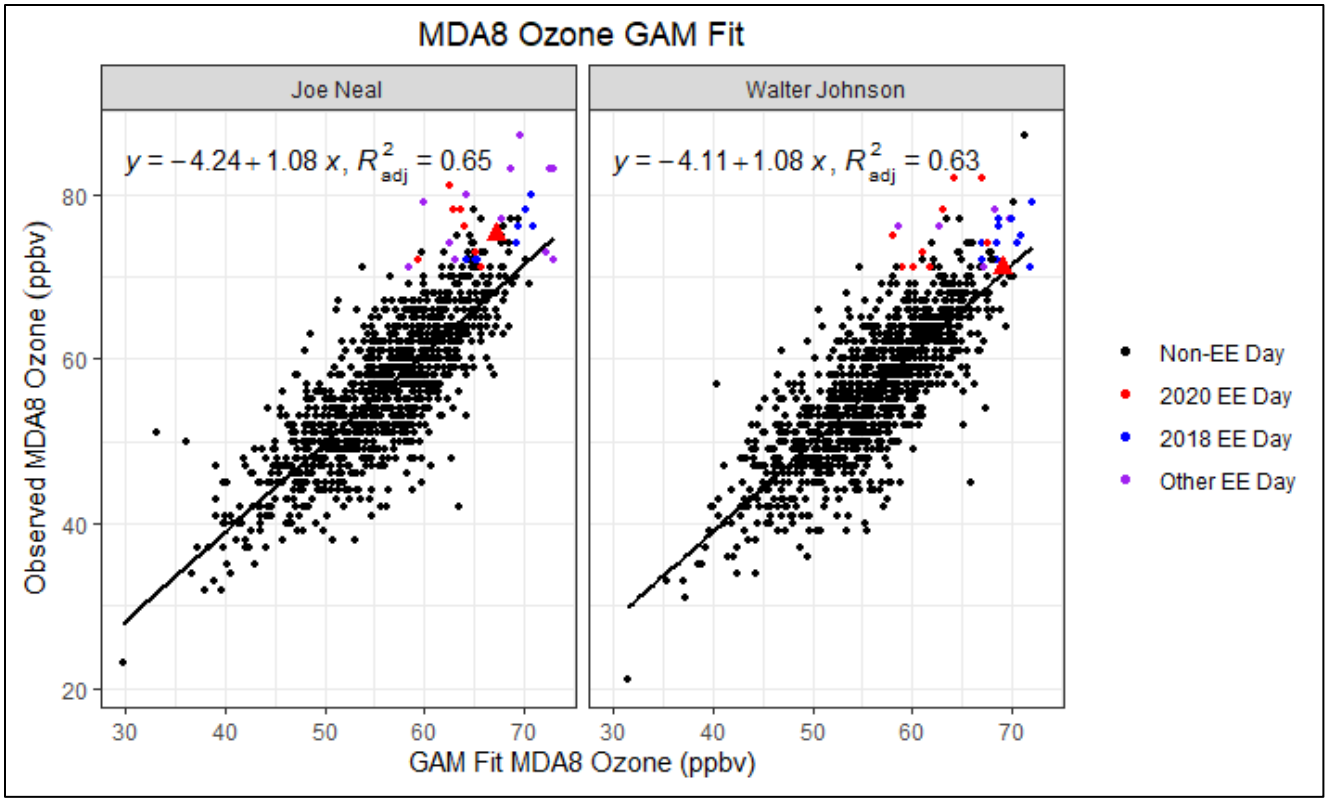

Figure 3-51. GAM MDA8 Fit versus Observed MDA8 ozone data from 2014 through 2020 for the EE affected sites on September 26, 2020. Black circles indicate data not associated with the 2018 or 2020 EE days, red circles indicate 2020 EE days, blue circles indicate 2018 EE days, and purple circles indicate 2014-2016 EE days. September 26 is shown as a red triangle. The black line is the linear regression of the data, and statistics (equation and r^2 value) are shown in the top of each sub-figure.

Table 3-18 provides the GAM results for September 26, 2020, at each monitoring site affected by the EE. GAM residuals show a modeled wildfire impact between 2 and 8 ppb for all monitoring sites, with MDA8 GAM prediction values below the 0.070 ppm standard. EPA guidance requires a further level of investigation. By adding the GAM MDA8 prediction value and the positive 95th quantile of residuals, we calculated the "No Fire" MDA8 ozone value. The difference between the observed and "No Fire" MDA8 ozone value (-8 to -2 ppb) is a conservative estimate of the influence of wildfire smoke at each site. Due to the large number of wildfires affecting Clark County during the 7-year modeling period, we also calculate the "No Fire" and minimum predicted fire influence given the 75th percentile (-3 to 2 ppb). This provides a range of minimum smoke enhancement (-8 to 2 ppb). The actual enhancement due to wildfire smoke likely lies between the minimum smoke enhancement estimate and the GAM residual. Previous studies and concurred EE demonstrations show and discuss the limitations of the 95th positive percentile evaluation (Miller et al., 2014; Arizona Department of Environmental Quality, 2016). Additionally, production of ozone is an extremely complex process that can only be predicted by meteorological variables in a GAM model with a 50%-80% correlation based on previously cited papers (our GAM model shows a 55%-61% correlation). In our case, this

leaves exceptional events, wildfire influence during high wildfire years, stratospheric intrusions, non-normal emissions, non-normal meteorology, etc., which make up the other 39%-45%. Due to the large number of high wildfire years used in the GAM model, we assert that the minimum predicted fire influence value (as determined by the positive 95th quantile) should not be used as strict guideline for actual fire influence. Although the "No Fire" predictions are low in this case, the MDA8 ozone concentrations at the Joe Neal and Walter Johnson monitoring stations are only above the standard by 1-5 ppb on September 26. Since the previous day's MDA8 ozone is used as a predictor in the GAM model, some wildfire influence may have been artificially included in the GAM prediction, accounting for part of the low "No Fire" predictions (smoke is present in Clark County on September 25, 2020). Whether the previous day's ozone added some wildfire influence or not, the GAM still shows MDA8 ozone predictions on September 26 below the 70-ppb standard at both sites. Based on the values from the GAM model, we see a non-typical enhancement in MDA8 ozone concentrations at the affected Clark County monitoring sites on September 26, 2020.

Table 3-18. September 26 GAM results and residuals for each site. The GAM residual is the difference between observed MDA8 ozone and the GAM Prediction. We also estimate the minimum predicted fire influence based on the positive 95th quantile and GAM prediction value.

Site Name	MDA8 Ozone Concentration[a] (ppm)	MDA8 GAM Prediction[b] (ppm)	GAM Residual (ppm)	Positive 75th-95th Quantile[c] (ppm)	"No Fire" MDA8[b+c] (ppm)	Minimum Predicted Fire Influence[a-(b+c)] (ppm)
Walter Johnson	0.071	0.069	0.002	0.006-0.010	0.074-0.079	-0.008 - -0.003
Joe Neal	0.075	0.067	0.008	0.005-0.010	0.073-0.077	-0.002 - 0.002

Finally, Figure 3-52 shows a 2-week time series of observed MDA8 ozone values across Clark County and the GAM prediction values at those sites. On September 26 (and September 25, which was a wildfire smoke-affected day in Clark County), we see a gap between observed MDA8 ozone and the GAM-predicted values. Outside of the possible EE day, the GAM prediction values are very close to the observed values, suggesting that immediately before and after the event, we are able to accurately predict typical fluctuations in ozone on non-event days.

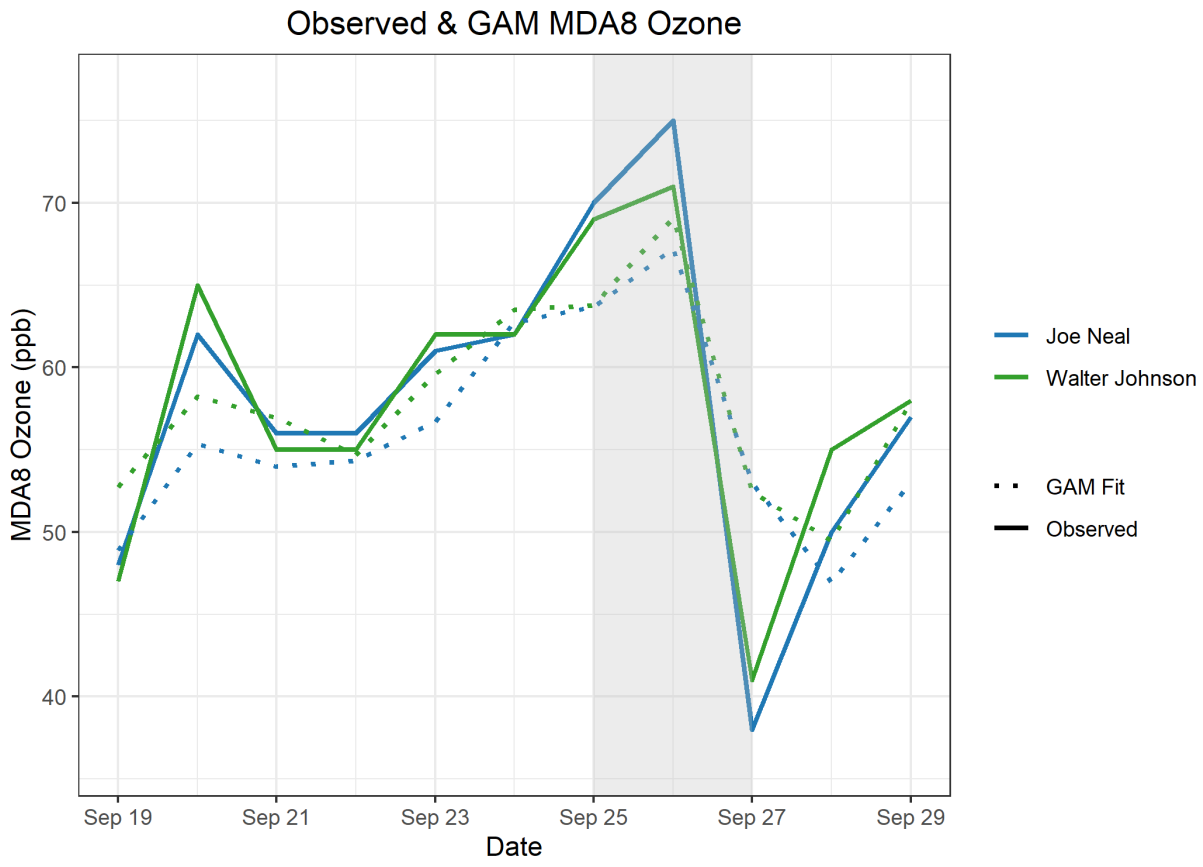

Figure 3-52. GAM time series showing observed MDA8 ozone for two weeks before and after the September 26 EE (solid lines). The GAM MDA8 ozone fit value is also shown for two weeks before and after September 2 (dotted line).

Overall, the GAM evidence clearly demonstrates that a non-typical source of ozone significantly impacted concentrations at both EE-affected Clark County sites on September 26, 2020. Coupled with wildfire smoke evidence from all other tiers of analyses, we can conclude by weight of evidence that the enhancement in ozone concentration was due to smoke from the large wildfires burning in southern and central California that was transported to Clark County, Nevada.

3.4 Clear Causal Relationship Conclusions

The analyses conducted in this report support the impact of smoke from the large wildfire complexes in central and southern California on ozone concentrations in Clark County, Nevada, on September 26, 2020. We find that:

1. Visible satellite imagery, news articles, and back trajectories support the conclusion of smoke transport from the wildfires in California to Clark County.
2. A large mixing layer, aerosols in the vertical profile, back trajectories starting aloft near the fire and ending at the surface in Clark County, and surface enhancements of wildfire-related pollutants and tracers in Clark County support the conclusion that smoke was mixed down to the surface in Clark County.
3. Comparisons with non-event concentrations, meteorologically similar matching day analysis, and GAM statistical modeling support the conclusion that the ozone concentrations seen in Clark County were well above typical summer concentrations.

The analyses presented in this report fulfill the requirements for a Tier 3 EE demonstration, and all conclusions for each type of analysis are summarized in Table 3-19. The effect of the wildfires in California on Clark County caused ozone exceedances at the Walter Johnson and Joe Neal monitoring stations. Based on the evidence shown that the wildfires in California were natural events and unlikely to recur, as well as the clear causal relationship between the wildfire event and the monitored exceedances, we conclude that the ozone exceedance event on September 26, 2020, in Clark County was not reasonably controllable or preventable.

Table 3-19. Results for each tier analysis for the September 26 EE.

Tier	Requirements	Finding
1	• Comparison of fire-influenced exceedance with historical concentrations • Key factor: Evidence that fire and monitor meet one of the following criteria: – Seasonality differs from typical season, or – Ozone concentrations are 5-10 ppb higher than non-event related concentrations • Evidence of transport of fire emissions to monitor: – Trajectories of fire emissions (reaching ground level), or – Satellite images and supporting evidence from surface measurements – Media coverage and photographic evidence of smoke	• The September 26, 2020, ozone exceedance occurred during a typical ozone season, but event concentrations were significantly higher than non-event concentrations. • Trajectories, satellite images, media coverage, and ground images support smoke transport from large complex wildfire in California into Clark County.
2	• All Tier 1 requirements • Key Factor #1: Fire emissions and distance of fires • Key Factor #2: Comparison of the event-related ozone concentration with non-event-related high ozone concentrations (high percentile rank over five years/seasons) – Annual and seasonal comparison • Evidence that fire emissions affected the monitor (at least one of the following): – Visibility impacts – Changes in supporting measurements – Satellite enhancements of fire-related species (i.e., NOx, CO, AOD, etc.) – Fire-related enhancement ratios and/or tracer species – Differences in spatial/temporal patterns	• Q/d values for the California fires were well below 100. • Ozone concentrations at all sites showed high percentile rank over the past five years and ozone seasons. • Surface concentrations of supporting pollutants show enhanced concentrations and changes in typical diurnal profiles, consistent with smoke. • Satellite measurements also show enhanced levels of fire-related species. • Levoglucosan, a wildfire tracer, showed a positive detection during this event.
3	• All Tier 2 requirements • Evidence of fire emissions effects on monitor: – Multiple analyses from those listed for Tier 2 • Evidence of fire emissions transport to the monitor: – Trajectory or satellite plume analysis, and – Additional discussion of meteorological conditions • Additional evidence such as: – Comparison to ozone concentrations on matching (meteorologically similar) days – Statistical regression modeling • Photochemical modeling of smoke contributions to ozone concentrations	• Meteorology patterns during this event show transport from the wildfires in California to Clark County. • Vertical profiles show vertical mixing and transport to the surface as well as increased aerosol in the column. • Meteorologically similar day analysis shows that average MDA8 ozone across similar days was well below the ozone NAAQS and 6-9 ppb lower than the September 26 exceedance at all affected sites. • GAM statistical modeling predicts ozone concentrations lower than observed, suggesting an impact from non-typical sources on ozone concentrations in Clark County during this event.

4. Natural Event Unlikely to Recur

A wildfire is defined in 40 CFR 50.1(n) as "any fire started by an unplanned ignition caused by lightning; volcanoes; other acts of nature; unauthorized activity; or accidental, human-caused actions, or a prescribed fire that has developed into a wildfire. A wildfire that predominantly occurs on wildland is a natural event." Furthermore, a "wildland" is "an area in which human activity and development are essentially non-existent, except for roads, railroads, power lines, and similar transportation facilities. Structures, if any, are widely scattered." 40 CFR 50.1(o). As shown in Table 3-3, the fires that contributed to this event were caused by human-caused actions or lightning and therefore meet the definition of wildfire (for fires where the cause is known). Based on the documentation provided in Section 3.2.1 of this submittal, the fires in California, which contributed to wildfire smoke in Clark County, predominately took place on wildlands designated as National Forests, as seen in Figure 3-20. Therefore, under 40 CFR §50.1, the fire listed in Table 3-3 can be classified as natural event that is unlikely to recur. Accordingly, the Clark County Department of Environment and Sustainability has shown in this submittal that smoke from California wildfires, which led to an ozone exceedance in Clark County of September 26, 2020, may be considered for treatment as an EE.

5. Not Reasonably Controllable or Preventable

As shown by the documentation provided in Section 3.2.1 of this submittal, each wildfire listed in Table 3-3 burned predominantly on wildland. The Exceptional Events rule stated in 40 CFR 50.1(j) indicates that a wildfire that occurs on wildland is not reasonably controllable or preventable. Previous sections of this report have shown that each fire referenced in this report was a wildfire that occurred on wildland. The InciWeb reports for each of these fires indicates that the wildfires burned across vast areas in generally inaccessible land, limiting firefighting efforts in each event (https://inciweb.nwcg.gov/). The Clark County Department of Environment and Sustainability is not aware of any evidence clearly demonstrating that prevention or control efforts beyond those made would have been reasonable. Therefore, the emissions that caused exceedances at monitors in Clark County on September 26, 2020, are neither reasonably controllable or preventable.

6. Public Comment

This exceptional event demonstration will undergo a 30-day public comment period concurrent with EPA's review beginning September 3, 2021. A copy of the public notice, along with any comments received and responses to those comments, will be submitted to EPA after the comment period has closed, consistent with the requirements of 40 CFR 50.14(c)(3)(v). **Appendix G** contains documentation of the public comment process.

7. Conclusions and Recommendations

The analyses conducted in this report support the conclusion that smoke from large wildfire complexes in central and southern California impacted ozone concentrations in Clark County, Nevada, on September 26, 2020. This EE demonstration has provided the following elements required by the EPA guidance for wildfire EEs (U.S. Environmental Protection Agency, 2016):

1. A narrative conceptual model that describes the wildfires burning in California and how the emissions from this wildfire led to ozone exceedances downwind in Clark County (Sections 1 and 2).
2. A clear causal relationship between the wildfires in California and the September 26 exceedance through ground and satellite-based measurements, trajectories, emission modeling, comparison with non-event concentrations, vertical profile analysis, and statistical modeling (Section 3).
3. Event ozone concentrations at or above the 99th percentile when compared with the last six years of observations at each site and among the four highest ozone days at each site (excluding other 2018 and 2020 EE events – Section 3).
4. The wildfires in California were determined to be caused by lightning or unknown/human-caused accidents that were coupled with a period of high temperatures, low humidity, and low fuel moisture and began in wildland areas where they grew rapidly and quickly beyond firefighting controls, which classifies this event as unlikely to recur (Section 4).
5. Demonstration that the emissions from the California wildfires being transported to Clark County was neither reasonably controllable or preventable (Section 5).
6. This demonstration went through the public comment process via Clark County's Department of Environment and Sustainability (Section 6).

The major conclusions and supporting analyses found in this report are:

1. Visible satellite imagery, news articles, and back trajectories support the conclusion of smoke transport from the wildfires in California to Clark County.
2. A large mixing layer, aerosols in the vertical profile, back trajectories starting aloft near the fire and ending at the surface in Clark County, and surface enhancements of wildfire-related pollutants and tracers in Clark County support the conclusion that smoke was mixed down to the surface in Clark County.
3. Comparisons with non-event concentrations, meteorologically similar matching day analysis, and GAM statistical modeling support the conclusion that the ozone concentrations seen in Clark County were well above typical summer concentrations.

The analyses presented in this report fulfill the requirements for a Tier 3 EE demonstration, and all conclusions for each type of analysis are summarized in Table 3-19. The effect of the large complex wildfires burning in central and southern California on Clark County caused ozone exceedances at the Walter Johnson and Joe Neal monitoring stations. Based on the evidence shown that the California wildfires natural events and unlikely to recur, as well as the clear causal relationship between the wildfire events and the monitored exceedances, we conclude that the ozone exceedance event on September 26, 2020, in Clark County was not reasonably controllable or preventable.

8. References

Alvarado M., Lonsdale C., Mountain M., and Hegarty J. (2015) Investigating the impact of meteorology on O_3 and $PM_{2.5}$ trends, background levels, and NAAQS exceedances. Final report prepared for the Texas Commission on Environmental Quality, Austin, TX, by Atmospheric and Environmental Research, Inc., Lexington, MA, August 31.

Arizona Department of Environmental Quality (2016) State of Arizona exceptional event documentation for wildfire-caused ozone exceedances on June 20, 2015 in the Maricopa nonattainment area. Final report, September. Available at https://static.azdeq.gov/pn/1609_ee_report.pdf.

Arizona Department of Environmental Quality (2018) State of Arizona exceptional event documentation for wildfire-caused ozone exceedances on July 7, 2017 in the Maricopa Nonattainment Area. Final report, May. Available at https://static.azdeq.gov/pn/Ozone_2017ExceptionalEvent.pdf.

Bhattarai H., Saikawa E., Wan X., Zhu H., Ram K., Gao S., Kang S., Zhang Q., Zhang Y., Wu G., Wang X., Kawamura K., Fu P., and Cong Z. (2019) Levoglucosan as a tracer of biomass burning: recent progress and perspectives. *Atmospheric Research*, 220, 20-33, doi: 10.1016/j.atmosres.2019.01.004. Available at http://www.sciencedirect.com/science/article/pii/S0169809518311098.

Brey S.J. and Fischer E.V. (2016) Smoke in the city: how often and where does smoke impact summertime ozone in the United States? *Environ. Sci. Technol.*, 50(3), 1288-1294, doi: 10.1021/acs.est.5b05218, 2016/02/02.

Bytnerowicz A., Cayan D., Riggan P., Schilling S., Dawson P., Tyree M., Wolden L., Tissell R., and Preisler H. (2010) Analysis of the effects of combustion emissions and Santa Ana winds on ambient ozone during the October 2007 southern California wildfires. *Atmos. Environ.*, 44, 678-687, doi: 10.1016/j.atmosenv.2009.11.014.

Camalier L., Cox W., and Dolwick P. (2007) The effects of meteorology on ozone in urban areas and their use in assessing ozone trends. *Atmos. Environ.*, 41, 7127-7137, doi: 10.1016/j.atmosenv.2007.04.061.

Clark County Department of Air Quality (2019) Ozone Advance program progress report update. August.

Clark County Department of Environment and Sustainability (2020) Revision to the Nevada state implementation plan for the 2015 Ozone NAAQS: emissions inventory and emissions statement requirements. September. Available at https://files.clarkcountynv.gov/clarknv/Environmental%20Sustainability/SIP%20Related%20Documents/O3/20200901_2015_O3%20EI-ES_SIP_FINAL.pdf?t=1617690564073&t=1617690564073.

Draxler R.R. (1991) The accuracy of rrajectories during ANATEX calculated using dynamic model analyses versus rawinsonde observations. *Journal of Applied Meteorology*, 30, 1446-1467, doi: 10.1175/1520-0450(1991)030<1446:TAOTDA>2.0.CO;2, February 25. Available at https://journals.ametsoc.org/doi/abs/10.1175/1520-0450%281991%29030%3C1446%3ATAOTDA%3E2.0.CO%3B2.

Finlayson-Pitts B.J. and Pitts Jr J.N. (1997) Tropospheric air pollution: Ozone, airborne toxics, polycyclic aromatic hydrocarbons, and particles. *Science*, 276, 1045-1051, (5315).

Gong X., Kaulfus A., Nair U., and Jaffe D.A. (2017) Quantifying O_3 impacts in urban areas due to wildfires using a generalized additive model. *Environ. Sci. Technol.*, 51(22), 13216-13223, doi: 10.1021/acs.est.7b03130.

Gong X., Hong S., and Jaffe D.A. (2018) Ozone in China: spatial distribution and leading meteorological factors controlling O_3 in 16 Chinese cities. *Aerosol and Air Quality Research*, 18(9), 2287-2300. Available at http://dx.doi.org/10.4209/aaqr.2017.10.0368.

Hennigan C.J., Sullivan A.P., Collett J.L., Jr., and Robinson A.L. (2010) Levoglucosan stability in biomass burning particles exposed to hydroxyl radicals. *Geophysical Research Letters*, 37(L09806), doi: 10.1029/2010GL043088. Available at https://www.firescience.gov/projects/09-1-03-1/project/09-1-03-1_hennigan_etal_grl_2010.pdf.

Hoffmann D., Tilgner A., Iinuma Y., and Herrmann H. (2009) Atmospheric stability of levoglucosan: a detailed laboratory and modeling study. *Environ. Sci. Technol.*, 44, 694–699.

Jaffe D., Chand D., Hafner W., Westerling A., and Spracklen D. (2008) Influence of fires on O_3 concentrations in the western U.S. *Environ. Sci. Technol.*, 42(16), 5885-5891, doi: 10.1021/es800084k.

Jaffe D.A., Bertschi I., Jaegle L., Novelli P., Reid J.S., Tanimoto H., Vingarzan R., and Westphal D.L. (2004) Long-range transport of Siberian biomass burning emissions and impact on surface ozone in western North America. *Geophys. Res. Let.*, 31(L16106).

Jaffe D.A., Wigder N., Downey N., Pfister G., Boynard A., and Reid S.B. (2013) Impact of wildfires on ozone exceptional events in the western U.S. *Environ. Sci. Technol.*, 47(19), 11065-11072, doi: 10.1021/es402164f, October 1. Available at http://pubs.acs.org/doi/abs/10.1021/es402164f.

Kimbrough S., Hays M., Preston B., Vallero D.A., and Hagler G.S.W. (2016) Episodic impacts from California wildfires identified in Las Vegas near-road air quality monitoring. *Environ. Sci. Technol.*, 50(1), 18-24. Available at https://doi.org/10.1021/acs.est.5b05038.

Lai C., Liu Y., Ma J., Ma Q., and He H. (2014) Degradation kinetics of levoglucosan initiated by hydroxyl radical under different environmental conditions. *Atmospheric Environment*, 91, 32-39, doi: 10.1016/j.atmosenv.2014.03.054, 2014/07/01/. Available at http://www.sciencedirect.com/science/article/pii/S1352231014002398.

Langford A.O., Senff C.J., Alvarez R.J., Brioude J., Cooper O.R., Holloway J.S., Lin M.Y., Marchbanks R.D., Pierce R.B., Sandberg S.P., Weickmann A.M., and Williams E.J. (2015) An overview of the 2013 Las Vegas Ozone Study (LVOS): impact of stratospheric intrusions and long-range transport on surface air quality. *Atmospheric Environment*, 109, 305-322, doi: 10.1016/j.atmosenv.2014.08.040, 2015/05/01/. Available at http://www.sciencedirect.com/science/article/pii/S1352231014006426.

Langford A.O. and Senff C.J. (2019) Fires, asian, and stratospheric transport-Las Vegas ozone study (FAST-LVOS). Report prepared for the Clark County Department of Air Quality, Las Vegas, NV, by the National Oceanic and Atmospheric Administration Earth System Research Laboratory, Chemical

Sciences Division, Boulder, CO, and the Cooperative Institute for Research in Environmental Sciences, University of Colorado, Boulder, CO, CBE 604318-16, December. Available at https://csl.noaa.gov/projects/fastlvos/FAST-LVOSfinalreport604318-16.pdf.

Louisiana Department of Environmental Quality (2018) Louisiana exceptional event of September 14, 2017: analysis of atmospheric processes associated with the ozone exceedance and supporting data. Report submitted to the U.S. EPA Region 6, Dallas, TX, March. Available at https://www.epa.gov/sites/production/files/2018-08/documents/ldeq_ee_demonstration_final_w_appendices.pdf.

Lu X., Zhang L., Yue X., Zhang J., Jaffe D., Stohl A., Zhao Y., and Shao J. (2016) Wildfire influences on the variability and trend of summer surface ozone in the mountainous western United States. *Atmospheric Chemistry & Physics*, 16, 14687-14702, doi: 10.5194/acp-16-14687-2016.

McClure C.D. and Jaffe D.A. (2018) Investigation of high ozone events due to wildfire smoke in an urban area. *Atmospheric Environment*, 194, 146-157, doi: 10.1016/j.atmosenv.2018.09.021, 2018/12/01/. Available at http://www.sciencedirect.com/science/article/pii/S1352231018306137.

McVey A., Pernak R., Hegarty J., and Alvarado M. (2018) El Paso ozone and $PM_{2.5}$ background and totals trend analysis. Final report prepared for the Texas Commission on Environmental Quality, Austin, Texas, by Atmospheric and Environmental Research, Inc., Lexington, MA, June. Available at https://www.tceq.texas.gov/assets/public/implementation/air/am/contracts/reports/da/582188176307-20180629-aer-ElPasoOzonePMBackgroundTotalsTrends.pdf.

Miller D., DeWinter J., and Reid S. (2014) Documentation of data portal and case study to support analysis of fire impacts on ground-level ozone concentrations. Technical memorandum prepared for the U.S. Environmental Protection Agency, Research Triangle Park, NC by Sonoma Technology, Inc., Petaluma, CA, STI-910507-6062, September 5.

National Weather Service Forecast Office (2020) Las Vegas, NV: general climatic summary. Available at https://www.wrh.noaa.gov/vef/lassum.php.

Pernak R., Alvarado M., Lonsdale C., Mountain M., Hegarty J., and Nehrkorn T. (2019) Forecasting surface O_3 in Texas urban areas using random forest and generalized additive models. *Aerosol and Air Quality Research*, 19, 2815-2826, doi: 10.4209/aaqr.2018.12.0464.

Sacramento Metropolitan Air Quality Management District (2011) Exceptional events demonstration for 1-hour ozone exceedances in the Sacramento regional nonattainment area due to 2008 wildfires. Report to the U.S. Environmental Protection Agency, March 30.

Simon H., Baker K.R., and Phillips S. (2012) Compilation and interpretation of photochemical model performance statistics published between 2006 and 2012. *Atmos. Environ.*, 61, 124-139, doi: 10.1016/j.atmosenv.2012.07.012.

Simoneit B.R.T., Schauer J.J., Nolte C.G., Oros D.R., Elias V.O., Fraser M.P., Rogge W.F., and Cass G.R. (1999) Levoglucosan, a tracer for cellulose in biomass burning and atmospheric particles. *Atmos. Environ.*, 33, 173-182.

Simoneit B.R.T. (2002) Biomass burning - a review of organic tracers for smoke from incomplete combustion. *Applied Geochemistry*, 17, 129-162.

Solberg S., Walker S.-E., Schneider P., Guerreiro C., and Colette A. (2018) Discounting the effect of meteorology on trends in surface ozone: development of statistical tools. Technical paper by the European Topic Centre on Air Pollution and Climate Change Mitigation, Bilthoven, the Netherlands, ETC/ACM Technical Paper 2017/15, August. Available at https://www.eionet.europa.eu/etcs/etc-atni/products/etc-atni-reports/etcacm_tp_2017_15_discount_meteo_on_o3_trends.

Solberg S., Walker S.-E., Guerreiro C., and Colette A. (2019) Statistical modelling for long-term trends of pollutants: use of a GAM model for the assessment of measurements of O_3, NO_2 and PM. Report by the European Topic Centre on Air pollution, transport, noise and industrial pollution, Kjeller, Norway, ETC/ATNI 2019/14, December. Available at https://www.eionet.europa.eu/etcs/etc-atni/products/etc-atni-reports/etc-atni-report-14-2019-statistical-modelling-for-long-term-trends-of-pollutants-use-of-a-gam-model-for-the-assessment-of-measurements-of-o3-no2-and-pm-1.

Texas Commission on Environmental Quality (2021) Dallas-Fort Worth area exceptional event demonstration for ozone on August 16, 17, and 21, 2020. April. Available at https://www.tceq.texas.gov/assets/public/airquality/airmod/docs/ozoneExceptionalEvent/2020-DFW-EE-Ozone.pdf.

U.S. Census Bureau (2010) State & County QuickFacts. Available at http://quickfacts.census.gov/qfd/states/.html.

U.S. Environmental Protection Agency (2008) Network design criteria for ambient air quality monitoring, 40 CFR Part 58, Appendix D.

U.S. Environmental Protection Agency (2015) 40 CFR Part 50, Appendix U: interpretation of the primary and secondary National Ambient Air Quality Standards for ozone. Available at https://www.ecfr.gov/cgi-bin/text-idx?SID=43eb095cc6751633290941788ab4f3bd&mc=true&node=ap40.2.50_119.u.

U.S. Environmental Protection Agency (2016) Guidance on the preparation of exceptional events demonstrations for wildfire events that may influence ozone concentrations. Final report, September. Available at www.epa.gov/sites/production/files/2016-09/documents/exceptional_events_guidance_9-16-16_final.pdf.

U.S. Environmental Protection Agency (2020) Green Book: 8-hour ozone (2015) area information. Available at https://www.epa.gov/green-book/green-book-8-hour-ozone-2015-area-information.

Wigder N.L., Jaffe D.A., and Saketa F.A. (2013) Ozone and particulate matter enhancements from regional wildfires observed at Mount Bachelor during 2004–2011. *Atmos. Environ.*, 75, 24-31, doi: 10.1016/j.atmosenv.2013.04.026, August. Available at http://www.sciencedirect.com/science/article/pii/S1352231013002719.

Wood S. (2020) Mixed GAM computation vehicle with automatic smoothness estimation. Available at https://cran.r-project.org/web/packages/mgcv/mgcv.pdf.

Wood S.N. (2017) *Generalized additive models: an introduction with R*, 2nd edition, CRC Press, Boca Raton, FL.

Zhang L., Lin M., Langford A.O., Horowitz L.W., Senff C.J., Klovenski E., Wang Y., Alvarez R.J., II, Petropavlovskikh I., Cullis P., Sterling C.W., Peischl J., Ryerson T.B., Brown S.S., Decker Z.C.J., Kirgis G., and Conley S. (2020) Characterizing sources of high surface ozone events in the southwestern US with intensive field measurements and two global models. *Atmospheric Chemistry & Physics*, 20, 10379-10400, doi: 10.5194/acp-20-10379-2020. Available at https://acp.copernicus.org/articles/20/10379/2020/acp-20-10379-2020.pdf.